SU-8 Cantilever Sensor with Integrated Read-Out

Johansson, Alicia Charlotte

Publication date:
2007

Document Version
Early version, also known as pre-print

Preface

This thesis has been written as a part of the requirements for obtaining the PhD degree at the Technical University of Denmark (DTU). The PhD project was carried out at the Department of Micro and Nanotechnology (MIC) at DTU during the period from the 1st of October 2003 to the 1st of October 2006.

The PhD project has been a part of the Nanoprobe group in the Nanoscience Engineering (NSE) division and was supervised by:

Professor Anja Boisen
Main supervisor

Associate Professor Oliver Geschke
Co-supervisor

The project was funded by the Danish Ministry of Science and Technology Innovation through the MiNap (Micro and Nano Products) Consortium.

The results I have obtained during this PhD project could not have been achieved without the contribution from a number of people both at MIC and outside the department. Most of all I would like to thank the present and previous members of the Nanoprobe group which have provided a open, friendly, helpful and inspiring atmosphere which have made these past three years a great experience. Especially I would like to thank Anja Boisen for being an outstanding leader and Maria Nordström for her friendship.

For the part of the project that involved the fabrication of the chip, I would like to acknowledge Peter Rasmussen and Monsterrat Calleja as well as the staff of DANCHIP. The electronic interconnection of the chip could not have been achieved without the help from DELTA and I would especially like to thank Jakob Janting, Karsten Hoppe and Inger Ninna Hansen. The microfluidic system was fabricated in the lab at the Danish Polymer Center at DTU with the help of mainly Gerardo Perozziello and Oliver Geschke. I would also like to acknowledge Jan Vasland Eriksen at DANCHIP for de-

veloping an amplifier for the measurements. The theory behind the surface stress and the temperature sensitivity was developed by Ole Hansen who provided an excellent help throughout the project. Martin Dufva, Gabriela Blagoi and Mogens Havsteen Jakobsen provided invaluable advice in terms of the biomolecular measurements.

A number of students have contributed to the work through courses they have followed at MIC. They are: Encarnacion Sánchez-Noguéron, Peter Schultz, Julie Wulff, Henrik Dam and Malene Erup Larsen. Malene Erup Larsen is especially acknowledged for contributing with results both in terms of chip fabrication and cell handling.

The collaboration within the MiNap project has been a highly educating experience for me and I would like to thank all the participants. Furthermore I would like to thank Jakob Thaysen and Cantion A/S for supplying the Cantion chips and Adama Sesay and Allan Hede Alstrup at Teknologisk Institut for performing the antibody spotting on the cantilevers. The results obtained by Lal Pinnaduwage and coworkers at Oak Ridge National Laboratory using the chips presented in this thesis are important to demonstrate the future applications of the SU-8 chip and I would like to thank them for their hard work. I would also like to thank Montserrat Calleja and Javier Tamayo for letting me work in their group at the Bionanomechanics Lab at Centro Nacional de Microelectronica (CNM) in Madrid for two months. Although we did not achieve the results we had expected, I learned a lot from working in your lab and I hope the collaboration between the groups will continue.

Finally I would like to thank my family and friends and most of all Simon.

Abstract

Cantilever based biosensors can be used for detection of surface stress changes due to recognition of a specific analyte in solution. The aim of this PhD project was to develop a micromechanical device which allows for label-free detection of biomolecules such as antibodies. Moreover, due to the small dimensions of the device, high-sensitivity and low reagent consumption is possible. This PhD thesis describes the fabrication of an SU-8 cantilever chip with integrated piezoresistive readout in form of Au resistors. SU-8 is an epoxy based negative photoresist which has been extensively used for microfluidic devices within the last few years. Normally, cantilever sensors are fabricated in Si but SU-8 has a number of advantages compared to Si such as being softer and less expensive. The SU-8 chip was electrically interconnected to a printed circuit board using flip chip bonding and a microfluidic system was fabricated by micromilling to enable measurements in liquid. The chip was characterized in terms of the gauge factor of the piezoresistor, the resonant frequency and the temperature sensitivity. To determine the surface stress sensitivity of the cantilevers, theoretical calculations are presented and the minimum detectable surface stress was estimated. Immobilization of thiol molecules on Au coated cantilevers in both air and liquid phase have been demonstrated and the induced surface stress changes were calculated from the obtained electrical signal. The results correspond reasonable well with results obtained using Si based cantilevers. The Au coated SU-8 cantilevers were also characterized in terms of pH sensitivity. In this thesis, it is demonstrated that it is possible to immobilize antibodies directly on the SU-8 surface and that subsequent recognition of antigens can be verified using fluorescently labelled antibodies. These results have been used to demonstrate that the cantilever chip can be used as a biosensor for detection of antigens in solution.

Contents

Chapter 1

Introduction

The adsorption of molecules from gas or liquid phase on solid surfaces is known to produce surface stress changes. This principle can be used to develop biosensors where the adsorption of biomolecules on one side of a beam results in a surface stress change that makes the beam bend, see Figure 1.1. The induced bending of the beam, or the so called cantilever, is a measure for how many molecules that are present in the solution.

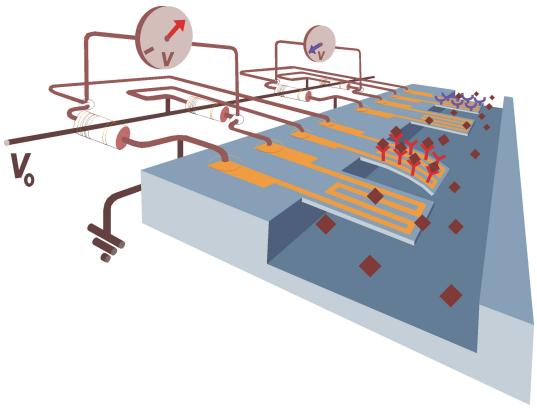

Figure 1.1: A schematic image of a micromechanical sensor. Adsorption of biomolecules induces a surface stress change that can be detected by measuring the deflection of the beam. The image shows a sensor with integrated piezoresistive readout [1].

1.1 Cantilever deflection readout

Cantilever based biosensors originate from the Atomic Force Microscope (AFM) which was invented in 1986 [2]. An AFM measures the topography of a surface by scanning a cantilever with a sharp tip over a surface area while measuring the deflection of the cantilever. The most common

method for detecting the bending of the AFM cantilever is by pointing a laser beam towards the apex of the cantilever and measure the reflection using a position sensitive diode, see Figure 1.2. This optical readout method has been inherited by cantilevers for surface stress sensing. However, other readout methods such as piezoresistive [3], piezoelectric [4], capacitive [5] and MOSFET-based [6] have also been demonstrated.

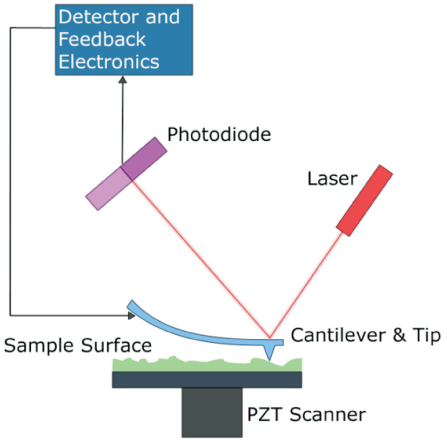

Figure 1.2: The deflection of a cantilever used for AFM measurements or biosensing is often monitored by using an optical setup [7].

Although the optical readout technique is very sensitive, the disadvantage is that it requires an optical setup and alignment of a laser beam. Moreover, due to the rather bulky optics the technique is difficult to use for portable devices [8]. Furthermore, changes in the optical properties of the liquid, such as the refractive index might influence the reflected light. By using piezoresistive readout these issues can be avoided. One of the first demonstrations of AFM cantilevers with piezoresistive readout was reported by Tortonese et al. in 1991 [9].

Instead of measuring the surface stress induced due to adsorption of molecules, it is also possible to detect an added mass or an induced temperature change. Mass detection requires a resonant cantilever where the added mass is detected as a change in resonant frequency of the cantilever [10]. Since liquids have a damping effect on resonating cantilevers, these cantilevers are mostly used for sensing in air and vacuum environments. Temperature changes on the surface of a cantilever can be detected by using a cantilever consisting of a sandwich of materials with different coefficients of thermal expansion. The deflection can be detected by using optical readout [11].

The idea of using cantilevers for chemical sensing has existed since the 1940s

[12]. The first demonstrations of cantilever based sensing used beams with dimensions in the millimeter range and the readout was done by visual inspection [13]. However, in order for a monolayer of biomolecules to induce a measurable deflection the beam has to be micrometer sized. Hence, it was not until the development of microtechnology and the invention of the optical readout method used for AFM that cantilevers became truly interesting as biochemical sensors. Some of the first publications using micrometer sized cantilevers for surface stress measurements were published in 1995 by Raiteri et al. [14] and Chen et al. [15] and in 1996 by Butt [16]. Since then, cantilevers for a wide range of applications have been developed. Detection of surface stress changes due to binding of complimentary deoxyribonucleic acid (DNA) strands [17][18], protein recognition [19], pesticides [20], explosives [21] and alcohols [22] has been reported. Although the principle of surface stress change detection is well established, the origin of the surface stress is not well understood and both electrostatic interactions and entropy changes are believed to influence the bending [23].

1.2 Cantilevers as biosensors

A biosensor is an analytical device consisting of a biocatalyst and a transducer, which can convert a biological or biochemical signal or response into an electrical signal. The biocatalyst is normally immobilized so that it is in intimate contact with the transducer. Biosensors are already of major commercial importance, and their significance is likely to increase as the technology develops [24][25]. The reason is that they are designed to respond specifically and with high sensitivity to a wide range of molecules that are important within industrial, clinical or environmental applications.

Cantilever based microchips are promising for biosensor applications due to the small size, low reagent consumption, fast response time, simple readout and relatively high sensitivity. Since the molecules are detected in real time it is possible to observe the kinetics of the molecular interactions. By using an array of cantilevers with different surface coatings, a high degree of parallelization is possible which is important for multiple detection of biological and chemical molecules and high-throughput screening. Although detection limits of proteins down to a few picograms can be achieved with microarrays, cantilever based sensors offers the advantage of being label-free which means that the biomolecules do not have to be fluorecently labelled before detection. Surface stress changes due to protein concentrations down to nM or ng/ml range have been reported for cantilever based sensors [26] and by using nanoscale resonating cantilevers, mass changes of only a few femtograms is possible [27]. In comparison, other label-free biosensors such as quartz crystal microbalance (QCM) and surface plasmon resonance

(SPR) have been demonstrated to have detection limits for proteins down to pg/ml and ng/ml respectively [28][29]. However, cantilever based biosensors are more suitable for miniaturization.

However, when a biosensor is developed not only the sensitivity but also the selectivity, the reproducibility and the response time are important parameters to consider. These issues are some of the greatest challenges for all types of biosensors.

1.3 Polymeric cantilevers

Within microtechnology and microfluidics there is a general trend towards replacing Si with polymeric materials. The reason is that polymers are less expensive and that the devices can be fabricated more rapidly using less expensive equipment. It is also possible that the surface properties make the polymeric materials more suitable for certain biomolecular applications than Si surfaces.

In 1999, Genolet et al. published one of the first articles presenting polymeric cantilevers for scanning probe microscopy [30]. Since then polymeric cantilevers have been fabricated by injection molding [31], razor blade cutting [32], laser ablation [33], photopolymerization using focused laser beams [34] and UV-lithography [35]. The polymeric materials that have been used include polyimide [36], polypropylene [31], polystyrene [31], polyethylene terephthalate [33], parylene [37] and SU-8 [38].

Most of these cantilevers have only been characterized in terms of the spring constant and resonant frequency while demonstrations of AFM measurements or surface stress measurements are relatively rare [33][38][39].

1.4 Cantilever research in the Nanoprobe group

Cantilevers for AFM were first fabricated at the Department of Micro and Nanotechnology (MIC) in 1994 [40]. Since the start of the Nanoprobe group in 1999, the focus has been on developing cantilevers using new fabrication methods and/or new readout techniques for both surface stress measurements and mass detection. Some ideas include using the cantilever as a lid to a reservoir, using hollow cantilevers where the liquid is guided into the cantilever or fabricating waveguides in the chip to enable integrated optical readout [41]. Initially, mainly Si based cantilevers were developed which resulted in the spin-off company Cantion A/S in 2001. Since then, the research on cantilevers for surface stress measurements has switched to development

of SU-8 based cantilevers. The first SU-8 cantilevers with piezoresistive readout that were fabricated at MIC were presented by Jakob Thaysen in 2002 [42] and by Montserrat Calleja in 2003 [43]. In 2003, SU-8 cantilevers for optical readout were also developed [35]. During the past few years the group has been front-runner in the field of developing SU-8 cantilevers for both optical and piezoresistive readout.

Although the main focus has been on the fabrication and development of cantilever devices, detection of surface stress changes due to DNA hybridization [44], binding of thiol molecules [45] and ethanol [22] have also been demonstrated.

1.5 Motivation

The motivation for this PhD thesis was to develop an SU-8 based cantilever biosensor with fully integrated piezoresistive readout and to perform surface stress measurements using this cantilever chip. The work was divided in four major areas

- Chip fabrication: To fabricate an SU-8 cantilever chip with integrated piezoresistive readout in the DANCHIP cleanroom.
- Packaging: To develop a method to obtain electrical interconnection to the chips and to fabricate a microfluidic system to enable measurements in liquid.
- Characterization: To investigate the performance of the chips in terms of the gauge factor, the resonant frequency and the temperature sensitivity.
- Biomolecular application: To find a potential application for the device and to measure the surface stress induce by molecular binding on the surface of the cantilever.

Moreover, the aim was also to compare the performance of the SU-8 chip to Si based cantilever chips. The work was carried out as a part of the Innovation Consortium MiNap. The consortium was created to build up knowledge that will enable the Danish industry to develop products based on nanotechnology.

1.6 Outline

The outline of the thesis is as follows. In Chapter 2, the principle of piezoresistive readout is described and the expected gauge factor of the resistors in the cantilevers is calculated.

The motivation for using SU-8 and the fabrication process of the SU-8 chips are described in Chapter 3. The packaging of the chip, including the investigations of different methods to achieve electrical interconnection to the chip is described in Chapter 4, while the fabrication of a microliquid handling system for the chip is presented in Chapter 5. Possible contamination from the materials used for the packaging is also discussed.

The characterization of the chip in terms of the spring constant, the resonant frequency, the gauge factor and the temperature sensitivity is presented in Chapter 6. To estimate the performance of the chip as a biosensor, the expected surface stress sensitivity and minimum detectable surface stress of the cantilevers are calculated in Chapter 7. Surface stress measurements in both air and liquid using thiol/Au chemistry are also presented.

Antibody immobilization and subsequent antigen detection has been performed directly on the SU-8 surface. This is presented in Chapter 8 combined with surface stress measurements using the SU-8 cantilever. In Chapter 9 the commercial cantilever measuring system developed by Cantion A/S is presented. To demonstrate that it is possible to replace Si based chips with polymeric chips, an SU-8 chip has been fabricated and integrated in the Cantion system. The performance of the chips was compared to the Si based chips. A conclusion is given in Chapter 10 and five appendices are included in the end of the thesis. The appendices describe the SU-8 patterning process, the chip fabrication process and some additional calculations that are useful to better understand the temperature sensitivity and the bending of the cantilever. Furthermore, a Danish abstract and a publication list is included.

Chapter 2

Piezoresistive readout

The principle of a cantilever sensor with integrated piezoresistive readout is illustrated in Figure 2.1. When molecules bind to the surface of a cantilever a surface stress is induced that results in a bending of the cantilever. If a resistor is embedded in the cantilever the bending will induce a strain in the resistor which thereby results in a resistance change.

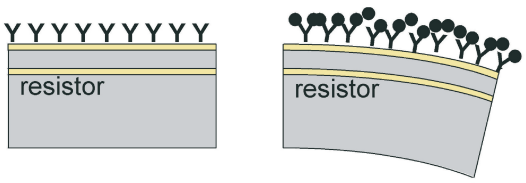

Figure 2.1: Microcantilevers coated with specific receptor molecules, are highly sensitive to surface stress changes that occur due to interactions with molecules in the surrounding air or liquid.

This principle has been used to develop a cantilever based biosensor where a Au resistor was embedded in an SU-8 cantilever. The cantilever has a length, L=215 μm, a width, W=280 μm and a thickness, H=3.5 μm, see Figure 2.2. The cantilever was designed to be a so called *clamped* cantilever where the length and width of the cantilever are about equal in size, $L \sim W$. If $L >> W$, the cantilever is considered to be a *beam* cantilever and the restriction imposed on the cantilever by the clamping at the base is considered negligible, see Figure 2.3. The surface stress sensitivity of the two types of cantilever designs is compared below.

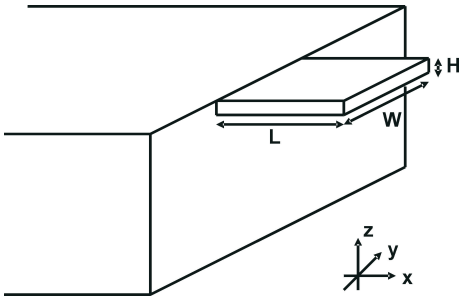

Figure 2.2: Geometry of the cantilever.

2.1 Piezoresistivity

The resistance of a conductive material will change due to an applied strain. The sensitivity to strain is generally termed the gauge factor, K, which is defined as

$$K = \frac{\Delta R}{R}\frac{1}{\epsilon} \tag{2.1}$$

where R is the resistance of the resistor, ΔR is the change in resistance and ϵ is the strain.

2.1.1 Strain

The relationship between strain and stress, σ, is for an elastic isotropic material in three dimensions given by [46]

$$\epsilon_x = \frac{1}{E}(\sigma_x - \nu(\sigma_y + \sigma_z)) \tag{2.2}$$

$$\epsilon_y = \frac{1}{E}(\sigma_y - \nu(\sigma_x + \sigma_z)) \tag{2.3}$$

$$\epsilon_z = \frac{1}{E}(\sigma_z - \nu(\sigma_x + \sigma_y)) \tag{2.4}$$

where E is the Young's modulus and ν is the Poisson's ratio.

For an isotropic surface stress, there is no strain in the y-direction, ϵ_y=0, for a clamped cantilever, while for a beam cantilever, σ_x=σ_y [46]. The out-of-plane stress, σ_z, is assumed to be zero for both cantilever designs. Thus the strains for a clamped cantilever becomes

$$\epsilon_x = (1 - \nu^2)\frac{\sigma_x}{E} \tag{2.5}$$

$$\epsilon_y = 0 \tag{2.6}$$

$$\epsilon_z = -\nu(1 + \nu)\frac{\sigma_x}{E} = \frac{-\nu}{1 - \nu}\epsilon_x \tag{2.7}$$

Hence, the clamped cantilever modulus is Y=E/(1-ν^2).

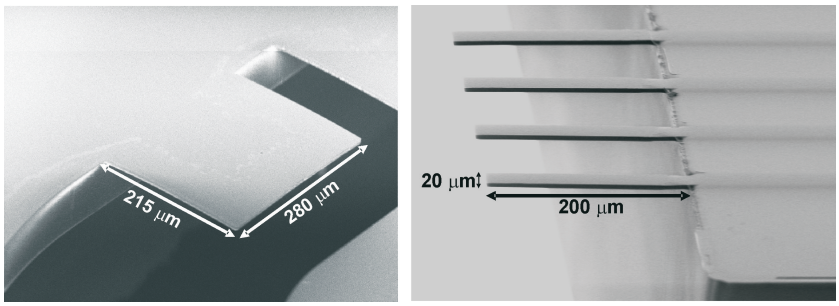

Figure 2.3: Scanning electron microscope (SEM) images of SU-8 cantilevers. The SU-8 cantilever with an integrated resistor (left) is considered to be a clamped cantilever while the SU-8 cantilever for optical readout (right) is an example of a beam cantilever [47]. The integrated resistor is not visible through the SU-8 layer.

2.1.2 Gauge factor

The resistance of a conductor can be expressed as

$$R = \rho \frac{l}{wt} \tag{2.8}$$

where ρ is the conductivity, l is the length, w is the width and t is the thickness of the resistor. The change in resistance of a conductive material when a strain is applied is due to a decrease in cross sectional area and an increase in length of the material under tension. In addition, the resistance also changes due to a change in the resistivity. The relative resistance change can be found by differentiation,

$$\frac{dR}{R} = \frac{d\rho}{\rho} + \frac{dl}{l} - \frac{dw}{w} - \frac{dt}{t} \tag{2.9}$$

if the dimensional changes are assumed to be small the expression becomes

$$\frac{dR}{R} = \frac{d\rho}{\rho} + \epsilon_x - \epsilon_y - \epsilon_z \tag{2.10}$$

by inserting Eq.(2.5)-(2.7),

$$\frac{dR}{R} = \frac{d\rho}{\rho} + \frac{1}{1-\nu}\epsilon_x \tag{2.11}$$

It can be seen that the gauge factor has two contributions - one physical, or so called piezoresistive term, and one geometric term. The geometric gauge factor is

$$K_{geo} = \frac{1}{1-\nu} \tag{2.12}$$

The piezoresistive term of the gauge factor can be estimated as described by Kuczynski [48]. The resistivity can be described by the Drude equation

$$\rho = \frac{m_e}{ne^2\tau} \tag{2.13}$$

where m_e is the effective mass of the electron, n is the electron density, e is the electron charge and τ is the average time between collisions. The electron mass and the charge are considered to be constant. By differentiation the resistivity change can be expressed as

$$\frac{d\rho}{\rho d\epsilon_x} = -\frac{dn}{nd\epsilon_x} - \frac{d\tau}{\tau d\epsilon_x} \tag{2.14}$$

and the electron density is

$$n = \frac{N}{V} \tag{2.15}$$

where N is the number of electrons and V is the volume. If the number of electrons is assumed to be constant and the terms are differentiated

$$\frac{dn}{nd\epsilon_x} = \frac{dN}{Nd\epsilon_x} - \frac{dV}{Vd\epsilon_x} = -\frac{dV}{Vd\epsilon_x} \tag{2.16}$$

The relative volume change can be found by using the strain equations for the clamped cantilever,

$$\frac{\Delta V}{V} = \epsilon_x + \epsilon_y + \epsilon_z = \frac{1-2\nu}{1-\nu}\epsilon_x \tag{2.17}$$

Hence Eq.(2.14) can be written as,

$$\frac{d\rho}{\rho d\epsilon_x} = \frac{1-2\nu}{1-\nu} - \frac{d\tau}{\tau d\epsilon_x} \tag{2.18}$$

The contribution from the change in the average time between collisions can be estimated by assuming that $\tau \sim \theta^2$, where θ is the characteristic temperature and by introducing Grüneisen's constant which is defined as

$$G = -\frac{dln\theta}{dlnV} \tag{2.19}$$

This expression can be written as $d\theta/\theta$=-$G\,d\,V/V$ so that

$$\frac{d\rho}{\rho d\epsilon_x} = \frac{1-2\nu}{1-\nu} - 2G\frac{dV}{Vd\epsilon_x} \tag{2.20}$$

Hence, by using Eq.(2.17) the piezoresistive term of the gauge factor becomes

$$K_{piezo} = \frac{1-2\nu}{1-\nu} - 2G\frac{1-2\nu}{1-\nu} \tag{2.21}$$

and the total gauge factor is

$$K = K_{geo} + K_{piezo} = 2(1 + G\frac{1-2\nu}{1-\nu}) \tag{2.22}$$

G is about 3 for Au and the total gauge factor for the clamped cantilever using ν_{Au}=0.42 is 3.7 [49]. The geometrical and piezoresistive gauge factor

are of the same order of magnitude. However, for Si which is known to have a high gauge factor, the piezoresistive part dominates and the geometrical contribution can be assumed to be negligible. It should also be observed that for clamped cantilevers, the gauge factor is expected to be the same for an isotropic stress as for a point forces applied at the end of the cantilever. However, for beam cantilevers the gauge factor values in the two situations differ [50].

2.1.3 Gauge factor in thin films

When the resistor has a thickness below 1000 Å it can be expected that the conductivity is influenced by surface scattering. The reason is that the thickness of the metal film is comparable to the mean free path length of the electrons. The mean free path length in Au is about 365 Å at room temperature [49]. For even smaller film thicknesses, below 100 Å, the metal layer can be assumed to be discontinuous and the resistivity increases significantly. Generally, the gauge factor has been observed to be slightly lower for films having thicknesses in the intermediate range, 100 Å to 1000 Å, than for layers of more than 1000 Å [51][52]. However, by using discontinuous films very large gauge factors, of up to 100 for Au, have been reported [51][53].

In the intermediate range, the electron transport is dominated by scattering from the film surface and it is assumed that the resistivity depends on the film thickness according to ρ=constant/t so that [51]

$$\frac{d\rho}{\rho} = -\frac{dt}{t} = \epsilon_z \tag{2.23}$$

and using ϵ_z from Eq.(2.7) the result becomes

$$K_{piezo,int} = \frac{d\rho}{\rho}\frac{1}{\epsilon_x} = \frac{\nu}{1-\nu} \tag{2.24}$$

Hence, the total gauge factor for the intermediate range is

$$K_{int} = K_{geo} + K_{piezo,int} = \frac{1}{1-\nu} + \frac{\nu}{1-\nu} = \frac{1+\nu}{1-\nu} \tag{2.25}$$

which is 2.4 for a Au resistor. Hence, the gauge factors for the two thickness ranges are approximately the same and a significant difference should not be detected experimentally. It is also seen that in the intermediate thickness range, the gauge factor increases for increasing values of the Poisson's ratio, while the opposite is true for the thicker resistors. The gauge factors for both 75 Å and 600 Å thick Au resistors were experimentally determined and the results are presented in Chapter 6 where the relationship between the resistivity and the thickness is also further discussed.

2.2 Clamped cantilever vs. Beam cantilever

The sensitivity of a clamped cantilever can be compared to the sensitivity of a beam cantilever for an applied isotropic stress. From Eq.(2.5) and Eq.(2.22) the sensitivity for a clamped cantilever is found

$$\frac{\Delta R}{R} = 2(1 + G\frac{1-2\nu}{1-\nu})\epsilon_x \cong 3\frac{\sigma_x}{E} \tag{2.26}$$

and the corresponding expression for a beam where ϵ_x=(1-ν)σ_x/E is

$$\frac{\Delta R}{R} = 2(1 + G\frac{2-4\nu}{1-\nu})\epsilon_x \cong 3\frac{\sigma_x}{E} \tag{2.27}$$

Hence, for an isotropic stress a clamped cantilever is expected to have about the same sensitivity as a beam cantilever when using an Au piezoresistor. However in the intermediate range, using Eq.(2.5) and Eq.(2.25), the sensitivity becomes

$$\frac{\Delta R}{R} = \frac{1+\nu}{1-\nu}\epsilon_x \cong 2\frac{\sigma_x}{E} \tag{2.28}$$

and the corresponding expression for a beam is

$$\frac{\Delta R}{R} = \frac{4\nu}{1-\nu}\epsilon_x \cong 1.7\frac{\sigma_x}{E} \tag{2.29}$$

Hence, for film thicknesses in the intermediate range the clamped cantilever should have a higher sensitivity than a beam cantilever. The design of the clamped SU-8 cantilever is based on these theoretical estimations.

2.3 SU-8 vs. Si

From Eq.(2.1)-(2.2) it is seen that to optimize the sensitivity, $\Delta R/R$, it is important to use a cantilever material with a low Young's modulus and to have a piezoresistor with a high gauge factor. SU-8 has a low Young's modulus of about 3.5 GPa, which makes it a suitable material for cantilevers for surface stress detection [54][55]. The Young's modulus of Si is about 170 GPa [50].

Normally, metallic layers such as Au, have low gauge factors compared to doped Si and Ge. Gauge factors of 50 to 95 have been demonstrated for doped single crystal Si piezoresistors [3][56] while gauge factors between 12 and 20 have been obtained for cantilevers with polycrystalline Si piezoresistors [3][57]. Unfortunately, Si and Ge are normally deposited at high temperatures ($>$ 700°C) which is well above the decomposition temperature of SU-8 [58][59]. Even so, the K/E-ratio is larger for an SU-8 cantilever with Au piezoresistor, $(K/E)_{\mathrm{Au/SU8}}$=1.1 GPa^{-1}, than for a Si based cantilever,

$(K/E)_{\mathrm{Si}}$=0.1-0.6 GPa^{-1}. It is also important to keep in mind that metallic resistors are expected to have lower noise levels than Si based resistors which makes the resolution of the SU-8/Au cantilever significantly better than for a Si based cantilever.

In conclusion, the SU-8 cantilever with piezoresistive readout presented in this project should have a slightly better sensitivity than Si based piezoresistive cantilevers. Furthermore, due to the clamped design of the cantilever the sensitivity should be somewhat higher than for a beam cantilever, at least when the resistor thickness is in the intermediate thickness range. The expected gauge factor for the Au piezoresistor is 2.4 or 3.7 depending on the Au thickness.

Chapter 3

Design and fabrication of the SU-8 chip

The SU-8 cantilever chip with piezoresistive readout was first presented in 2002 by Jakob Thaysen [42] and a year later, Monserrat Calleja and Peter Rasmussen presented a new design which combined the cantilevers with a microchannel [43]. The chips were fabricated entirely from SU-8 except for the integrated Au resistors and contact pads, see Figure 3.1.

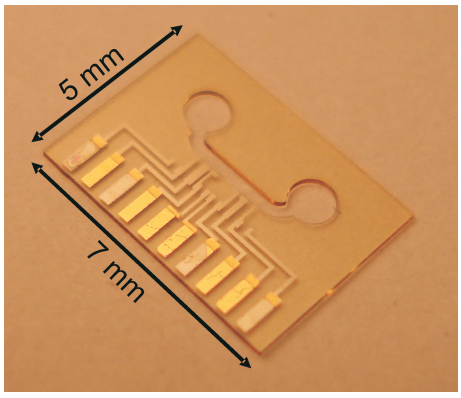

Figure 3.1: The second generation SU-8 cantilever chip with integrated Au resistors, Au contact pads and a microchannel.

3.1 SU-8

SU-8 is an epoxy-based negative photoresist which was invented by IBM in 1989 [58][60]. The SU-8 monomer has eight epoxy groups, see Figure 3.2. The SU-8 used for the cantilever chips was supplied by Micro Resist Technology (Germany) and consisted of the SU-8 monomers, a photoinitiator and a solvent. The photoinitiator, triaryl sulfonium salt (SbF_6^-), is sensi-

tive to near-ultraviolet light (350-400 nm). Upon UV-exposure an acid is produced which opens the epoxy bonds and starts the crosslinking process. Above 350 nm, the SU-8 is highly optically transparent which makes it possible to fabricate vertical sidewalls in thick films. Hence, SU-8 was initially marketed as a high-aspect ratio resist. However, in the last few years the trend has turned towards microfluidic applications where the SU-8 is left as the constitutional material of the device. SU-8 has been used for a number of applications such as microfluidic chambers and optical components including lasers, lenses and waveguides [61][62][63]. This is due to the good mechanical and thermal properties as well as the excellent chemical resistance and biocompatibility [64]. SU-8 is highly resistant to solvents, acids and bases. In fact, crosslinked SU-8 is almost impossible to remove.

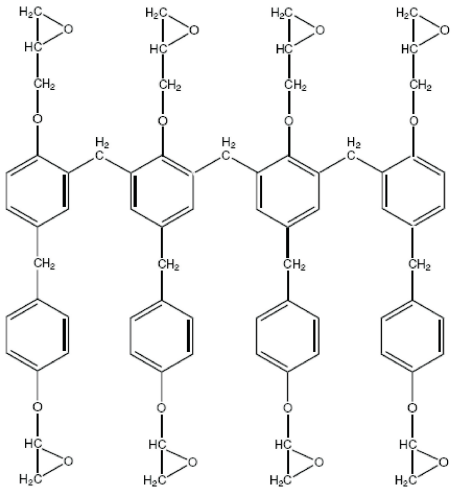

Figure 3.2: The SU-8 monomer with the eight epoxy groups.

3.1.1 Motivation for using SU-8

The low Young's modulus of SU-8, compared to Si, makes the SU-8 ideal for mechanical structures, such as cantilevers, where a low stiffness is often required. This is the one of the main motivations for using SU-8 instead of Si for the cantilevers. Another important reason for using SU-8 is that the finished chip is expected to become considerably cheaper. The reason is not only that the material itself is less expensive but also that the fabrication time is shorter. In the cleanroom at DANCHIP, the total fabrication time for the SU-8 chips with piezoresistive readout was about 6-8 days compared to 6-8 weeks for piezoresistive Si chips [65]. Since access to cleanroom facilities is expensive, this is an important motivation for using SU-8. Furthermore, it is also less expensive to set up a lab for SU-8 processing compared to Si

processing. Reducing the chip cost is of great interest if the devices are to be used for commercial products and especially for single-use devices.

Compared to other polymeric materials that have been used for fabrication of cantilevers, such as polyethylene terephthalate and parylene [33][37], SU-8 has the advantage that it can be spin-coated in very thin layers and subsequently patterned by UV-lithography.

3.1.2 SU-8 processing

The SU-8 processing includes spin coating, soft baking to remove the solvents, UV-exposure and a post-exposure bake to fully crosslink the epoxy groups of the SU-8. Since the SU-8 is a negative resist, the nonexposed and thereby the noncrosslinked SU-8, is dissolved during development. The development is done using propylene glycol methyl ether acetate (PGMEA). The optimization of the patterning process of the SU-8 layers for the cantilever chip was rather straightforward. Although the spin process required some optimization, the baking and the development processes were performed as recommended by MicroChem Corp. [66]. The resolution was not a critical issue and the SU-8 layers could simply be overexposed.

The SU-8 that was used during this project was the so called SU-8 2002 and 2075, which contains the solvent cyclopentanone. SU-8 2002 is more diluted than SU-8 2075 to enable layer thicknesses of around 2 µm while 2075 should be optimal for layer thicknesses around 75 µm. SU-8 2002 was used for the cantilever layers, while 2075 was used for defining the channels and lids. A detailed process sequence for the SU-8 layers is given in Appendix A.

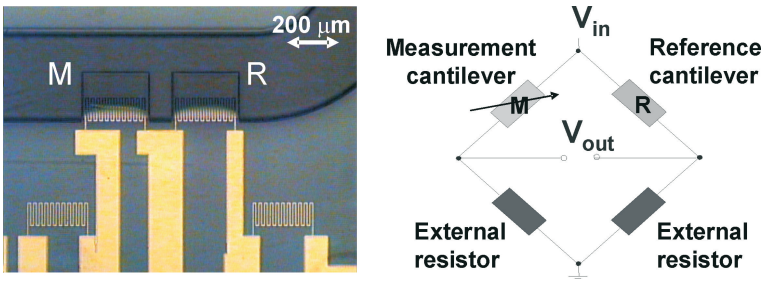

Figure 3.3: The resistors in the measuring and in the reference cantilever were connected with two external SMD resistors in a Wheatstone bridge configuration. The on-chip resistors are also seen in the image.

3.2 Design of the chips

The SU-8 chips are 5 by 7 mm and have a microchannel with four cantilevers. The channel has a large well in each end for inlet and outlet. Each cantilever has an integrated piezoresistor. There are four additional resistors, or so called on-chip resistors, which are integrated in the bulk of the chips, see Figure 3.3. The resistors can be connected in two Wheatstone bridge configurations, each consisting of two cantilever resistors and two on-chip resistors. However, instead of the on-chip resistors, external SMD resistors were normally used.

The cantilevers are 215 μm long, 280 μm wide and about 3.5 μm thick. The resistors are meander-shaped to increase the resistance and are extending 100 μm from the clamping. The width of the resistors is 4 μm. Normally, the thickness of the resistors is 600 Å and the resistance is about 500 Ω.

3.2.1 Three generations of SU-8 chips

The first generation of the SU-8 the chips with a microchannel had some problems with the fabrication and packaging processes:

- The resistors were fabricated by etching which resulted in an inhomogeneous width of the Au and large resistance variations.
- The electrical connection between the contact pads on the chip and the encapsulated resistors was unreliable.
- There was no reliable method to achieve electrical interconnection to the chip from a printed circuit board which made it difficult to characterize the chip.
- The channel in the chip did not have a lid or a bottom.

During this PhD project these problems were solved and a second and third generation of SU-8 chips with integrated piezoresistive readout were fabricated and characterized, see Figure 3.4.

Below, the fabrication process of the second generation of the SU-8 chip is described, referred to as *the SU-8 chip* while the third generation chip, *the SU-8 Cantion chip*, is described in Chapter 9. In principle, the second generation chips have the same design as the first generation chips. However, some of the process steps have been optimized or altered. Unless otherwise stated, it was the second generation chips that were used for the packaging processes, the characterization and the surface stress measurements presented in this thesis. Except for the electroplated Ni contact pads, all the fabrication steps were performed in the cleanroom at DANCHIP. The fabrication process has been published elsewhere [67].

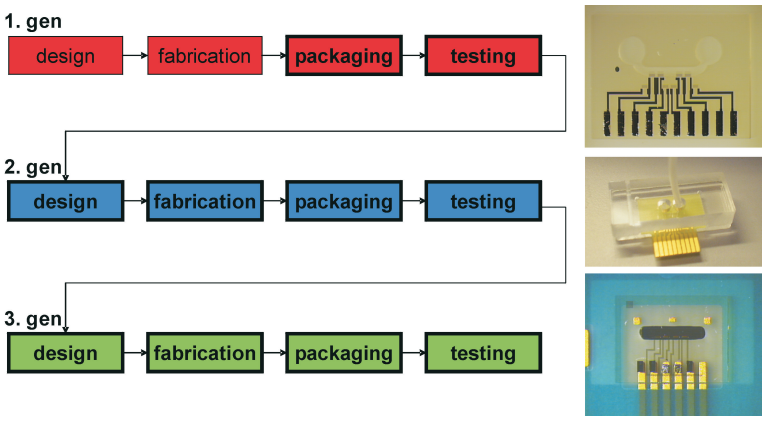

Figure 3.4: The three generations of the SU-8 cantilever chips with piezoresistive readout. The bold text and the bold outline of the boxes indicate the work included in this PhD project. It should be noted that although the packaging processes were different for the three generations of chips, the design of the first and second generation chips was the same while the fabrication process of the second and third generation chips was the same.

3.3 Chip fabrication process

The process sequence is shown in Figure 3.5 and the process parameters are given in Appendix B. A batch of wafers normally consisted of four or five wafers where each wafer had 148 chips.

The first step of the fabrication process was to deposit a release layer consisting of 50/500/500 Å Cr/Au/Cr on four inch Si wafers using a Leybold E-beam evaporator. The reason for using this metal combination is discussed in Section 3.3.6. The purpose of the metallic layer was to enable release of the chips from the wafer at the end of the fabrication process.

3.3.1 Top SU-8 cantilever layer

The chips were fabricated with the cantilevers facing towards the surface of a carrier Si wafer. The reason was that there is no straightforward method to fabricate thin free-hanging cantilevers in SU-8, especially not with integrated readout [68][69]. Hence, the first SU-8 layer that was deposited on the wafer was going to be the top layer of the cantilever where biomolecules were going to be immobilized. The top SU-8 layer should be as thin as possible to achieve maximum sensitivity. This is further explained in Chapter 7. Thicknesses down to 0.16 µm was achieved by diluting the SU-8 2002 but the chips delaminated during the release process and could not be used for measuring. The reason could be due to inhomogeneous mixing of the SU-8 and the solvent. Instead, SU-8 2002 that was not diluted and a layer thickness of 1 µm was used.

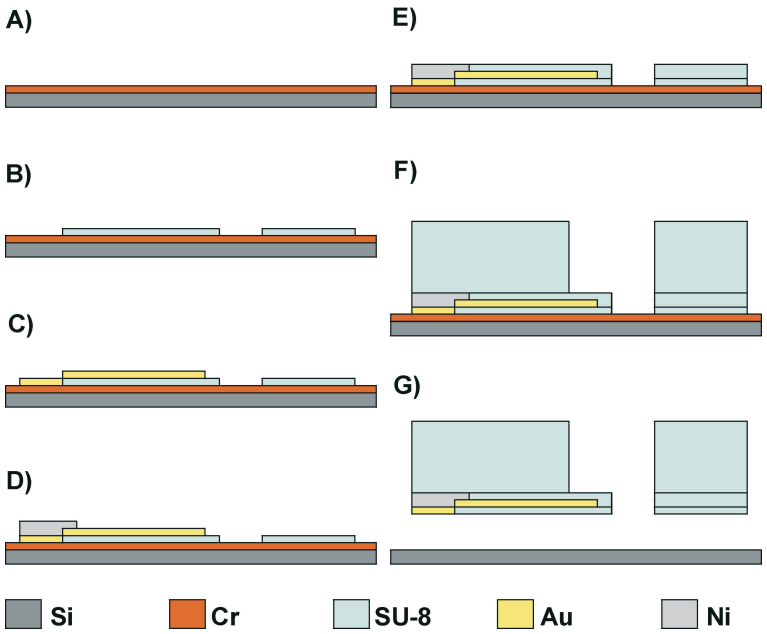

Figure 3.5: Schematic image of the fabrication process. A) Evaporation of a Cr/Au/Cr layer on a Si wafer. B) Patterning of the first SU-8 cantilever layer (1 µm thick). C) Patterning of a Ti/Au layer for the piezoresistors and for the electroplating seed layer (20/600 Å). D) Ni electroplating (5-10 µm). E) Patterning of the second SU-8 cantilever layer (2.5 µm). F) Patterning of the channel SU-8 layer (150 µm). G) Release of the chips by etching the Cr layer.

3.3.2 Au resistors

Figure 3.6 (left) shows the mask used for the first cantilever layer and the mask used for the resistors and the contact pads. The resistors for the first generation design were fabricated by etching the Au in KI using a AZ5214E photoresist mask. However, when the chips were characterized only about half of the resistors on each chip were working and the variation in the resistance was quite large (from about 2 kΩ to 11 kΩ). This indicated that the width of the resistors was inhomogeneous.

Instead, the resistors for the SU-8 chips were fabricated by lift-off. First, a 1.5 µm thick photoresist layer was patterned on the SU-8 layer. An oxygen plasma treatment (240/40 sccm O_2/N_2) was performed to increase the adhesion of the Au layer to the SU-8. The Au layer for the resistors of the SU-8 chip was deposited by using an Alcatel E-beam evaporator. The thickness was normally 20/600 Å Ti/Au, where the Ti layer was used for adhesion. Alternatively, chips with piezoresistor thicknesses down to 75 Å were also fabricated. The reason that the thickness was normally 600 Å was that for larger thicknesses the resistance would be very small and the stiffness of the cantilever would increase. For smaller Au thicknesses, on the other

hand, the Au would start to become discontinuous and the resistors would become fragile. In the same process as for the resistors, a metallic layer for the contact pads was also patterned. The lift-off was done by dissolving the resist in acetone. Figure 3.6 (right) shows the meander-structured piezoresistor in the cantilever.

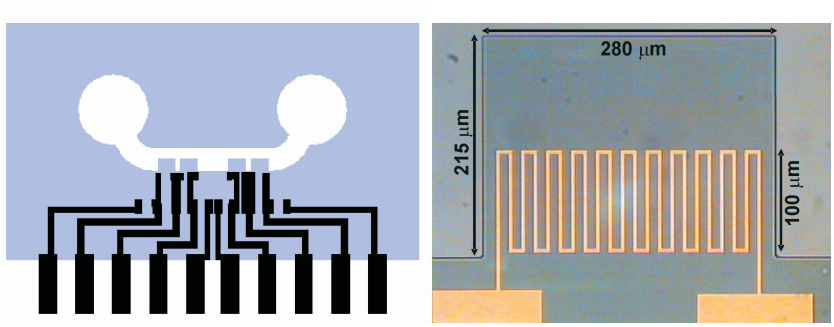

Figure 3.6: Left: The masks used for the top cantilever layer and the metallic layer for the resistors and the contact pads. The resistors in the cantilevers are too small to be visible. Right: The cantilever with the integrated Au resistor.

An ultra sound treatment is normally applied in lift-off processes. However, since the adhesion between the SU-8 and the Ti/Au layer was lower than between Ti/Au and Si, ultra sound would remove most of the metal from the SU-8. Instead, the acetone treatment was prolonged to fully remove the resist from the wafer. As long as ultra sound was not used, the adhesion between the Ti/Au layer and the SU-8 was sufficiently strong for the resistors. An oxygen plasma treatment was performed to remove any resist residues.

In collaboration with Maria Nordström and Encarnacion Sánchez-Noguéron, the bond strength between SU-8 and Au was measured and the influence of using adhesion promoters such as Ti, 4-aminothiolphenol (4-ATP) and Omnicoat (MicroChem Corp.) was investigated. The pull-test method was used to investigate the bond strength and the results are described elsewhere [70]. It was found that Omnicoat gave the best results followed by 4-ATP and Ti. A similar study was presented by Dai et al. where the bond strength between SU-8 and various metals was tested [71]. It was found that Ti had the largest adhesion to SU-8 followed by Cr, Au, Cu and Ni.

The reason for using Au resistors was that it is a good conductor that does not form an oxide on the surface. However, as mentioned in Chapter 2 the sensitivity of the cantilevers might increase by using a material which has a large gauge factor compared to Au and other metals. Although Si has a large gauge factor, it is normally deposited at temperatures which are too high for the SU-8 and the two materials are thereby not compatible [59]. During

this project, sputtered Si and Ge was deposited on SU-8 but the measured resistivity was too high. Another possibility is to use SU-8 based conducting polymers as the piezoresistive material. This has been investigated in the Nanoprobe group at MIC [72]. However, one of the disadvantages by using conductive SU-8 is the lower reproducibility and the increasing noise level.

3.3.3 Contact pads for electrical interconnection

To achieve electrical interconnection from the contact pads on the wafer to the resistors on the first SU-8 layer, it was important that the metallic layer had a good step-coverage, see Figure 3.5C. However, when using the Alcatel for metal evaporation the step-coverage was normally low, unless a metallic layer of approximately the same thickness as the SU-8 layer was used. Hence, the 600 Å Au layer that was evaporated for the resistors was not sufficient to form an electrical connection from the contact pad to the resistor when the thickness of the first SU-8 layer was 1 µm. For the first generation chips the problem was solved by evaporating another thicker metal layer and patterning it for the contact pads. However, even though a Au layer of up to 1.5 µm was deposited, reliable electrical connection to the resistors was not achieved.

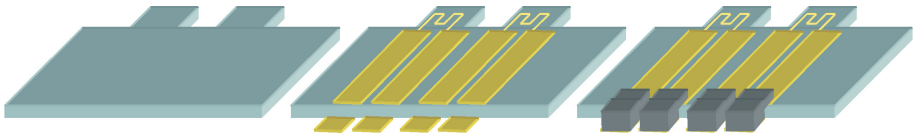

Figure 3.7: Schematic image showing the first SU-8 layer, the thin Au layer for the resistors and the electroplated Ni contact pads. The Au was too thin to form a reliable electrical connection from the contact pad to the metallic layer on the SU-8.

For the second generation chips, the problem was solved by electroplating the contact pads which enabled metallic layers of several microns to be deposited, see Figure 3.7.

3.3.4 Electroplating

Electroplating requires a conductive seed layer on the wafer and a photoresist mould. Au is excellent to use as the seed layer since it has a high conductivity and does not form an insulating oxide on the surface [73]. Hence, the thin layer of Ti/Au for the resistors could also be used as the seed layer for the contact pads and 2.2 µm AZ5214E resist was used as the mould, see Figure 3.8. The Au contact pads, that were going to be electroplated, were in electrical contact with the release layer on the wafer. To achieve a good electrical connection to the seed layer, the Cr layer at the rim of the wafer was etched so that the Au layer underneath was exposed.

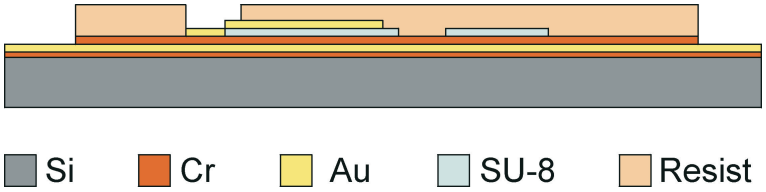

Figure 3.8: Schematic image showing the resist mould used for electroplating. The resist covered the entire wafer except for the rim of the wafer and the contact pads where the Ni was going to be electroplated. The upper Cr layer of the Cr/Au/Cr release layer was etched at the rim of the wafer.

Electroplating is done by applying a voltage between the item to be plated and a counter electrode in a container with an electrolyte with metal ions, see Figure 3.9 (left). When a negative voltage is applied, metal ions are reduced and metal is deposited on the metallic plating base.

The wafers were placed on a holder having three pins for electrical contact that each were protected by an O-ring, see Figure 3.9 (right). A so called current thief was placed around the wafer and was connected to the same potential as the wafer. The current thief ensured a more homogeneous distribution of the current density and thereby a more uniform thickness.

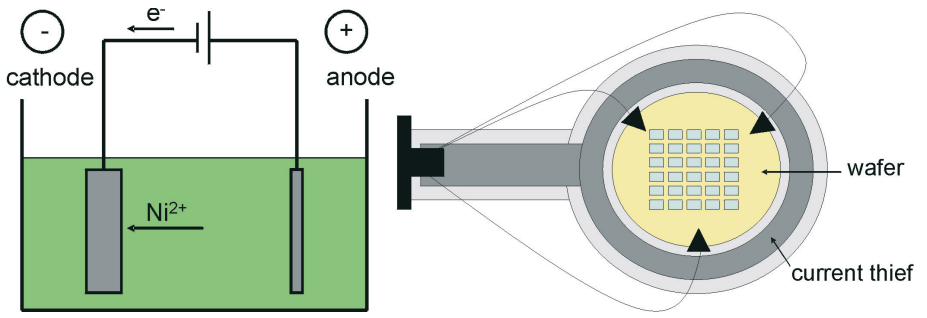

Figure 3.9: Schematic image showing the principle of Ni electroplating (left) and the holder for the wafer which was used while electroplating (right).

The wafers were electroplated with the help of Peter Torben Tang at the Department of Manufacturing Engineering (IPL) at DTU. Both Ni and Au were electroplated on the Au seed layer. The Au was electroplated using 1 A/dm^2 with a rate of 0.2 µm/min. The calculated area to be electroplated was about 0.16 dm^2 and the Au electroplating was performed for 20 min. The Ni was electroplated in a sulfamate-based electrolyte at 40°C using a current density of 4 A/dm^2. The wafers were electroplated between 2.5 min and 6 min and the thickness of the electroplated Ni was about 5-10 µm. As long as the thickness of the contact pads was more than 1 µm a robust

electrical connection was obtained.

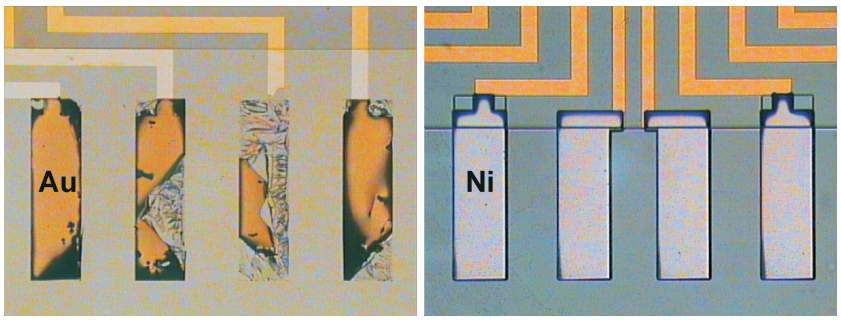

Figure 3.10: Both Au and Ni were electroplated for the contact pads. The Au pads (left) fell off the wafer due to stress in the material while the Ni pads (right) adhered well.

Due to stress in the electroplated Au pads the adhesion was low, while Ni electroplating resulted in smooth and stress-free contact pads, see Figure 3.10 (left) and (right). Although Ni layers have been observed to have low adhesion to SU-8, the Ni contact pads adhered well to the SU-8 chip. The reason was probably that the contact pads were rather thick and well anchored in the chip. The resistance from the contact pads to the piezoresistors was less than 10 Ω. Hence, it was decided to use electroplated Ni for the contact pads. After electroplating, the resist was removed in acetone and by oxygen plasma treatment.

3.3.5 Second SU-8 cantilever layer and the channel walls

The resistors were encapsulated in a 2.5 μm thick SU-8 layer, which formed the second layer of the cantilever, see Figure 3.5E. The reason that the resistors were fully encapsulated in the SU-8 was to enable measurements in liquid. The mask for the second cantilever layer was similar to the mask used for the top cantilever layer. After the patterning of the cantilever, a thick layer (150 μm) of SU-8 2075 was spin coated and patterned to form the walls of the microfluidic channel, see Figure 3.5F. The mask had exactly the same dimensions as the second cantilever layer but the cantilevers had been removed.

3.3.6 Release layer

When the fabrication of the chips was finished, the chips had to be released from the Si wafer. Although Teflon and polymeric layers can be used as release layers, a metallic release layer was required for the fabrication of the SU-8 chips with integrated readout [74][75][76]. The reason was that the electroplating step required that the chips were fabricated on a conductive substrate.

For the fabrication of the SU-8 chips, a Cr layer was used to release the chips. However, other metallic layers were also investigated including Ti, Cu and Al. All of these metals could be evaporated in the cleanroom using the Alcatel or the Leybold. The requirement for the metallic layer was that it could be underetched in a few hours in an etchant which would not harm the SU-8 or etch the Au and Ni used for the contact pads on the chip. Once the chips were released, they were picked up from the etchant one by one using a pair of tweezers. Finally, they were rinsed in water.

Ti is normally etched in hydrofluoric acid (HF) but since it is highly hazardous to use, was not considered to be a good option. However, a single test was made where the wafer with the SU-8 chips on a Ti release layer was immersed in 5% HF for a few minutes. The chips were observed to delaminate and only the thick SU-8 layer came off the wafer while the thin SU-8 and the contact pads stayed on the Ti layer. Delamination was also observed when the Ti layer was etched in NH_4OH:H_2O_2 (1:3). Etching in RCA-1 (NH_3:H_2O_2:H_2O) (18:25:100) was also attempted but no underetch was observed even after 24 h. Based on these results, Ti was not considered to be a promising material for the release process.

The idea of using Cu as release layer was first investigated by Malene Erup Larsen during her Master thesis [77]. Both electroplated and evaporated Cu were tested. The electroplated Cu was found to be too rough and it was not possible to perform lithography with good line-width on the wafer. Instead, evaporated Cu was investigated but unfortunately the adhesion between the SU-8 and Cu was found to be very low and most structures delaminated from the wafer during development.

The SU-8 chips on the Al release layer were underetched in NaOH and Type D etchant (Transene). In NaOH, the etch rate was very inhomogeneous and the chips appeared to float to the surface before the cantilevers were released and thereby ripping the cantilevers off the surface and breaking them. The Type D etchant was etching the Al layer very slowly and not a single chip was released after 24 h. The reason could be that the etchant was too old but the test was never repeated to confirm this.

For the Cr based release process, the Cr layer was etched in Cr etchants 1020A, CRE-473 or 8002A, all supplied by Transene. 1020A is based on ceric ammonium nitrate (CAN) and 5-6 % nitric acid and is a fast etchant but not compatible with Ni. In 8002A, the nitric acid has been exchanged with 10-20 % acetic acid which makes the etchant compatible with Ni. CRE-473 is based on HCl (20-25 %) and is also compatible with Ni. However, since SU-8 chips had been observed to delaminate in HCl, 8002A was chosen to

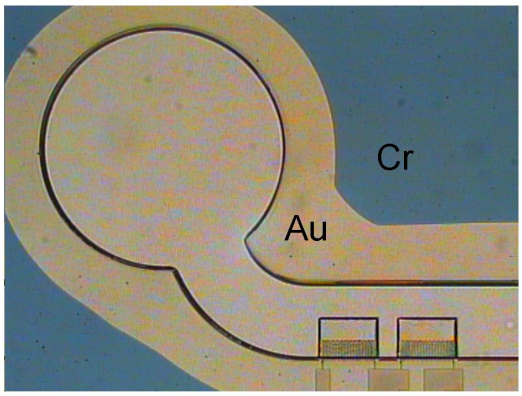

Figure 3.11: The Cr layer under the SU-8 chip has been etched around the channel.

be the most suitable etchant for Cr. As long as the bottle was used within two months of opening, the chips were released within 1-3 h, see Figure 3.11. After two months the etch rate decreased significantly and it could take several days to underetch all the chips. The chips were rarely observed to delaminate and the cantilevers were rarely broken.

Hence, the Cr release was found to be the preferred release process and the first step in the fabrication process was to evaporate a 50/500/500 Å thick Cr/Au/Cr layer on Si wafers. The Au layer was used to form a voltaic cell with the Cr layer which increased the etch rate. The first Cr layer was used as an adhesion layer for the Au. This release process was developed by Genolet [78].

To investigate if any Cr residues were left on the chip surface, X-ray photoelectron spectroscopy (XPS) measurements were performed on the SU-8 surface that had been in contact with the Cr layer. The XPS analysis was performed by John Larsen at the Interdisciplinary Research Center for Catalysis (ICAT) at DTU. The measurements did not indicate that there were any Cr molecules left on the SU-8 surface.

3.4 Au coating of the measuring cantilever

After the fabrication and the release of the chips, the cantilevers could be coated with Au to enable immobilization of thiol molecules. The cantilevers were coated on the top surface which is the side that was facing down towards the wafer during fabrication. Normally, a 20/200 Å thick Ti/Au layer was evaporated using the Alcatel. The evaporation rate was 10 Å/s. A shadow-mask could be used while evaporating the metal so that only some of the cantilevers were coated, see Figure 3.12. The shadow-mask was also used to

protect the contact pads so that they were not short circuited.

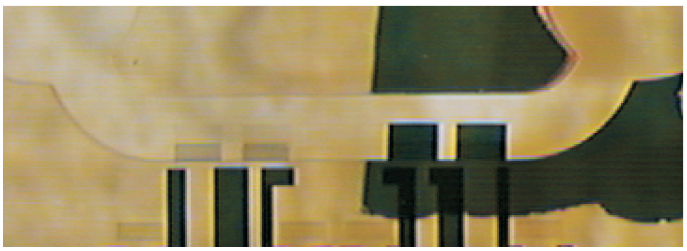

Figure 3.12: Optical image showing two Au coated cantilevers. A shadow-mask was used to ensure that only two of the cantilevers were coated.

The grain size of the Au on the SU-8 cantilevers was measured using tapping mode AFM. The grain size diameter was found to be 20-40 nm and the height variation was about 5-7 nm.

3.5 Fabrication process yield

During this project a total of 32 wafers with SU-8 chips were fabricated. Only about ten of these wafers were fabricated following the optimized process described above using 600 Å thick Au resistors. The fabrication process in the rest of the cases involved f. ex. Ti, Cu or Al as the release layer, another Cr release than 8002A, sputtered Si or Ge piezoresistors, diluted SU-8, varying thicknesses of the Au layer for the resistors or another type of SU-8.

Out of the ten wafers that were fabricated using the optimized process, five wafers could not be used. In four of the cases the reason was due to problems during patterning of the resistors. Hence, this step was regarded as the most critical part of the process. In the last case, all of the cantilevers were bending a lot without any apparent reason. The five successful wafers that were fabricated using the process described above had a resistor yield of more than 90 %. A resistor was considered to be functioning when the resistance was not deviating with more than 2 % from the average resistance of that chip. As the thickness of the Au layer for the resistors was reduced, the yield was observed to decrease. The reason was probably that the resistors were becoming more fragile. However, a yield of up to 75 % was observed for resistor thicknesses as small as 75 Å which was sufficiently large to enable characterization of the chips.

Hence, it could be concluded that as long as the process described above was followed, the yield was likely to be very high for the SU-8 chips.

3.6 Bonding a lid on the microchannel

After release of the SU-8 chips, the microfluidic channel in the chip had no bottom or lid. While a lid should be bonded onto one side of the chip, the opposite side had to be open to allow for the liquid to be introduced through a microfluidic system.

Patterning the SU-8 lid as a last step of the fabrication process and before the chips were released is one possible option [68][79]. However, due to the high UV-transmission of SU-8 it was difficult to control the exposure dosage so that only the lid layer was exposed and not the SU-8 in the channel under the lid. Instead, the SU-8 lids were fabricated on a separate wafer and were subsequently bonded to the chips. The channel walls and the lids could be bonded either before or after the release of the chips. If the bonding was done before the release, all the chips were bonded simultaneously, see Figure 3.13 (right). This is referred to as wafer scale bonding. If the lids were bonded to the channel walls after the release, the chips were bonded one by one, or so called single chip bonding, see Figure 3.13 (left).

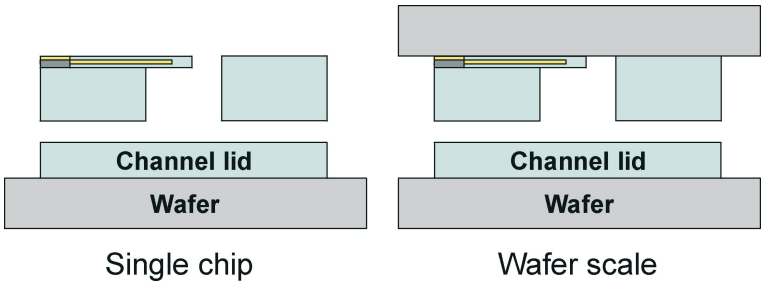

Figure 3.13: Schematic image showing two different methods of bonding a lid to the SU-8 channel. The SU-8 layers could be bonded using either single chips that were released from the wafer (left) or by using wafer scale bonding where the chips were still attached to the wafer (right).

Bonding SU-8 to SU-8 is not straightforward and has been addressed in several research articles [75][80]. If the SU-8 layers are crosslinked before bonding the adhesion might be low. On the other hand, if the layers are crosslinked after bonding, clogging might be a problem. Blanco et al. have demonstrated successful results when bonding two 20 µm thick crosslinked layers of SU-8 together using a commercial wafer bonder [80]. However, thickness uniformity, bonding pressure and crosslinking density were reported to be important parameters that had to be carefully optimized.

Here, the SU-8 lids had a thickness of about 35 µm and were patterned on either Si wafers, Teflon coated Si wafers or on Pyrex wafers. The SU-8 patterning is further described in Appendix A. The Teflon layer was used as

a release layer and was deposited using an Advanced Silicon Etcher (ASE) (STS) [74]. The Teflon release did not require any wet-etching and was done by simply pulling the lids off the wafer after bonding to the SU-8 chips.

3.6.1 Single chip bonding

Standard cantilever chips having a channel wall thickness of about 150 µm were used for the single chip tests presented here. The bonding of the SU-8 cantilever chips to crosslinked and developed lids was done by placing the chips on the lid structures and gently pressing using tweezers. The wafer with the lids was placed on a hotplate at 90°C and a weight was placed on top to press the two structures together.

The adhesion between the chips and the lids turned out to be very low. The reason for the low adhesion was probably that the SU-8 was fully crosslinked before bonding. However, the results were not improved by minimizing the crosslinking density. The crosslinking density was reduced by using short exposure times and by bonding directly after exposure of the lids without post-exposure baking the SU-8 first. Since it did not seem to be possible to bond the chips to the lids after exposure of the lids, the structures had to be bonded before the SU-8 lids had been exposed. However, when single SU-8 chips were placed on the SU-8 lid layer before it was exposed, their placement were random and mask alignment during the subsequent exposure was a problem.

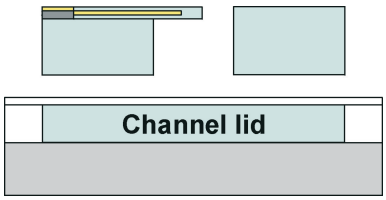

Figure 3.14: The SU-8 chip was glued to the crosslinked lid using an unexposed SU-8 layer as glue. To achieve a homogeneous thickness of the glue layer it was important that it was spin coated before the channel lid layer was developed.

Another approach was to expose and post-exposure bake the lid and spin coat another layer of SU-8 on top which was used for gluing, see Figure 3.14. By spin coating the glue layer before the channel lid layer was developed, the glue layer obtained a homogeneous thickness distribution over the wafer. Since the lid was already crosslinked it was visible through the glue layer and the chip could be aligned to it by the eye. The chip was glued to the lid at the end of the soft bake process of the glue layer when the wafer had cooled down to about 70°C. It was important that the temperature was above the glass transition temperature, T_g, of the SU-8 which is about 50°C, so that

any thickness variations could be levelled out. The chips were pressed gently to the glue layer using tweezers. The glue layer was then exposed through a mask followed by post-exposure bake and development of both the glue layer and the lid layer. Both SU-8 2005 and 2075 could be used as the glue layer and no clogging of the channel was observed and the adhesion was good, see Figure 3.15 (right). When liquid was introduced in the channel, leakage was not observed which indicated that the glue layer had sealed the interface properly, see Figure 3.15 (left).

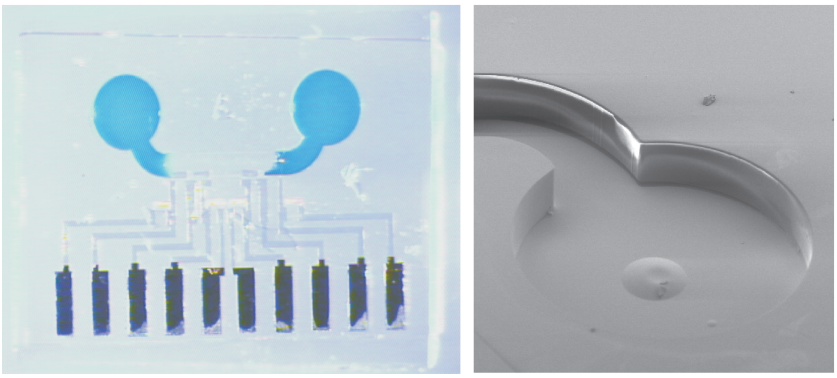

Figure 3.15: Left: Optical image of a chip that was bonded to an SU-8 lid using an SU-8 glue layer. Before bonding, the glue layer had been soft baked but not UV-exposure. A colored liquid was introduced in the channel to verify that the sealing was tight. Right: SEM image of a channel glued to a lid.

3.6.2 Wafer scale bonding

When bonding two wafers with SU-8 structures together it is very important that both wafers have a flat surface with thickness variations of maximum a few microns. For the wafers scale bonding, a mask was designed with 88 lid structures, see Figure 3.16 (Inset). The thickness of eight lids was measured across the wafer and the relative thickness variation was plotted, see Figure 3.16. The thickness variation decreased when the spin speed, spin time and acceleration were increased. Moreover, the thickness of the SU-8 layer decreased from 60 µm to 25 µm when the spin speed was increased from 3000 rpm to 5000 rpm.

The channel walls of the SU-8 chips were fabricated using a spin speed of only 1000 rpm and the measured height variation across the wafer was up to 100 µm. Such a large thickness variation made it impossible to bond lids to the cantilever chips on wafer scale. Hence, for the wafer scale bonding tests, channel structures instead of cantilever chips, having a thickness of about 35 µm were used. In principle, it is possible to fabricate the cantilever

chips with much thinner channel walls which would thereby enable wafer scale bonding of the chips.

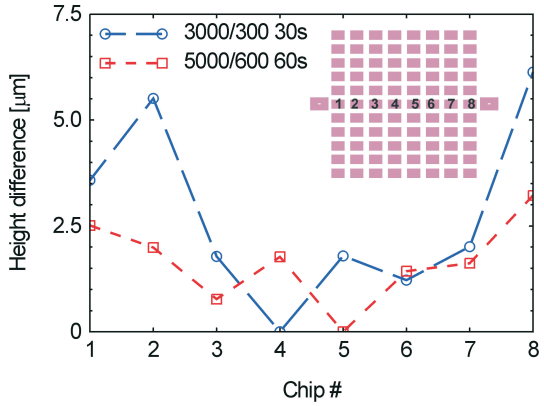

Figure 3.16: The thickness of eight SU-8 lids on two wafers have been measured and the height difference between the thinnest and the thickest lid has been measured. To enable bonding of two crosslinked SU-8 structures it was important that the thickness variation was as small as possible.

An EVG-NIL bonder was used for the wafer to wafer bonding of SU-8 channels and lids. The work was done by Henrik Dam and Julie Wulff as part of a course at MIC. If both the channels and the lids were fabricated on Si wafers the alignment required alignment marks on the backside of the wafers. To avoid this extra process step, the lids were fabricated on transparent Pyrex wafers while the channels were fabricated on Teflon coated wafers for fast and easy release. If the two wafers were bonded before the lid layer had been fully processed, it was difficult to develop the SU-8 between the two wafers after bonding. Instead, both the channel structure and the lid structures were crosslinked and developed before bonding. To minimize the crosslinking density the wafers were exposed as little as possible (about 50 s) while still maintaining a good adhesion to the wafer. The bonding time, temperature and pressure were varied and it was found that good adhesion could be obtained using a bonding temperature of 150°C, a bonding pressure of 2400 N and a bonding time of 20 min. The bond strength was investigated by simply pulling the two wafers apart.

The reason that two crosslinked SU-8 structures could be bonded using wafer scale bonding, while low adhesion was observed using single chips, was probably due to the better control of the bonding pressure when using the EVG-NIL compared to manually bonding of the chips.

In this chapter the design and fabrication of the second generation of SU-8 chips with integrated readout have been described. The resistors were

fabricated by lift-off and the thickness was normally 600 Å resulting in a resistance of 500 Ω. By electroplating the contact pads a robust electrical connection could be achieved. Several metallic layers were investigated as release layers and Cr was found to give the best results. The SU-8 chips could be fabricated with a yield of more than 90 %. An SU-8 lid could be bonded to the channel walls of the SU-8 chip using single chip or wafer scale bonding. However, most of the surface stress measurements were done by simply gluing the chips without lids to a printed circuit board. This is discussed further in Chapter 5.

Chapter 4

Electrical interconnection

Although there is an enormous interest in the future applications of micromechanical devices there are relatively few publications that address the packaging of such devices [81]. However, for microsystems to function properly the packaging is essential. Packaging can include fluidic, optical and electrical interconnections. In this chapter, the electrical interconnection of the chips is described while in the next chapter the microfluidic system will be described. All the packaging processes were performed using both the SU-8 chips and Si cantilever chips supplied by Cantion A/S [82]. This made it possible to compare the packaging process of polymeric chips to Si based chips. The Si Cantion chips are 2.5 mm by 3.5 mm and the contact pads have approximately the same dimensions as the contact pads on the SU-8 chip, see Figure 4.1.

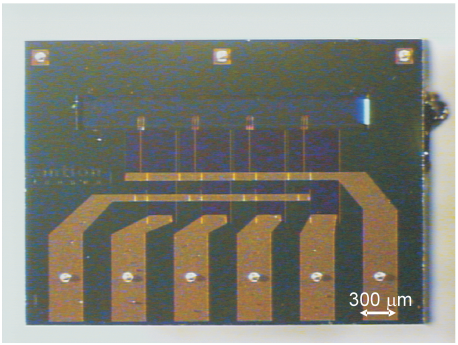

Figure 4.1: The Si Cantion chip is a cantilever chip with piezoresistive readout which was supplied by Cantion A/S. The chips were packaged using the same method as for the SU-8 chips. The Au bumps used for the flip chip bonding are seen on the contact pads on the chip.

The aim was to find a reasonable fast and reliable method to electrically interconnect SU-8 based chips by using methods that are well established

in the semiconductor industry. The motivation for these investigations was that if Si based devices are going to be replaced by polymeric materials, it is important that the interconnection methods are optimized to better suit these devices. The tested electrical interconnection techniques described here are: wirebonding, silver paste, flip chip bonding using underfill and flip chip bonding using Anisotropic Conductive Film (ACF). Although SU-8 is becoming a widely used material within research and development of micromechanical and microfluidic devices it is not common to integrate metallic conductors in the resist. Hence, how to achieve reliable electrical interconnection to metallic conductors in SU-8 has not been extensively addressed in the literature. The results presented in this chapter has been published elsewhere [83].

4.1 Substrate for electrical interconnection

The contact pads on the chip had to be electrically interconnected to a Printed Circuit Board (PCB) that could be easily inserted in a Flat Flexible Cable connector (FFC). Connecting the chip directly in a connector was not an option since i) a connector with a small enough pitch was difficult to find, ii) the contact pads on the SU-8 chip were considered to be too fragile and iii) it would be difficult to integrate the chip with a fluidic system so close to the connector.

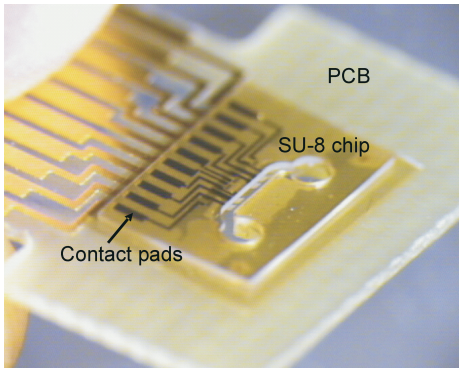

Figure 4.2: The optical image shows an SU-8 chip that has been flip chip bonded on a PCB. The conductors on the PCB have the same width and pitch as the contact pads on the SU-8 chip. A microfluidic channel, corresponding to the channel in the SU-8, have been micromilled in the PCB. The four cantilevers can be seen in the channel.

There are a number of different PCB materials such as ceramics, flex prints and FR-4 [84]. Ceramics are medium expensive and has a low coefficient of thermal expansion (CTE) (about 7 ppm/K for Al_2O_3) which is suitable for Si based materials having a CTE of 2.5 ppm/K. However, since SU-8 has a CTE of 52 ppm/K thermal, stress might be a problem if a ceramic print

is used. Flex prints have thickness of about 100-150 µm and are used when thin and flexible prints are required. Flex prints are often made of polyimide which is a biocompatible material. The drawback of flex prints is the high cost. FR-4 is based on multiple layers of epoxy and glass and is the most widely used material for PCBs. FR-4 is relatively inexpensive (10-20 times less than flex print) and has a CTE of about 16 ppm/K.

For the SU-8 chips, a FR-4 PCB (Printline, Denmark) was used for chip interfacing, see Figure 4.2. The main reasons for using FR-4 was due to the low cost and that it was possible to micromill a channel in the print. This is further discussed in Chapter 5. The PCB was T-shaped and 15 mm long, 12.5 mm wide and 400 µm thick and was designed specifically for the SU-8 chip. It had ten equally spaced 35/5/0.8 µm thick Cu/Ni/Au conductors. The conductors had the same width and pitch as the contact pads on the SU-8 chip. To facilitate electrical interconnection to the PCB, it was designed to fit in an FFC connector (Deltron Conelec AS). A similar FR-4 PCB was used for the Si Cantion chips.

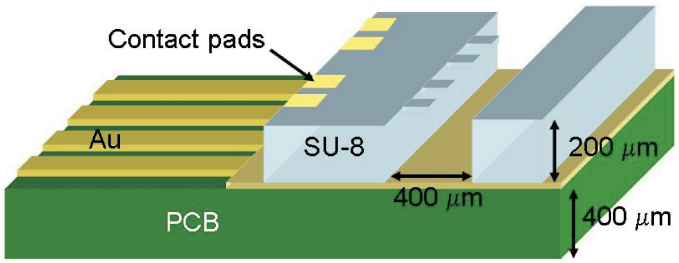

Figure 4.3: When interconnecting the chip using wirebonding or silver paste, the chip was mounted on the PCB with the contact pads and the cantilevers facing up.

4.2 Wire bonding

The most common method to electrically interconnect microchips is probably wire bonding. Wire bonding includes ball- and wedge bonding which require heat, pressure and/or ultrasonic energy to attach the wire to the contact pad. The wire can be made of Au, Al or Cu. Wire bonding from the Au coated Ni contact pads on the SU-8 chip to the PCB was done using a ball-wedge bonder (WestBond 454647E) with a 25 µm thick Au wire. The chips were mounted on the PCB with the contact pads and the cantilevers facing up, see Figure 4.3. Wire bonding was mainly investigated using chips from the first generation of the SU-8 chips and from the first batch of the second generation, see Figure 4.4.

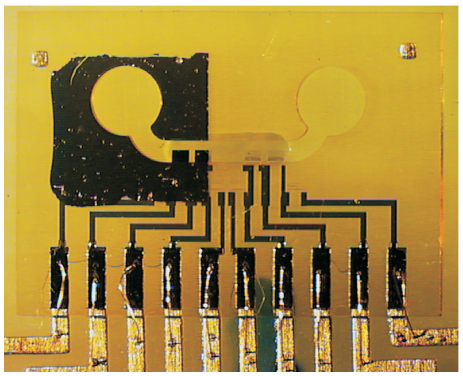

Figure 4.4: The contact pads on the SU-8 chip from the second generation were wire bonded to the PCB. However, due to SU-8 residues on the contact pads the wire bonding yield was normally very low and other methods had to be investigated to interconnect the chips.

For the first generation chips, the adhesion between the contact pads and the chip turned out to be too low. The result was that the wire pulled the contact pad from the chip. By electroplating the contact pad, the adhesion improved significantly for the second generation chips. Furthermore, since electroplating resulted in a thicker and thereby harder contact pad, it was assumed that the wire bonding yield would increase [85]. Unfortunately, regardless of the parameters that were used, it proved to be very difficult to attach the wires to the contact pads on the chips. Initially, it was assumed that the reason was due to the softness of the SU-8 chip. However, by visual inspection traces of residues could clearly be seen on the contact pads on some of the chips. These residues could not be removed by using acetone, O_2 plasma or UV-ozone cleaning, indicating that it probably was crosslinked SU-8. These residues were likely to be the cause of the low adhesion of the wire. When a few 200 µm thick SU-8 substrates with electroplated contact pads, without any visible residues were wire bonded the yield was close to 100 %, indicating that the problem was mainly caused by the residues. However, since many of the chips showed signs of residues on the contact pads it was decided that wire bonding was not a suitable interconnection method to use for the SU-8 chips.

Compared to the SU-8 chips it was considerably easier to wire bond to the Si Cantion chips. This confirmed that the low yield, when using the SU-8 chips, had nothing to do with the wire bonding technique but was due to the properties of the polymeric chip.

4.3 Silver paste

Instead of wire bonding, isotropic conductive pastes can be used to electrically interconnect microchips. Different silver pastes were manually applied between the contact pads on the chip and the conductors on the PCB using a small probe needle, see Figure 4.5.

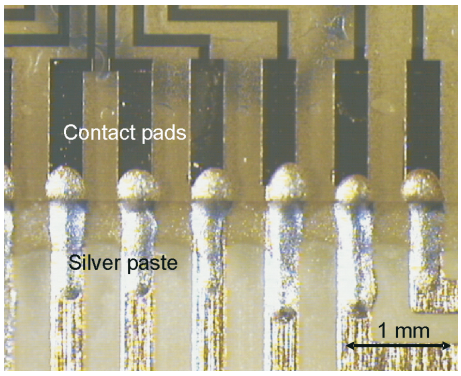

Figure 4.5: The contact pads on the SU-8 chip were connected to the PCB using silver paste. The silver paste was manually applied.

Since the distance between the contact pads was only about 300 µm it was important that the paste had a high viscosity so that it would not spread on the surface and cause short circuits. Out of a number of silver pastes that were investigated, Namics H9807 (Namics, Japan) proved to give the best results. The paste was cured in an oven at 80°C for 2 h or at room temperature overnight. This method was very fast and flexible and resulted in a yield of 100 % even when the surfaces of the contact pads had visible SU-8 residues. The contact resistance was less than 10 Ω.

The silver paste interconnection method could also be applied to the Si Cantion chips and resulted in equally good results. Although the method is currently not suitable for large scale production it could be imagined that an automatic dispensing system could be used in the future.

4.4 Flip chip bonding

The flip chip bonding technique was introduced in the 1960's by IBM as an alternative to wire bonding. When using flip chip bonding, the chip is placed with the contact pads facing towards the printed circuit board, see Figure 4.6.

The electrical interconnection is established by bump structures on the con-

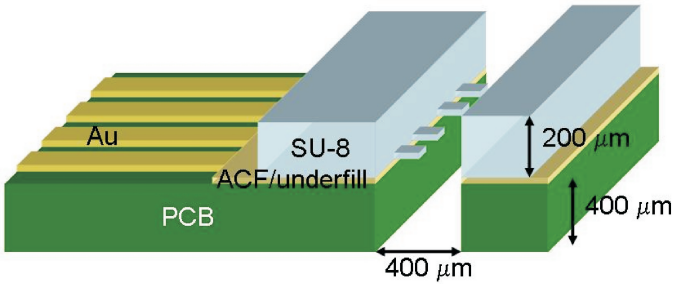

Figure 4.6: When the SU-8 cantilever chip was electrically interconnected using ACF or underfill the contact pads and the cantilevers were facing down towards the PCB. To allow for a microchannel under the cantilevers a channel was micromilled in the PCB.

tact pads on the chip. Here, Au bumps were used but solder and polymeric bumps can also be used. Flip chip bonding offers good electrical performance due to the short signal path and a high interconnection density. Furthermore, this interconnection method is compact and robust since all the interconnection sites are protected between the chip and the PCB [84].

Figure 4.7: SEM image of two bumps that were placed on a conductor on the PCB. The bumps have been coined using the fine placer.

4.4.1 Flip chip bonding using isotropic conductive glue and an underfill

Two bumps were made on each contact pad to increase the chances of electrical interconnection and to increase the support of the chip. The bumps were made by Inger Ninna Hansen at DELTA using a technique which is similar to ball-wedge bonding. The height of the bumps was about 50 μm and the diameter about 70 μm. A fine placer (Omni Bonder Model 860, Semiconductor Equipment Corp.) at DELTA was used for the flip chip bonding. The fine placer had a vacuum tool that could lift the chips and a camera to align the chip and the PCB. The bumps on the chip were pressed against a flat surface, so that all the bumps got the same height. This process is called coining, see Figure 4.7. The bumps were coined using 10 grams/bump, cor-

responding to a pressure of about 35 MPa, and were subsequently dipped in a well with conductive glue (Namics H9807), see Figure 4.8. The conductive glue was used to increase the chances of a good electrical interconnection.

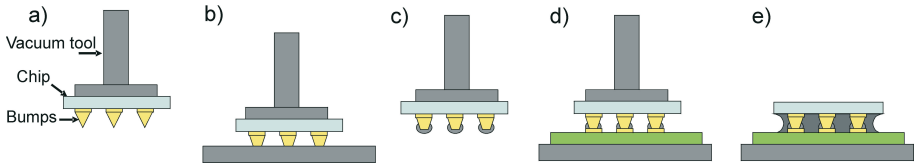

Figure 4.8: Schematic drawing of the flip chip bonding process. The chips were a) bumped, b) coined, c) dipped in conductive glue, d) bonded to the contact pads on the chip and e) the underfill was applied and cured.

The chip and the PCB were then aligned and electrical interconnection was established by pressing the chip against the conductors on the PCB using a pressure of 20-40 grams/bump (70-140 MPa). Afterwards, the conductive paste was cured in an oven at 120°C for 2 h followed by 2 h at 150°C. A nonconductive epoxy underfill (Namics 8422) was dispensed at the edges of the chip and the underfill was dragged in between the PCB and the chip by capillary forces. The underfill was used to increase the reliability of the bond and to compensate for the difference in the CTE between the chip, the PCB and the Au bumps. The FR-4 PCB, the underfill and the SU-8 had a CTE of 16 ppm/K, 20-25 ppm/K and 52 ppm/K, respectively. The underfill covered not only the area around the contact pads but the entire area under the chip except where the channel was placed. Thereby, the underfill could also be used as the sealing layer between the chip and the PCB, see Figure 4.9.

The major problem with the flip chip bonding process was that warpage of the SU-8 chips made it difficult to dip the bumps in the conductive glue without also covering the entire chip area with glue. Another issue was the process of adhering the Au bumps on the chips. Since the bumps were placed on the contact pads on the chip, the SU-8 residues on the contact pads, which were a problem for the wire bonding process, was still an issue. However, the bumps could also be placed on the conductors on the PCB instead of on the contact pads on the SU-8 chip. However, in this case it was not possible to dip the bumps in the conductive glue since the vacuum tool of the fine placer was not able hold the large PCB.

Despite the problems with the SU-8 residues and the process of dipping the bumps in the conductive glue, a few chips were interconnected using flip chip bonding. In order to investigate the quality of the electrical interconnects, a cut was made through an SU-8 chip on a PCB and the cut was imaged

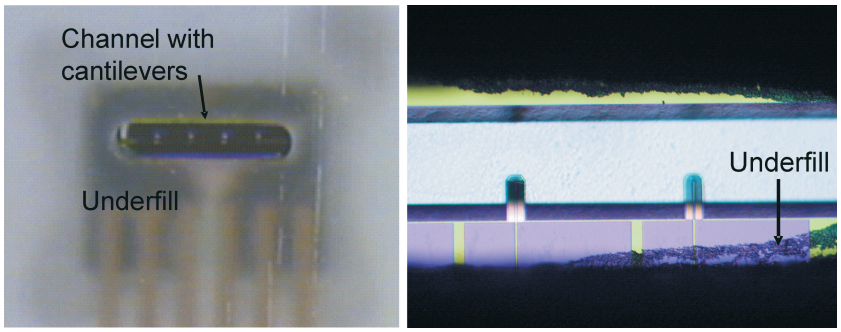

Figure 4.9: Flip chip bonding using the Si Cantion chip. The chip is seen through the backside of the PCB. Left: The underfill covered the area between the chip and the PCB but did not spread into the channel where the cantilevers were placed. The bright stripe parallel to the conductors was a sign that the underfill had not filled the entire area under the chip. Right: To avoid damage of the cantilevers, the channel in the PCB was made slightly larger than the channel in the chip, so that the underfill would stop before it reached the cantilevers.

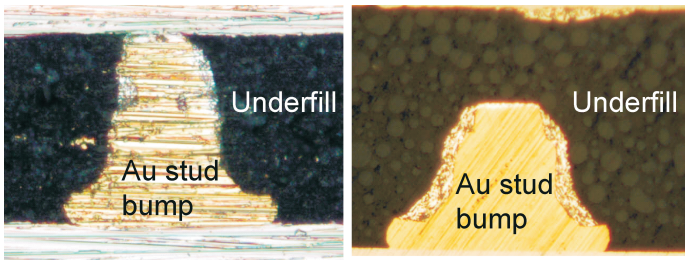

Figure 4.10: Microscope image of a cut through the bumps between the SU-8 chip and PCB after flip chip bonding using an underfill. Left: Electrical interconnection was formed when the bump was in contact with the wires on the PCB. Right: Unfortunately, most of the time the underfill lifted the chip from the PCB and damaged the interconnection.

in a Scanning Electron Microscope (SEM). Figure 4.10 (left) shows a bump on the SU-8 chip in contact with the PCB metallization. However, most contact pads had no electrical connection to the PCB. The reason was that due to capillary forces, the underfill had moved in between the bump and the PCB, see Figure 4.10 (right). For this reason, electrical interconnection was not achieved to a single resistor. Most likely, the bumps did not adhere well to the contact pads on the PCB and when the underfill was applied it simply lifted the chip from the PCB. Flip chip bonding using underfill was repeated several times for the SU-8 chips using varying conditions before it was finally concluded that it was not a successful method.

When the Si Cantion chips were flip chip bonded, a robust electrical interconnection was achieved every time. The bumps on the Si Cantion chips could easily be dipped in the conductive glue. This demonstrated that the reason that an electrical interconnection could not be achieved to the SU-8

chip was due to the material properties of the SU-8.

4.4.2 Flip chip bonding using Anisotropic Conductive Film

Since the flip chip bonding process using an underfill was not successful, another flip chip method based on an Anisotropic Conductive Film (ACF) was investigated. By using a solid conducting film with conductive particles, the conductive glue and the underfill process could be avoided.

Anisotropic conductive films consist of a thermoset polymer matrix mixed with conducting particles such as Ni or Ni/Au-coated polymer balls [86][87], see Figure 4.11. The electrical interconnection is established through the bumps on the contact pads and the conducting particles that are trapped between the contact pads and the conductors on the PCB. The adhesive polymer matrix also protects the metallic contacts and provides a stable interconnection.

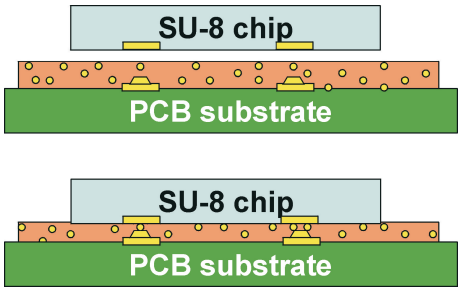

Figure 4.11: The ACF has conducting particles that contributes to the formation of an electrical interconnection between the chip and the PCB. The density of particles is low so that no electrical current will flow in the horizontal direction.

Here, a 30 µm thick ACF with Au coated polymer balls with a size of 5 µm and a particle concentration of 4500 pcs/mm^2 was used (TFA22000, Telephus, Korea). A non-conductive film (NCF) without any conductive particles was also tested using the same parameters as for the ACF. The ACF had a CTE of 68 ppm/K and was attached to a separator film to facilitate easy handling. A contact resistance of less than 0.1 Ω should be achievable using this film [88]. The Au bumps were placed on the PCB instead of on the SU-8 chips and the same coining procedure, as described above was used. The ACF was cut using a razor blade and was placed on a PCB with a micromilled channel. After a pre-cure at 80°C for 10 s, the film was slightly melted and a small channel corresponding to the one in the PCB was cut using tweezers and a razor blade, see Figure 4.12. Just as for the underfill, the film could also be used as a tight sealing layer between the chip and the PCB.

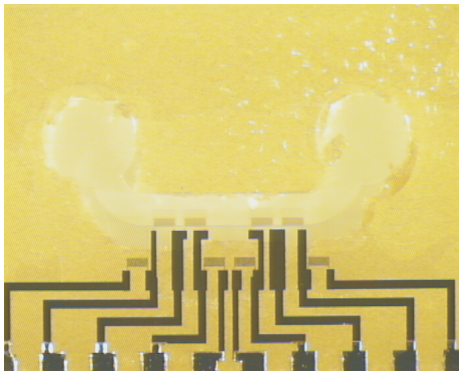

Figure 4.12: A channel having the same shape as the channel in the SU-8 chip was micromilled in the PCB. The ACF and NCF could be used both for electrical interconnection but also as the sealing layer around the channel. However, it was important that the hole in the film, to allow for the channel, was made large enough so that clogging would not be an issue. The channel in the film was cut using a razor blade which unfortunately also resulted in rough edges.

The SU-8 chip was then aligned to the PCB using the fine placer. According to the supplier, the ACF should be cured at 180°C for 20 s while applying a bonding pressure of 50-150 MPa. However, it was observed that at 200°C the cantilevers became slightly deformed and the contact pads fell off the chips due to thermal stress. These effects were not observed at 150°C. Hence, the chips were flip chip bonded both at 180°C but also at either 110°C or 133°C to investigate if the temperature had any influence on the chip and on the flip chip process. When using low temperatures, the bonding times were extended to cure the film properly. The tested bonding times and temperatures as well as the resulting yield for a bonding pressure of 50 grams/bump (175 MPa) can be seen in Table 4.1.

Time [s]	Temperature [°C]	Yield [%]
80	110	65
20-80	133	75
20	180	80

Table 4.1: The table shows the bonding time, temperature and yield for a coining pressure of 10 grams/bump and a bonding pressure of 50 grams/bump. Varying the bonding time between 20 s and 80 s, when using a bonding temperature of 133°C, did not influence the yield. The highest yield was obtained when using a bonding temperature of 180°C.

Since the contact pads were facing towards the substrate it was not possible to directly measure the resistance between each contact pad on the chips and the conductors on the PCB. Instead, the number of successful

interconnected contact pads was found by measuring the resistances of each integrated Au resistor by placing probes on the PCB after bonding. If there was no electrical connection to the integrated resistor it was assumed that at least one of the contact pads was not interconnected to the PCB. The yield was estimated from analysis of 30 chips in total and determined within 48 h after flip chip bonding. The highest yield (80 %) was obtained when the film was cured at 180°C for 20 s, which corresponds to the parameters obtained from the supplier. When using a bonding temperature of 133°C the yield was slightly lower and increasing the bonding time from 20 s to 80 s did not have any significant influence on the yield. The contact resistance was found to be less than 2 Ω. Only a few chips were interconnected using the non-conducting film instead of the ACF. The yield was fond to be slightly lower when using the NCF compared to the ACF, indicating that the conductive particles contributed to the electrical interconnection.

Flip chip bonding of the Si Cantion chips using the ACF resulted in a good electrical interconnection with a yield of almost 100 % as long as the parameters in Table 4.1 were used. The tests using the Si Cantion chips were done in collaboration with Peter Schultz as part of a course at MIC.

4.4.3 Investigation of the ACF interconnection

To further investigate why the ACF interconnection yield was lower for the SU-8 chips than for the Si chips, a cut was made through the SU-8 chip and the PCB. This clearly showed that the bumps were in close contact with the contact pads, see Figure 4.13, which should give a robust electrical interconnection to all contact pads.

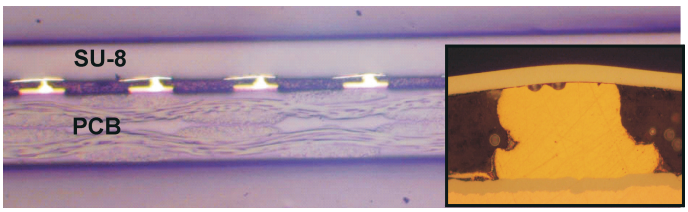

Figure 4.13: SEM image of a cut through the SU-8 chip and the PCB after ACF flip chip bonding. The bumps on the PCB were clearly in contact with the contact pads on the SU-8 chip. The inset shows a close up of a single bump and two conducting particles. The contact pad on the SU-8 chip was deflecting due to the pressure from the bump.

Some of the flip chip bonded SU-8 chips were also removed from the PCB and electrically characterized. It was found that some of the resistors had an infinitely large resistance. This suggested that the interconnection through the ACF was working and that it instead was the integrated Au resistors that had broken during flip chip bonding. Thus, the actual yield of the ACF

flip chip bonding was probably higher than 80 %. Although the SU-8 chip is transparent, it was not possible by visual inspection to determine where the damage had occurred. Normally, the cantilevers were not observe to bend due to the flip chip bonding process.

One cause of chip damage could be the application of pressure during flip chip bonding, breaking the Au resistors. The pressure might strain the Au and thereby create small fractures in the integrated resistor. In Figure 4.13, it is clearly observed that the contact pads were deformed after flip chip bonding. It is also possible that the connection between the Ni contact pad and the thin Au conductors was damaged due to the pressure. However, the yield was only 25 % when the bonding pressure was reduced to 40 grams/bump, indicating that it was not possible to reduce the pressure. SEM investigation verified that the Au bumps had the same height after coining which suggested that inhomogeneous distribution of pressure was not a problem.

Another reason why the resistors in the SU-8 chip were damaged during the bonding could be the temperature. The difference in CTE of Au and the SU-8 could result in damaged resistors in the chip. Furthermore, inhomogeneous crosslinking of the SU-8 could give rise to differences in the thermal properties of the SU-8. However, since the results were not improved by using a lower bonding temperature this is not likely to be the case.

In conclusion, achieving electrical interconnection proved to be significantly more difficult for the SU-8 chips compared to the Si Cantion chips. Wire bonding was not feasible with the tested chips, but it is likely that if chips with cleaner contact pads were used, the results would improve. Although flip chip bonding using an underfill did not prove successful, ACF flip chip bonding on the other hand, was fast and resulted in a very high yield with regard to electrical interconnection. However, due to damage to the chip, the maximum resulting yield was 80 %. The main difference between the SU-8 chips and the Si chips was that SU-8 is much softer having a Young's modulus of only 3.5 GPa compared to about 170 GPa for Si chip. Thus, when the SU-8 chip was pressed against the PCB it was not the Au bumps but instead the chip that was deformed which probably caused damage to the chip. The most reliable interconnection method was the silver paste gluing. Moreover, it was the fastest method and it did not require any equipment such as a fine placer. Hence, most of the presented measurements in this report were performed using chips that were electrically connected to a PCB using silver paste.

Chapter 5

Microfluidic system

In this chapter the design and fabrication of the microfluidic system for the SU-8 chip is described. The inlet and outlet system was fabricated in polymethyl methacrylate (PMMA) while polydimethylsiloxane (PDMS) was used for sealing. Both PDMS and PMMA are well-known materials for microfluidic systems. A micromilling machine was used for the fabrication of the microfluidic system. During the development of the system, I received invaluable advice from Gerardo Perozziello regarding micromilling and methods to solve fluidic interconnection problems.

For all the packaging systems that were tested for the SU-8 chip, a similar packaging system was fabricated for the Si chip supplied by Cantion A/S. It was thereby possible to compare the packaging process of a polymeric chip to a Si chip.

5.1 The initial idea: Microchannels in the PCB

As described in the previous chapter, electrical interconnection to the chip was achieved by interconnecting the chip to a PCB. To enable a very compact and easy to use system, it was initially investigated whether it was possible to combine the fluidic system with a PCB so that all the fluidic channels were integrated in the PCB, see Figure 5.1.

However, it was not possible to find a PCB supplier that had experience with microfluidic systems and that could fabricate such a board in a suitable material and for a reasonable prize. The alternative was to fabricate the system in-house using a polymeric material such as PMMA or Topas®. However, the drawback of using such a substrate for the PCB would be the low adhesion to metallic layers making wire bonding and flip chip bonding difficult. Furthermore, fabrication of a large number of such substrates would be very time consuming, especially if they could not be reused. Another important

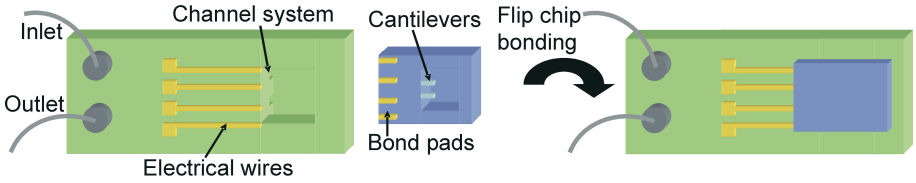

Figure 5.1: The initial idea was to integrate the microfluidic system in the printed circuit board that was used for electrical interconnection. Although such a fully integrated system would have a number of advantages it did not prove to be a feasible solution for the SU-8 cantilever chips.

drawback with this design was that it was impossible to get access to the cantilever surface after flip chip bonding in order to functionalize it with biological molecules.

Instead, it was decided to use a standard PCB for electrical interconnection and a separate system for the microfluidic system. It was thereby possible to reuse the microfluidic system.

5.2 Packaging designs

The microfluidic packaging system was designed so that it would be possible to use it for chips that were electrically interconnected to the PCB using both silver paste or the anisotropic conductive film (ACF) flip chip bonding. It should also be possible to use the system for SU-8 chips with and without an SU-8 lid, as described in Chapter 3. Since the chip was rather small and the separation between the contact pads and the microfluidic channel in the chip was only 1 mm, one of the challenges was to design a packaging system with a tight sealing.

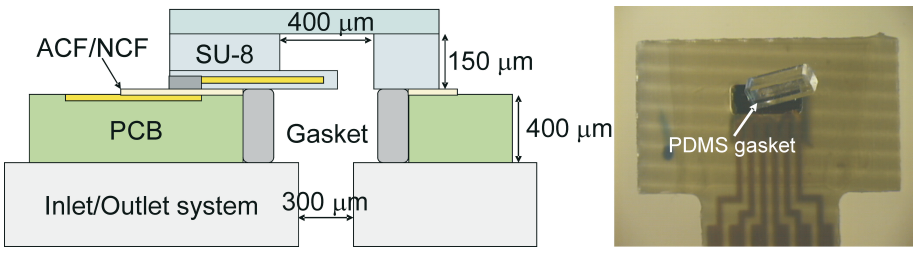

Figure 5.2: Left: Schematic image of the chip, the PCB and the microfluidic system. The channel was sealed using a small gasket. Right: The PDMS gasket before placing it in the micromilled channel in the PCB.

One of the most simple approaches would be to use the design shown in Figure 5.2 (left) where a chip with a lid was flip chip bonded to a PCB. To allow for a microfluidic channel, a hole was made through the PCB. To

avoid that the liquid would be in contact with the PCB and the ACF, a small gasket was fabricated in PDMS and placed in the channel of the PCB, see Figure 5.2 (right). However, leakage was often observed, especially for the Si Cantion chip since the gasket had to be very thin (about 300 µm) to fit into the channel. The problem was solved by combining the gasket with a thin sheet of PDMS that was placed between the PCB and the fluidic system, see Figure 5.3 (left) and (right). This made the gasket more stable.

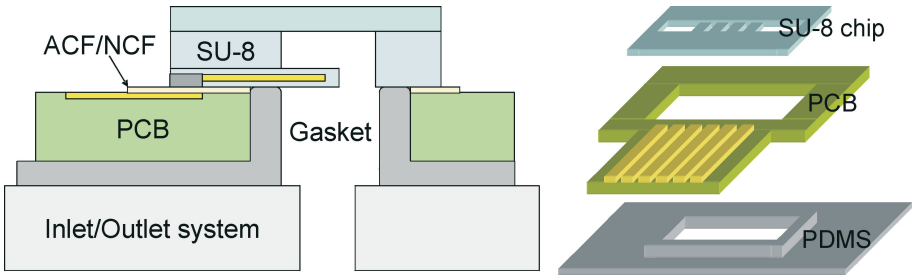

Figure 5.3: Schematic drawings of the large PDMS gasket. Left and right: By making the gasket and the sealing layer between the PCB and the microfluidic system as one part, a tight sealing was obtained.

It should also be possible to use the microfluidic system when the chips had no lid. In this case, the inlet and outlet system was placed on top of the chip and the PCB, while an additional thick PDMS gasket was used for sealing. The bottom side of the system consisted of a similar gasket to the one previously described and a PMMA plate to make it more rigid, see Figure 5.4 (left).

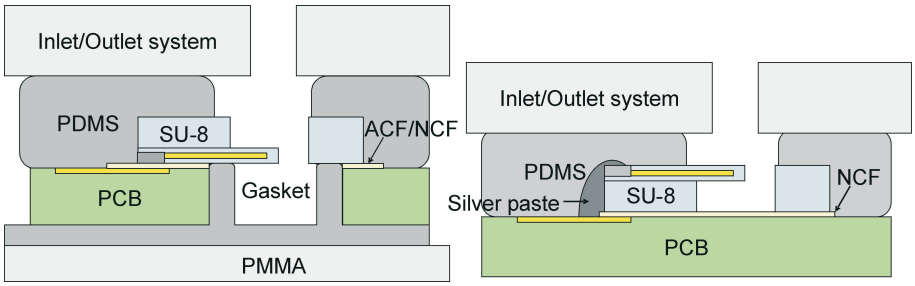

Figure 5.4: Left: Schematic drawing of the packaging system used for a flip chip bonded chip without a lid. Right: The packaging system for a chip without a lid that was interconnected using silver paste. This design was normally used for measurements in liquid. As seen in the image, the lower part of the channel walls was made from SU-8, while the part above the cantilevers was made from PDMS. Note that many of the packaging parts, were similar and could be used regardless of how the chips were electrically interconnected.

If instead, the chips were electrically interconnected using silver paste and

not flip chip bonding, the chips would have to turn upside down. This was achieved using the same inlet system but gluing the chip directly on a PCB (without a micromilled channel), see Figure 5.4 (right). The gluing could be done using the ACF, NCF (nonconductive film) or PDMS. Since this design was the most straightforward to assemble, it was used for most measurements presented in this thesis. This packaging design could be used for chips both with and without an SU-8 lid.

5.3 Fabrication by micromilling

Milling is a standard process on the macro scale, but is not as well-known for micromachining. However, the micromilling process can create trench-like features with vertical sidewalls and low roughness using tools with diameters down to a few tens of microns. Furthermore, micromilling is a flexible method for fast and inexpensive prototyping and allows for fabrication of three-dimensional structures [89][90]. Micromilling was used for several different applications in this project, such as

- Fabrication of a channel in the PCB by milling a trench or a hole
- Fabrication of an inlet and outlet system in PMMA
- Fabrication of molds in PMMA to be used for the PDMS gaskets

A micromilling machine (MicroMill 2000, MicroProto Systems, USA) with an air turbine motor that enabled velocities up to 30,000 rpm was used for the fabrication of the microfluidic system. Microtools having diameters of 300 µm, 400 µm and 1 mm (Micro End Mills, Performance Micro Tool, USA) were used. The designs were made using Dolphin 3D CAM software and the data were imported by the milling machine software.

Although it was difficult to obtain buried channels in the PCB, it was possible to drill holes or trenches. PCBs with holes could be obtained from many print suppliers but could also be fabricated at MIC using the micromilling machine. It was considerably easier to drill holes and trenches in FR-4 compared to ceramics due to the hardness of the ceramic material. This, in combination with the low cost, was the reason why FR-4 PCBs were used.

A number of different inlet and outlet systems were designed and implemented before an optimized design was achieved. The final version was fabricated by drilling two holes for inlet and outlet having a diameter of 300 µm through a 5 mm thick plate of PMMA. The connection for the silicone tubes were made by milling a circular trench around the inlet and outlet hole into which the tubes were attached. The silicone tubes (Reichelt Chemitechnik GmbH., Germany) could be easily and reversible assembled into the PMMA,

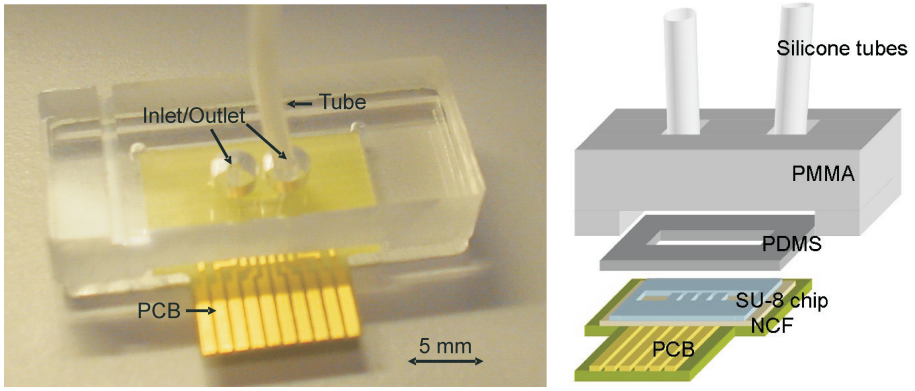

Figure 5.5: Left: The final version of the PMMA microfluidic inlet and outlet system. One silicone tube has been inserted. Right: Schematic drawing of all the packaging parts used for most of the measurements performed in liquid. In the drawing, the channel in the PDMS and in the chip has a rectangular shape. In reality, the channel had a rounded shape with a well in each end. It was also possible to fabricate a channel in the PDMS having the exact same shape as the channel in the chip.

see Figure 5.5 (left). As long as the tubes were inserted at least 2 mm into the PMMA, the connection was very reliable even though glue was not applied. On the opposite side of the PMMA plate, a recess with the same size as the PCB was milled. This recess allowed for easy alignment of the packaging parts, see Figure 5.5 (right). Finally, the plate was cut around the edges to a final size of about 10 mm by 20 mm using a saw or the micromilling machine. The PDMS was made by micromilling a mould in PMMA. The mould was filled with PDMS (Sylgard 184, Dow Corning) that was cured for 2 h at 80°C. The thickness of the PDMS gaskets were 200-600 µm.

All the packaging parts were fabricated in a few hours and design changes could relatively easily be made and implemented. The idea was that the SU-8 chip, together with the PCB and the PDMS, were disposable parts while the PMMA could be reused. The packaging system has been presented elsewhere [91]. There was no significant difference between the fluidic system developed for the SU-8 chip compared to the fluidic systems which were made for the Si Cantion chip. The only significant difference was that the SU-8 chip was slightly larger which made it easier to fabricate and assemble the parts.

5.4 Clamping and sealing

The PMMA housing, the PDMS gasket and the SU-8 chip could be clamped or screwed together. Figure 5.6 shows examples of fabricated systems that were sealed using either screws, two plastic clamps or a metallic holder in

which the system was inserted. The advantage with the metallic holder was that it was small and easy to use. However, to properly seal the channel it required that the fluidic system fitted perfectly into the holder. The screws also offered a compact system but were quite time consuming to assemble and were sensitive to wear. The plastic clamps were the most straightforward method and were used for the surface stress measurements in liquid.

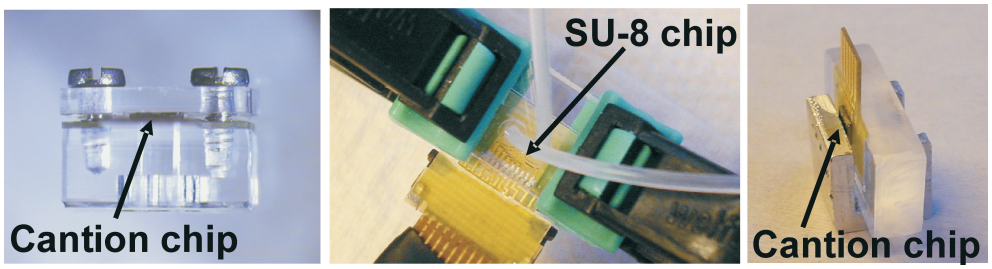

Figure 5.6: Optical images of the microfluidic systems fabricated for the SU-8 chip and for the Si Cantion chip. The microsystems were sealed by using screws (left), plastic clamps (middle) or a metal holder (right).

The microfluidic systems and the clamping methods were characterized by pumping liquid through the system at a pump rate of 10-100 μL/min. In general, for both the SU-8 chips and the Si Cantion chips, leakage was rarely observed. In case of leakage, the system was reassembled and the problem was normally solved.

It was also investigated how the flip chip bonding interconnections were influenced by immersion in water. In principle, the PDMS gasket should protect the ACF but if the film absorb liquid it might swell, which could damage the electrical interconnection, see Figure 5.3. According to the supplier, the moisture adsorption of the ACF was 2.0 wt% but information about how the film reacted in direct contact with liquid for a long time was nonexistent [88]. A few ACF interconnected SU-8 chips were immersed in liquid for two days. However, no change in the electrical resistance was observed which indicated that the film did not swell and break the interconnection.

5.5 Contamination from the packaging process

To immobilize molecules on the cantilever surface it is very important that the surface is clean. Since the Au coating was deposited as the last step of the fabrication process (except for the lid bonding) the chemical treatments during processing should not influence the Au surface. However, since the chip was electrically interconnected after the Au was deposited it is likely

that the materials used for the packaging, such as the underfill and the silver paste, could contaminate the surface. The silver paste was applied about 1 mm from the cantilevers while the ACF was placed only a few hundred microns from the cantilevers. Another source of contamination was the materials used for the microfluidic system such as PMMA and PDMS. Furthermore, it is important that the materials do not dissolve into the liquid in the channel or release any toxic chemicals.

The last part of this chapter deals with investigations of possible contamination from PDMS as well as from the anisotropic and the nonconductive films.

5.5.1 ACF and NCF for liquid systems

The ACF or NCF, used for attaching the chips to the PCB, see Figure 5.4 (right), was in direct contact with the liquid in the microfluidic system. If the film was dissolving due to contact with the liquid or releasing toxic chemicals, it might contaminate the liquid in the system. Thus, pieces of cured ACF and NCF were placed in flasks with HeLa cells in cell-medium and were left for three days in a 35°C environment to promote cell growth. The cells were obtained from Michael Stangegaard at MIC. The results were compared to a reference flask without any ACF or NCF.

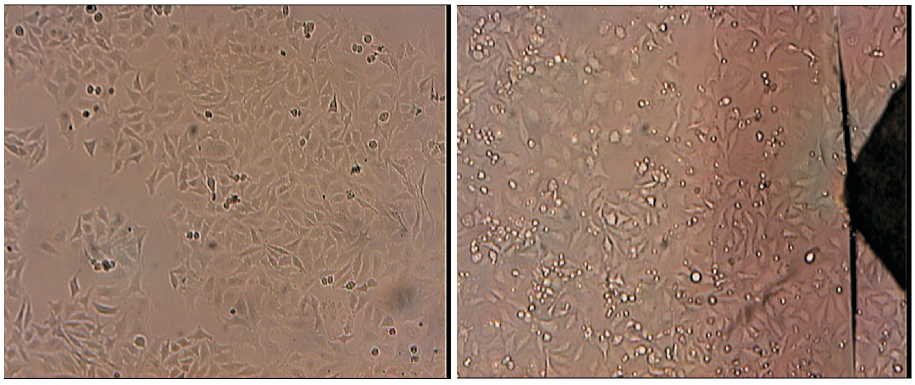

Figure 5.7: Left: Cells in reference flask after three days. Right: Cells in flask with ACF sample. No significant difference was observed.

Most of the cells in the flasks with the ACF or NCF were found to be viable after three days. Although there were slightly more viable cells in the reference flask the difference was not significant. Figure 5.7 (left) shows an image of the cells in the reference flask while Figure 5.7 (right) shows the cells in the flask with the ACF. The test indicated that the ACF was not directly toxic to the cells and that the microfluidic system could probably be used for cell analysis [77]. For comparison, a test was also made where

a PCB was immersed in the cell solution for one day. In this case, the cells were clearly affected and were not observed to be viable. The reason was most likely that the conductors on the PCB contained Cu. To fully establish the biocompatibility of the ACF film more tests should be performed where the number of cells should be counted.

5.5.2 Contamination by PDMS

Silicone based materials are known to contaminate surrounding surfaces [92]. PDMS is the most widely used silicone and it is used extensively within microtechnology, due to its many favorable properties such as low cost, good sealing properties, highly flexible structure and biocompatibility [93]. The contamination is caused by noncrosslinked low-molecular weight components that migrate from the from the bulk to the surface of the PDMS. The molecules continue to spread from the surface by evaporation of volatile compounds or by a process known as creep. Contact angle measurements were done to study the contamination by PDMS. Similar studies of creep by PDMS have previously been published [92][94].

Contact angle measurements can be used to quantitatively reveal surface modifications with monolayer sensitivity and are fast and easy to perform compared to other methods for surface analysis such as x-ray photoelectron spectroscopy (XPS) or time-of-flight secondary-ion mass spectroscopy (TOF-SIMS). The contact angle is determined by placing a droplet of water on the surface and measure the angle between the baseline and the tangent to the drop at the interface, see Figure 5.8.

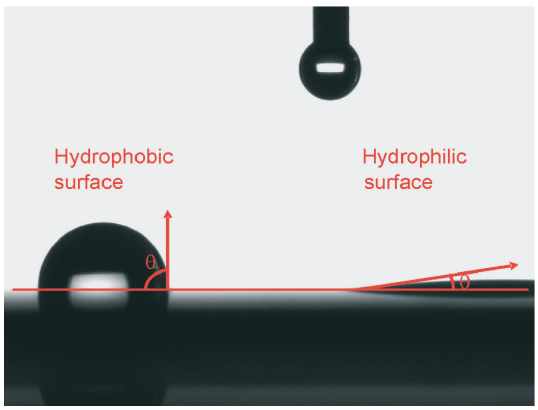

Figure 5.8: The right droplet was placed on a clean Si surface while the left droplet was placed in an area that was contaminated by PDMS. The contaminated surface was hydrophobic while the clean surface was hydrophilic.

By measuring the contact angle, the wetting and adhesion properties of a

surface can be determined. On hydrophilic surfaces the water droplet will spread and the contact angle is below 90° while on hydrophobic surfaces the contact angle is above 90°. Superhydrophobic surfaces can have contact angles up to 180°. By measuring the contact angle using liquids with known surface tensions, the surface free energy can be determined.

Here, the contact angle measurements were performed using a contact angle meter (DSA 10, Krüss GmBH) having an automatic dispensing system and a drop shape analysis software. Only deionized water (DI) was used for the presented measurements.

Si surfaces were used to investigate how the contact angle changed due to PDMS contamination. Two types of tests were prepared - Si samples in air and Si samples in MilliQ water. Si wafers were cleaned in UV/ozone for 10 min and diced into 1.5 mm by 1.5 mm sample pieces. The UV/ozone treatment is described in more detail in Chapter 7. The Si samples were placed on a thin layer of PDMS (Sylgard 184, Dow Corning) that had been cured for 2 h at 80°C, see Figure 5.9. The samples and the PDMS were stored in a closed single wafer tray made from polypropylene (Entegris). Reference samples were also prepared and the samples were placed directly into a tray without any PDMS.

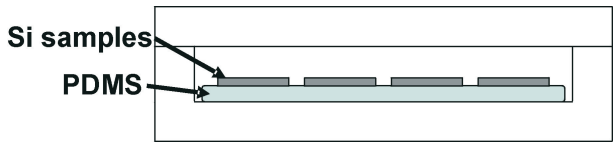

Figure 5.9: Clean Si samples were placed on a cured piece of PDMS in a closed single wafer tray. To perform a contact angle measurement, the lid was opened and a Si sample was quickly removed. The contact angle was measured on the top side of the Si sample and not on the side that had been in direct contact with the PDMS.

The UV/ozone treated Si surfaces were hydrophilic with a contact angle of about 5° which indicated that the surfaces were clean. The contact angle was measured by opening the tray and quickly removing one sample to avoid air contamination of the rest of the samples. The contact angle was measured on the top side of the sample which had not been in direct contact with the PDMS. Once the contact angle had been measured, the sample was discarded.

The contact angle of the samples that had been stored with the PDMS in air, was observed to increase rapidly over a few days and after about three weeks the contact angle had stabilized at a value of about 75°, see Figure 5.10 (left). Similar measurements have been presented by Lo et al.

and the results correspond very well, as seen in the graph [95]. The reference samples showed a much slower increase of the contact angle, which only reached about 20° after about three weeks. The increased contact angle was probably due to hydrocarbon contaminations from the air.

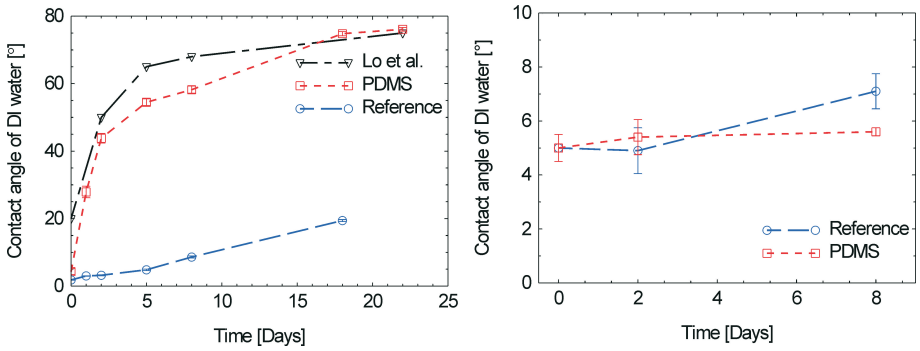

Figure 5.10: Left: The contact angle measurements clearly identified PDMS contamination on the surface of the Si samples that had been placed on the PDMS and stored in air. After a few days the surface coverage started to saturate. The results obtained by Lo et al. are also shown in the graph [95]. Right: Corresponding measurements using samples stored in a liquid environment. No significant difference in contact angle was observed between the Si samples that had been placed on the PDMS compared to the reference samples. This indicated that there was no contamination from PDMS in liquid.

However, for the samples that had been stored in liquid the contact angle was not observed to increase. After eight days the contact angle was still about 5° on both the samples placed on PDMS and the reference samples, see Figure 5.10 (right).

The results indicate that PDMS contamination only occur in air and not in liquid. The results can be explained by assuming that the molecular adsorption is depending on the surface free energy of the surface, where the adsorption is higher on surfaces with large surface energy compared to low surface energy. In liquid, it is the interfacial energy between the surface and the liquid rather than the surface free energy that has to be considered. For metals, the interfacial energy is lower than the surface free energy and thus, the PDMS is more likely to creep in air than in liquid [96].

To investigate if PDMS dissolves in water, a piece of cured PDMS was placed in a syringe filled with MilliQ water. After one week, a clean Si surface was covered by the water from the syringe and the Si surface was placed on a hotplate to quickly let the water evaporate, see Figure 5.11. Afterwards, the contact angle of the Si surface was measured. The test was repeated for water that had been in a syringe without PDMS. While the contact angle of the reference Si surface did not change (about 3.5°), the contact angle of the Si

surface that had been covered by the PDMS contaminated water had a contact angle of 47°. This clearly indicated that the PDMS had dissolved into the water. This could be a problem since it might influence the biochemical measurements. However, for the presented microsystem, the SU-8 chip and the PDMS were only assembled while measuring. Between measurements, the microfluidic system and the SU-8 chips were stored separately.

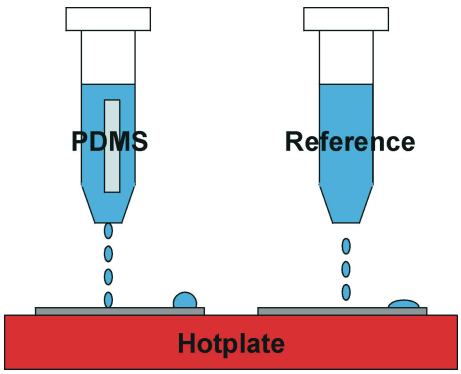

Figure 5.11: Schematic image of two syringes - one contained a cured piece of PDMS in water while the other contained only water. The water that had been in contact with PDMS for one week was observed to contaminate Si surfaces which indicated that the PDMS dissolved in water.

In conclusion, microsystems with inlet and outlet channels have been designed and fabricated using micromilling. By exchanging the PDMS gaskets, the system could be used for both flip chip bonded chips as well as silver paste interconnected chips. Moreover, it could also be used for SU-8 and Si chips both with and without a lid. Leakage was rarely observed to be a problem. Although the ACF and NCF did not seem to adsorb enough water to damage the interconnection and the films were not observed to be toxic to cells, it is still possible that the packaging materials might contaminate the surfaces of the chip. The PDMS was found to contaminate surrounding surfaces when left in air and was observed to dissolve in water. Since surface contamination is a very important issue for microsystems and cantilever based biosensors it should be further investigated.

Chapter 6

Characterization of the chips

Before the cantilevers were used for biological measurements in liquid, the chips were characterized in air. The resistances and the gauge factors of the resistors were measured. These parameters could give an indication of chip to chip variations and the reproducibility from batch to batch. The resonant frequency of the cantilevers was also measured and the results were compared to theoretical calculations. Finally, the temperature sensitivity of the chips was characterized. This was done to get a better understanding of how the chips reacted to fluctuations in the ambient temperature and to estimate the self-heating of the cantilever due to the applied voltage.

6.1 Electronic measurement setup

The results presented in this chapter involve characterization of single cantilever resistors and resistors connected in Wheatstone bridge configurations. The measurement setup used for the Wheatstone bridge configuration consisted of a lock-in amplifier (SR830, Stanford Research System), a laptop computer, a shielded box with two SMD resistors and an FFC connector (Deltron Conelec) where the chips could be plugged in, see Figure 6.1.

The lock-in amplifier was used to amplify the signal and to filter out the noise components at other frequencies than that of the applied frequency. Unless otherwise stated the input voltage, which was set on the lock-in amplifier, was V_{in}=0.5 V, the frequency was f_{in}=3 kHz and the time constant was T_{in}=300 ms. The output signal was obtained from the A and B ports on the lock-in amplifier and the output voltage and the phase were recorded via a GPIB interface to a Labview program run on the laptop. The Labview program was obtained from Rodolphe Marie.

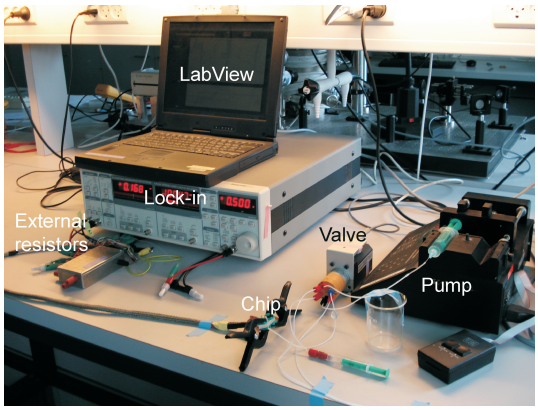

Figure 6.1: The electronic setup used for the Wheatstone bridge measurements included an FFC cable where the chip was attached, a box with SMD resistors, a lock-in amplifier and a laptop computer. The pump and the valve were used for measurements in liquid.

6.1.1 Wheatstone bridge configuration

To minimize noise, drift and temperature effects, the resistor in the measuring cantilever was connected to a resistor in a reference cantilever and with two external SMD resistors in a Wheatstone bridge configuration, see Figure 6.2.

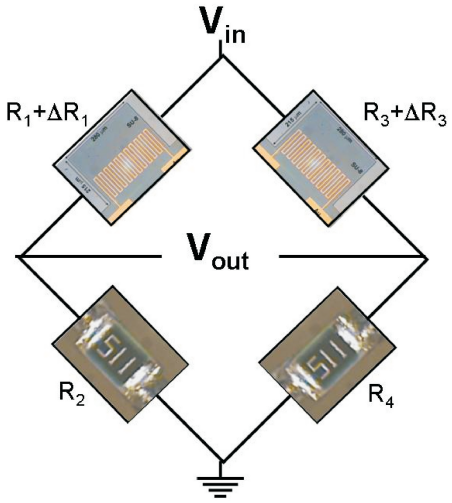

Figure 6.2: Two cantilever resistors and two SMD resistors were connected in a Wheatstone bridge configuration. All four resistors were assumed to have approximately the same resistance.

The Wheatstone bridge configuration converted the resistance change to a change in output voltage. The resistances of the SMD resistors were assumed to be constant while measuring. The output voltage change, ΔV_{out}, can be

described as

$$\Delta V_{out} = (\frac{R_2}{R_1 + R_2 + \Delta R_1} - \frac{R_4}{R_3 + R_4 + \Delta R_3})V_{in} \quad (6.1)$$

where R_1 and R_3 are the resistances of the two cantilever resistors, R_2 and R_4 are the resistances of the two SMD resistors, ΔR_1 is the resistance change of the measuring resistor and ΔR_3 is the resistance change of the reference resistor. The cantilever resistors are assumed to have approximately the same resistances, $R_1 \simeq R_3$ and the SMD resistors are also assumed to have the same resistances, $R_2 \simeq R_4$. Hence,

$$\Delta V_{out} \simeq \frac{R_2}{(R_2 + R_1)^2}(\Delta R_3 - \Delta R_1)V_{in} \quad (6.2)$$

If the resistances of the SMD resistors and the cantilever resistors are assumed to be approximately the same, $R_1 \simeq R_2 = R$, and if $\Delta R = \Delta R_3 - \Delta R_1$ the output voltage change becomes

$$\Delta V_{out} = \frac{1}{4}\frac{\Delta R}{R}V_{in} \quad (6.3)$$

Since the SMD resistors that were normally used have a resistance of 511 Ω compared to about 500 Ω for the cantilever resistors this approximation was assumed to be valid.

6.2 Resistance and resistivity

The resistances of the integrated resistors were measured for each new batch of chips. The thickness of the Au layer for the resistors was varied between 75 Å and 800 Å but was normally 600 Å which resulted in a resistance of about 500 Ω. Usually, the resistances of the four cantilever resistors on each chip did not differ with more than about 1-2%. The measured resistances as a function of the Au thickness, t, are plotted in Figure 6.3 (left) together with the theoretically estimated results assuming that the resistivity, ρ, of the Au is $2.2 \cdot 10^{-8}$ Ωm and $R = \rho(l/wt)$, where l is the resistor length and w is the width.

The total length of the meander-shaped resistor is about 2.3 mm and the width is 4 μm. The resistivity was calculated and was plotted as a function of the Au thickness, see Figure 6.3 (right). As the Au thickness decreased the resistivity was observed to increase. When the Au thickness was 75 Å the measured resistivity was almost five times larger than expected. The reason was probably that surface roughness and surface scattering started to influence the resistivity. The relationship between the resistivity and the thickness was observed to be $\rho \sim t^{-\alpha}$, where α was found to be about 0.7 from

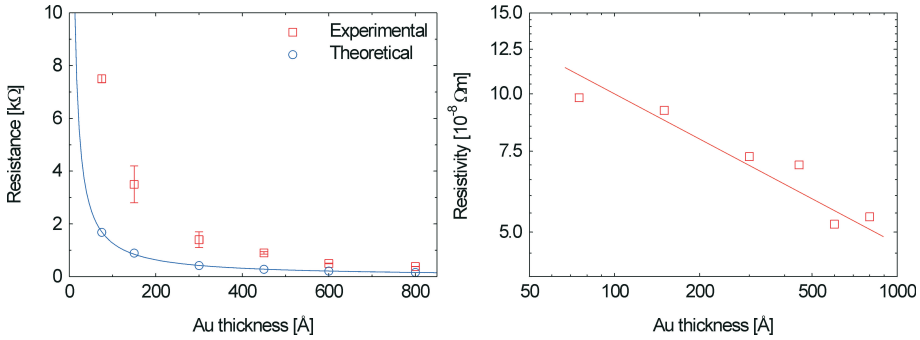

Figure 6.3: Left: The theoretical and the measured resistances for different Au thickness of the piezoresistors. Right: As the Au layer becomes thinner, the resistivity was observed to increase.

the slope in Figure 6.3 (right). Hence, the assumption that ρ=constant/t, used for the calculation of the intermediate gauge factor in Chapter 2, was observed to be in rather good agreement with the measured resistivity.

6.3 Spring constant and resonant frequency

The spring constant, k, and the resonance frequency, f_{res}, are two of the fundamental mechanical properties of a cantilever. The cantilever considered here has a length L, a width W and a thickness H and is assumed to consist of a single SU-8 layer. The spring constant of a cantilever is found from Hooke's law F=-kz, where z is the deflection of the cantilever caused by an applied force, F, at the apex of the cantilever, see Figure 6.4. The derivation is only valid when the deflection is small compared to the length of the cantilever.

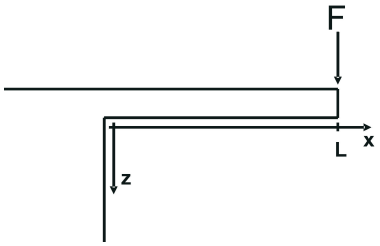

Figure 6.4: Schematic image of a point-force acting on the cantilever.

The spring constant of a cantilever can be calculated from [46]

$$k = \frac{3EI}{L^3} \tag{6.4}$$

where E is Young's modulus and I is the cross sectional area moment of inertia which is $I{=}WH^3/12$ for a rectangular cantilever. The resonance frequency for the fundamental mode of the cantilever is [50]

$$f_{res} = 0.3231\sqrt{\frac{k}{m}} \tag{6.5}$$

where m is the mass of the cantilever. For the SU-8 cantilever where L=215 µm, W=280 µm, and H=3.5 µm, the spring constant and the resonant frequency are

$$k{=}1.1 \text{ N/m} \quad \text{and} \quad f_{res}{=}21 \text{ kHz}$$

The values are obtained by assuming that E_{SU8}=3.5 GPa and the density of SU-8 is 1200 kg/m^3. The contribution from the resistor is assumed to be negligible.

The resonant frequency was measured by inserting the chips in an AFM. The measurements were done by the help of Zachary Davis. To get a strong reflection from the laser beam in the AFM, the cantilever was coated with 200 Å of Au. Resonant peaks were observed both at 24.5 kHz and at 25.7 kHz, see Figure 6.5. The double peak was probably due to coupling between the cantilevers. The reason could be misalignment of the channel wall structure so that the clamping of the cantilevers was shifted away from the base of the cantilever. Two cantilevers on the same chip were used for the measurements and the results were found to be highly reproducible. The reason that the resonant frequency was slightly larger than expected was probably due to the Au coating on the cantilever which was not included in the calculation. The Q-factor, $Q{=}f_{res}/\Delta f$, was about 20 which is comparable to previously presented results using SU-8 cantilevers in air [97].

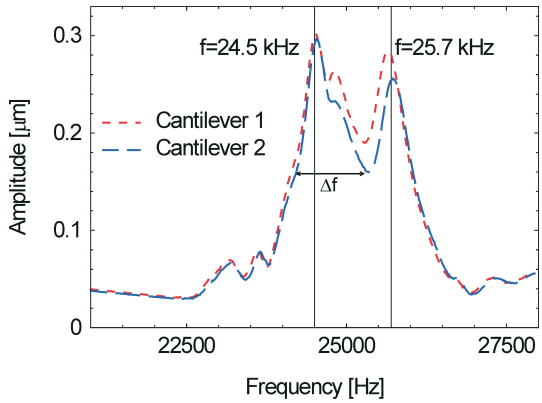

Figure 6.5: The resonant frequency of the SU-8 cantilever was measured in an AFM. The double peak was probably due to coupling between the two cantilevers.

6.4 Gauge factor

The gauge factor is a measure for the sensitivity of the piezoresistor to strain and was theoretically estimated in Chapter 2. The gauge factor can experimentally be determined by measuring the resistance change as a function of the deflection of the cantilever. Only a bending of the cantilever is assumed and any elongation is assumed to be negligible. If the force is acting at the apex of the cantilever, the resistance change per unit length, or the deflection sensitivity is [50]

$$\frac{\Delta R}{R} z^{-1} = \frac{k(L - \frac{\lambda}{2})d}{EI} K \tag{6.6}$$

where λ is the length of the resistor, d is the distance from the neutral plane to the resistor and K is the gauge factor.

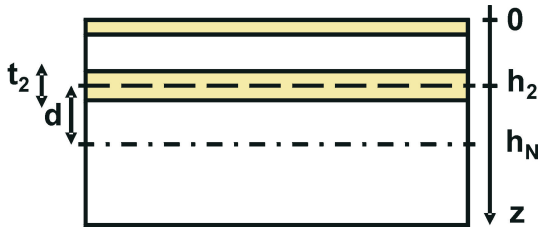

Figure 6.6: Schematic cross section of the cantilever with a top Au coating and an embedded piezoresistor. t_2 is the thickness of the piezoresistive layer and d is the distance from the neutral plane to the piezoresistor. h_N and h_2 are the positions of the neutral plane and the piezoresistive layer, respectively.

The neutral plane of the cantilever, h_N, is the position where there is no stress when the cantilever is deflecting. The neutral plane can be found from

$$h_N = \frac{\sum_i E_i h_i t_i}{\sum_i E_i t_i} \tag{6.7}$$

where h_i is the position, h_i=$(\sum_{j=0}^{i} t_j - \frac{t_i}{2})$, t_i is the thickness and E_i is the Young's modulus of the i'th layer, see Figure 6.6. For the SU-8 cantilever, with and without Au coating, the distance from the resistor to the neutral plane was about 0.5 µm and 0.7 µm, respectively. The length of the resistor was 100 µm.

To measure the gauge factor, a probe was placed at the apex of the cantilevers by using a probe station. The probe was moved down in steps of about 5 µm while the resistance was measured. As mentioned in Chapter 2, the measured gauge factor is expected to be the same for an applied point force as for a isotropic surface stress. However, for a beam cantilever the

values differ slightly.

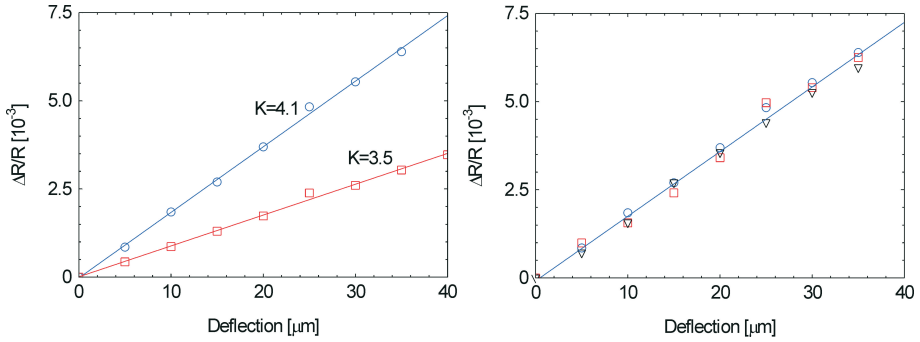

Figure 6.7: Left: The graph shows two gauge factor measurements using two cantilevers from different batches. The gauge factors were found to be 3.5 and 4.1. Right: The gauge factor was measured three times for the same chip and the reproducibility was found to be very high.

The gauge factor was measured using cantilever resistors from four different wafers. Figure 6.7 (left) shows typical measurements for two resistors where the cantilevers had slightly different thicknesses. From the slope, the gauge factors from these measurements were found to be 3.5 and 4.1. The average gauge factor calculated from all measurements was 3.7. This is in very good agreement with the theoretical gauge factor of 3.7 which was found in Chapter 2 for resistors were surface scattering was not assumed to influence the gauge factor. However, since the intermediate range gauge factor was only slightly lower (2.4) these results could not be used to conclude that surface scattering was not influencing the gauge factor for the 600 Å resistors.

The gauge factor measurement could be repeated several times using the same cantilever, without any signs of hysteresis, see Figure 6.7 (right). This indicated that the cantilevers were not plastically deformed by the probe. Moreover, the cantilevers were found to be highly flexible and could be deflected up to 100 μm without breaking the resistors or the cantilevers.

The gauge factor has been observed to depend on the thickness of the film layer and the applied strain. Li et al. observed that very large gauge factors, of up to 50, could be achieved for films below 100 Å if small strains were used (ϵ_x<3·10^{-5}). To investigate if the gauge factor would increase by using thinner Au layers, the gauge factor was also measured for cantilevers were the Au resistor thickness was only 75 Å. The gauge factor was measured both using the probe station as described above but also using a nanomanipulator setup. The nanomanipulator enabled strains on the order of 10^{-5} by moving the probe in steps of 0.1 μm. The gauge factor was measured for eight chips and was found to be about 5.1 for large strain regimes. Using

the nanomanipulator, only a single resistor was investigated and the gauge factor was found to be between 2 and 7. This was not a significant improvement compared to when cantilevers with 600 Å thick resistors were used. Hence, it did not seem that a significant increase in gauge factor could be achieved by using 75 Å Au layers compared to 600 Å or by decreasing the applied strains. The reason was probably that the 75 Å thick Au layer was not as discontinuous as reported by Li et al. Although it is possible that the gauge factor would increase by using even thinner films, the reproducibility is likely to be reduced when discontinuous films are used.

6.5 Noise

The inherent noise sources that influence the output voltage signal obtained from the lock-in amplifier are thermal and electrical noise. For piezoresistive cantilevers, the electrical noise has been estimated to be an order of magnitude larger than the thermal noise [98]. The electrical noise sources that are assumed to contribute is *Johnson noise* and *1/f-noise*. 1/f-noise is electrical noise that is dominating at small frequencies and has been described by Hooge et al. [99]. For the SU-8 cantilevers, it has been demonstrated that the 1/f-noise do not contribute for frequencies above f_{in}=1 kHz, which is well below the 3 kHz used here [43]. Moreover, due to the larger number of charge carriers in metals compared to Si, the 1/f-noise is assumed to be small compared to the 1/f-noise in Si. Hence, the Johnson noise was assumed to be the dominating noise source. The Johnson noise, V_J, is caused by thermal fluctuations of charge carriers and is described by

$$V_J = \sqrt{4k_B T R \Delta f} \tag{6.8}$$

where k_B is Boltzman's constant, T is the temperature, R is the resistance and Δf is the bandwidth. When using a lock-in amplifier, the equivalent noise band width (ENBW) determines the detection bandwidth, $\Delta f = ENBW$. $ENBW$ is determined by the time constant which was set on the lock-in amplifier, $ENBW = 5/(64\,T_{in})$, where T_{in} was normally 300 ms [100]. For a resistor with a resistance of R=500 Ω, the expected voltage noise was about 2 nV. Assuming that there was no self-heating of the cantilever due to the applied voltage, the resistance should be as small as possible to minimize the Johnson noise. However, the smaller the resistance the larger the dissipated power and thereby the self-heating.

As the resolution of the measurement signal was limited by the noise it is important to estimate the expected noise level to get an idea of the minimum detectable surface stress. Although the estimated Johnson noise was around 2 nV, the measured peak-to-peak output noise was larger. This could be due to external noise from the measurements setup and the surrounding

environment. The experimentally found noise level was about 0.05-1 μV for a resistor of 500 Ω using the electronic setup described above. However, when testchips based on two SMD resistors were used, instead of the two cantilever resistors, the noise level was generally lower than for the SU-8 chips. This indicated that the limiting factor was not the measurement setup but rather the noise level of the chip.

Assuming that the minimum detectable voltage, $\Delta V_{out,det}$, equals the voltage noise level, ΔV_{noise}, the minimum detectable surface stress change, σ_{det}, becomes,

$$\sigma_{det} \propto \frac{\Delta V_{out,det}}{V_{in}} = \frac{\Delta V_{noise}}{V_{in}} \tag{6.9}$$

To find the optimal signal to noise ratio it is important to maximize the V_{in} while maintaining a low noise level. In principle, the input voltage should be as high as its power dissipation abilities can tolerate. The peak-to-peak noise level was measured as a function of the input voltage using a Wheatstone bridge configuration. When the resistance was 500 Ω the signal to noise ratio was found to have its maximum at V_{in}=0.5 V while the maximum signal to noise ratio for resistors having a resistance of 7.5 kΩ was about V_{in}=1 V. In general, the measured noise level of the 7.5 kΩ resistors was about ten times lower than for the 500 Ω resistors using the same input voltage. The reason was most likely that the dissipated power was smaller. Hence, the sensitivity of the cantilevers could be significantly increased by increasing the resistance of the piezoresistor.

6.6 Temperature effects

The last part of this chapter deals with temperature effects of the cantilever. Temperature fluctuations can result in unwanted output signals which might influence the signal due to the detection of biomolecules. Hence, the temperature sensitivity of the resistances was estimated and the bending of the cantilevers due to temperature variations was measured. Temperature changes can be minimized by working in a temperature controlled environment. However, since such a setup was not available for this project it was necessary to understand how the chips reacted to variations in temperature.

It was also investigated how the input voltage influenced the cantilevers in terms of plastic deformation and increase of temperature. If the surface of the cantilever was heated due to the input voltage, it might influence molecular interactions with the surface. Some of the obtained results have been presented elsewhere [101].

6.6.1 Bimorph and TCR-effect

Au coated cantilevers for optical and piezoresistive readout are sensitive to temperature changes due to the bimorph effect which makes the cantilever bend. The bimorph effect is caused by the difference in coefficients of thermal expansion (CTE) of the materials in the cantilever. Bimorph microprobes using SU-8 and metallic layers have previously been presented [102][103]. Assuming that the cantilever has two layers - the SU-8 and a 200 Å Au coating and neglecting the Au layer for the resistor, the deflection, z_B, of the free end of the cantilever due to the bimorph effect can be calculated from [104]

$$z_B = 3\Delta\alpha_B \Delta T \frac{(t_{Au}+t_{SU8})}{t_{SU8}^2\left(4+6\frac{t_{Au}}{t_{SU8}}+4\frac{t_{Au}^2}{t_{SU8}^2}+\frac{E_{Au}t_{Au}^3}{E_{SU8}t_{SU8}^3}+\frac{E_{SU8}t_{SU8}}{E_{Au}t_{Au}}\right)} \tag{6.10}$$

where $\Delta\alpha_B$ is the difference in thermal expansion for the two materials ($\Delta\alpha_B$=$\alpha_{B,SU8}$-$\alpha_{B,Au}$), ΔT is the temperature change t_{Au} is the thickness of the Au layer, t_{SU8} is the thickness of the SU-8 layer, E_{Au} is the Young's modulus of Au and E_{SU8} is the Young's modulus of SU-8. The expected resistance change can be estimated from the deflection (see Appendix C)

$$\frac{\Delta R}{R} = K\epsilon_x = \frac{2dKz_B}{L^2} \tag{6.11}$$

Assuming that $\alpha_{B,SU8}$ = 52 ppm/K, $\alpha_{B,Au}$ = 14.2 ppm/K, E_{Au}=78 GPa, E_{SU8}=3.5 GPa, d=0.5 µm and K=3.7, the bimorph contribution to the resistance change is $\Delta R/(R\Delta T)$=1.0·10^{-5}/K.

Cantilevers for optical readout are heated due to the laser beam that is reflected from the surface of the cantilever. Although this is not an issue here, cantilevers with piezoresistive readout are also sensitive to temperature changes due to the thermal coefficient of resistance (TCR) effect. Theoretically, the resistance of a material varies with the temperature as

$$\frac{\Delta R}{R} = \alpha_{TCR}\Delta T \tag{6.12}$$

where α_{TCR} is the temperature coefficient which is 3.3·10^{-3}/K for Au in the temperature range 0-100°C [105]. The TCR-effect is about ten times larger for a Au resistor compared to a Si based piezoresistor [3].

It is seen that the TCR-effect is about two orders of magnitude larger than the bimorph effect for the Au coated cantilever. While the TCR-effect increases the resistance, the bimorph effect bends the cantilever upward and thereby induces a compressive strain in the piezoresistor which to some extend compensates for the resistance increase caused by the CTE. The change

in resistance of a resistor in a Au coated cantilever and in an uncoated cantilever, as well as for an on-chip resistor was measured as a function of temperature, see Figure 6.8 (left). The measurements were done by placing the SU-8 chip on a Peltier element and slowly increasing the temperature from 24°C to 30°C while monitoring the resistance change.

From the slope of the curves the α_{TCR}-values were found to be $2.5{\cdot}10^{-3}$/K for both the Au coated and the uncoated cantilever resistors and $2.8{\cdot}10^{-3}$/K for the integrated on-chip resistors. The measured TCR-values were slightly smaller than expected. The on-chip resistors were found to have a different thermal behavior compared to the resistors in the cantilevers. A similar behavior has been observed for Si based cantilevers [3]. The bimorph effect from the Au coating was too small to be observed.

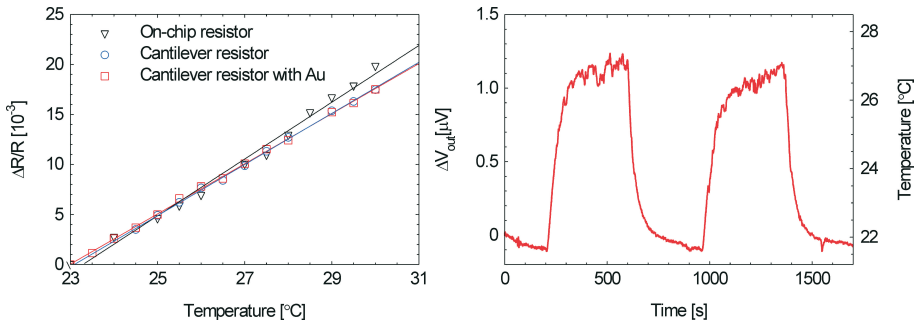

Figure 6.8: Left: The increase of the resistance was measured as a function of temperature for three different types of resistors. Right: The output voltage change from a Wheatstone bridge due to temperature changes.

Since the resistance of the Au resistors was sensitive to temperature changes, a reference cantilever should always be used when measuring surface stress changes. Ideally, all temperature effects should be cancelled out when two identical cantilever resistors were connected in a symmetrical Wheatstone bridge configuration. However, small differences between the resistors and between the cantilevers might result in changes in the output voltage if the temperature varies. Hence, the temperature measurements were repeated using Wheatstone bridge configurations. The temperature was cycled from about 22°C to 27°C and the results were recorded by a Labview program. To avoid self-heating of the resistors, a bridge input voltage of only 0.5 V was used.

If the measuring and the reference cantilevers were identical, the output voltage changed about 0.24 μV/K, see Figure 6.8 (right). Although the output voltage change should be zero, the measurements indicated that the difference in temperature sensitivity between the two cantilevers was small

and that they balanced each other well. Hence, although the individual Au resistors were very sensitive to temperature changes, most of the TCR effect could be balanced out by using a symmetrical Wheatstone bridge configuration.

When the reference cantilever was Au coated, the output voltage change was approximately 0.4 μV/K. This voltage change was due to differences in the resistors as well as cantilever deflections due to the bimorph effect. From Eq.(6.3) and Eq.(6.11), the expected output voltage change due to the bimorph effect was found to be 1.25 μV/K. Hence, the observed bimorph effect was slightly smaller than expected but still in rather good agreement with the theoretical results.

Since the bimorph effect appeared to be smaller than expected and comparable to the signal obtained from differences in the resistors, it should be possible to use a Au coated cantilever for measuring while using an uncoated cantilever as reference. This would allow for simple immobilization of thiolated biomolecules since binding would mainly occur on the Au and not on the SU-8 surface of the reference cantilever. Moreover, ambient temperature changes will normally occur slowly compared to surface stress changes due to binding of biomolecules. Hence, it should be possible to perform surface stress measurements without using a temperature controlled environment, as long as all the liquids used for the measurements would have the same temperature. However, when detecting very small surface stress changes, a temperature controlled environment might be required.

6.6.2 Plastic deformation

When a voltage is applied across the resistors, the cantilevers heat up. Due to the thermal mismatch between Au and SU-8, a thermal stress and cantilever bending is induced. If the voltage, and thus the temperature, is large the cantilevers will plastically deform, see Figure 6.9 (right). The deformation of the cantilever due to heating by the resistor was investigated by applying a voltage across the resistor and afterwards measuring the bending of the cantilever. The bending was measured by visual inspection using a microscope. The deflection caused by the applied power is plotted in Figure 6.9 (left). The maximum voltage that could be applied before plastic deformation occured was about 1.5 V for a resistor of 500 Ω corresponding to a power, P, of 4.5 mW, where $P = V_{in}^2/R$. For a resistor of 7.5 kΩ the maximum voltage was 3 V which corresponds to a power of 1.2 mW. It should be noted that single resistors and not Wheatstone bridge configurations were used for the measurements.

As the cantilevers started to plastically deform, the resistances also started

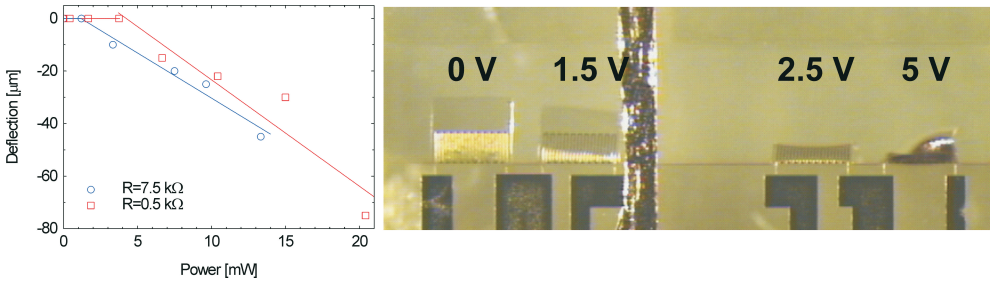

Figure 6.9: Left: The deflection of two cantilevers is plotted as a function of the applied power. One of the cantilever resistors had a resistance of 500 Ω while the other had a resistance of 7.5 kΩ. Right: A voltage of 0-5 V was applied over four 500 Ω resistors on the same chip. At around 1.5 V the cantilever started to deflect while at 5 V the cantilevers were completely melted.

to permanently change. However, the resistances of the on-chip resistors were also changing after applying a voltage. Since the on-chip resistors could not deflect, the increase of the resistance must be due to electromigration. Electromigration for Au can be expected for a current density of 1-2·10^6 A/cm^2 [42]. For an on-chip resistor of 500 Ω, the resistance change was observed around 3 V which corresponds to a current density of 1.4·10^6 A/cm^2.

6.6.3 Heating of the cantilever due to the applied voltage

If the cantilevers are going to be used for protein detection, it is important that the cantilever is not heated to more than 37°C to avoid damage of the protein structure. The binding strength between biotin and avidin has for example been demonstrated to be highly dependant on the temperature [106].

According to Eq.(6.3), the output voltage should increase linearly with the input voltage. However, the output voltage will also increase due to self-heating of the resistors. Two different Wheatstone bridge configurations were used to measure the relationship between the input voltage and the output voltage. An uncoated cantilever was always used as the measuring cantilever while the reference was either an uncoated cantilever or an external SMD resistor. The resistance of the external resistor was expected to be independent of temperature. Cantilever resistors of either 500 Ω or 7.5 kΩ were used. Figure 6.10 shows the output voltage as a function of the input voltage in the interval 0 V to 2 V. For the bridge configurations using two identical cantilever resistors, the relationship between the input and the output voltage was found to be slightly non-linear when using a 500 Ω resistor and completely linear when using 7.5 kΩ resistors. As expected, the bridge configuration with an external resistor as a reference was found to behave highly non-linear. The reason for the non-linear behavior was that

the resistance of the Au resistor was increasing due to self-heating. A curve with the expression $V_{out}{=}aV_{in}{+}bV_{in}^3$ was fitted to the results for the uncoated reference cantilever having a resistance of 500 Ω, while $V_{out}{=}bV_{in}^3$ was fitted to the results from the Wheatstone bridge configuration with the external SMD reference resistor.

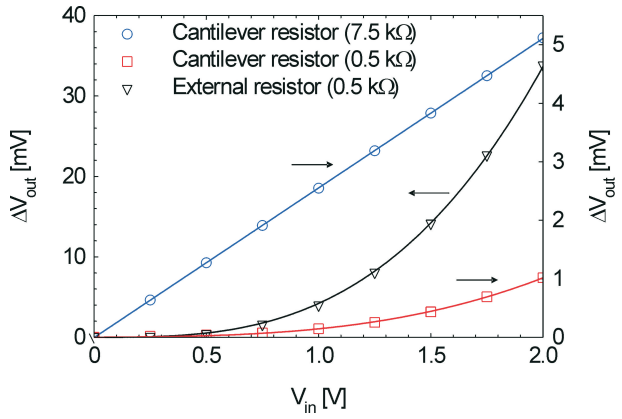

Figure 6.10: The graph shows the output voltage as a function of the input voltage for two different Wheatstone bridge configurations. The relationship was highly non-linear when an external resistor was used as a reference for a cantilever resistor. The non-linear behavior was due to self-heating. This was not observed when using resistances of 7.5 kΩ.

If the temperature change was only caused by the dissipated power and there was no change in the ambient temperature, the temperature increase could be related to the dissipated power through, $\Delta T{=}R_{TH}P$, where R_{TH} is the thermal resistance. If all the initial resistances in the Wheatstone bridge were assumed to be the equal, but the thermal resistances were different, the output voltage can be related to the input voltage by (see Appendix C)

$$\Delta V_{out} = \alpha_{TCR}\frac{\Delta R_{TH}}{16R}V_{in}^3 \tag{6.13}$$

where ΔR_{TH} is the difference in thermal resistance between the cantilever resistor and the reference resistor, $\Delta R_{TH}{=}R_{TH,CANT}{-}R_{TH,REF}$. When two identical cantilever resistors of 500 Ω were used for the Wheatstone bridge configuration, the non-linear term $\Delta V_{out}/V_{in}^3$, found from the graph was 121 μV/V^3 and the corresponding difference in thermal resistances was 290 K/W.

To minimize the dissipated power and thereby the self-heating, without lowering the input voltage, resistors having a resistance of 7.5 kΩ could be used instead of the 500 Ω resistors. As expected, the relationship between V_{in} and ΔV_{out} was linear which indicated that there was basically no self-heating of the cantilevers.

The non-linear term and the difference in thermal resistances, when using a cantilever resistor of 500 Ω and an external resistor, was found to be 4200 μV/V^3 and 10000 K /W, respectively. The temperature increase of the external SMD resistor due to the input voltage was assumed to be negligible and thus the thermal resistance, $R_{TH,REF}$, was zero. Hence, $R_{TH,CANT}$ was 10000 K/W. It is thereby possible to calculate the temperature increase in the cantilever due to the dissipated power, $P_W = V_{in}^2/(4R)$, for a Wheatstone bridge configuration. For an input voltage of 0.5 V the cantilever was theoretically heated about 1 K and for an input voltage of 1 V the temperature increase was 5 K.

Coventor simulations were also performed by Jan Hales to estimate the heating of the cantilevers due to the input voltage. It was found that if a voltage of 0.25 V was applied across a single resistor of 500 Ω (0.5 V across the bridge) the temperature of the cantilever increased about 6 K while for an applied voltage of 0.5 V (1 V bridge input) the temperature increased about 24 K. Hence, an input voltage of maximum 0.5 V should be used for biochemical measurements to avoid severe heating of the cantilevers.

In conclusion, the gauge factor and the resonant frequency have been measured and were found to correspond well with theoretical results. The TCR-effect and the bimorph effect have also been measured and were found to be slightly smaller than expected. The resistors were found to balance each other well when connected in a Wheatstone bridge configuration. A low input voltage was required to avoid plastic deformation and self-heating of the cantilevers. However, by increasing the resistance (by decreasing the thickness of the Au) the self-heating was significantly reduced and a larger sensitivity was obtained. The drawback was that the resistors became more fragile as the resistor thickness decreased.

Chapter 7

Surface stress measurements in vapor and liquid phase

Cantilever based sensors have been used for detection of DNA [17], proteins [19], pesticides [20] and TNT explosives [21]. Since the surface stress changes induced by DNA hybridization and antigen-antibody recognition have been observed to be small, some initial measurements were performed using chemistry that was expected to generate relatively large surface stresses. Although the measurements presented in this chapter are not related to a specific biosensor application, they are useful to get an understanding of the surface stress sensitivity of the SU-8 cantilever.

To characterize the surface stress sensitivity of the cantilever, three test systems were investigated:

- Etching the Au on the cantilever surface
- Immobilization of thiol molecules in vapor and liquid phase
- Characterization of pH and salt sensitivity

Due to the strong binding between thiols and Au, thiol-based chemistry is the most common method of binding biomolecules on cantilevers and has been used to immobilize DNA [17] and antibodies [20]. Unless otherwise stated, the measuring cantilever was coated with a 20/200 Å thick layer of Ti/Au. By using a shadow mask the reference cantilever was left uncoated.

The electronic measurement setup and the Wheatstone bridge configuration presented in Chapter 6 was used for all measurements unless otherwise stated.

7.1 Surface stress sensitivity

To understand the relationship between the change in the resistance of the piezoresistor and the surface stress, results from the mechanical theory of bending cantilevers is presented here. A more thorough description of the surface stress equations is give by Peter Rasmussen in his PhD thesis [50][107]. The theory gives an estimate of the expected surface stress sensitivity of the SU-8 cantilevers in terms of the Young's modulus and the thickness of the cantilever and an understanding of which parameters that are important in order to optimize the sensitivity.

The relationship between the deflection of the cantilever, z, and the surface stress, σ_s, was first reported by Stoney in 1909 [108]

$$\sigma_s = -\frac{YH^2}{3L^2}z \tag{7.1}$$

where $Y{=}E/(1\text{-}\nu^2)$ is the clamped cantilever modulus, E is the Young's modulus, ν is the Poisson's ratio, H is the thickness of the cantilever and L is the length of the cantilever. Although this expression is derived for a one-layer cantilever it is also a good approximation for a cantilever with a Au coating of a few hundred Å. This equation can be used to compare the sensitivity of piezoresistive cantilevers with cantilevers for optical readout.

To obtain a relationship between the surface stress due to molecular binding and the change in output voltage from the Wheatstone bridge, a model has been developed by Ole Hansen at MIC. As already seen in Chapter 2, the resistance change, ΔR, can be related to the strain, ϵ, through $\Delta R/R{=}K\epsilon$ where K is the gauge factor. The strain in the cantilever at a distance z_N from the neutral plane is assumed to consist of an elongation/contraction part, ϵ_0, and a bending part, βz_N,

$$\epsilon = \epsilon_0 + \beta z_N \tag{7.2}$$

Since it is only the surface stress change that is of interest here, any built-in stress in the cantilever has been ignored. The surface stress is defined as, $\sigma_s = \sigma_T t_T$, where σ_T is the stress in a thin layer having a thickness of t_T. The thickness of the stressed layer is assumed to be close to zero. The surface stress is given in units of [N/m]. The contributions to the strain are [50]

$$\epsilon_0 = -\frac{\sigma_s}{\sum_i Y_i t_i} \tag{7.3}$$

$$\beta = -\frac{\sigma_s h_N}{\sum_i Y_i t_i \Big((h_N - \sum_{j=0}^{i} t_j + \frac{t_i}{2})^2 + \frac{1}{3}(\frac{t_i}{2})^2 \Big)} \tag{7.4}$$

where $Y_i{=}E_i/(1-\nu_i^2)$ is the clamped cantilever modulus and t_i is the thickness of the i'th layer. h_N is the distance from the top of the cantilever to the neutral axis and was defined in Eq.(6.7). From these equations it is possible to find an expression for the surface stress sensitivity of the piezoresistors. If the distance from the piezoresistor to the neutral plane is called d, so that $z_N{=}d$ the surface stress sensitivity becomes,

$$\frac{\Delta R}{R\sigma_s} = K\Big(- \frac{1}{\sum_i Y_i t_i} - \frac{h_N d}{\sum_i Y_i t_i \Big((h_N - \sum_{j=0}^{i} t_j + \frac{t_i}{2})^2 + \frac{1}{3}(\frac{t_i}{2})^2 \Big)} \Big) \quad (7.5)$$

It can be seen that the important parameters that influence the sensitivity of the cantilever is the thickness, the Young's modulus, the distance from the resistor to the surface and the gauge factor. The surface stress sensitivity, for a so called standard cantilever having the layer thicknesses seen in Figure 7.1 and a 200 Å Au coating, is about $3.9{\cdot}10^{-4}$ $(\mathrm{N/m})^{-1}$. The parameters from Table 7.1 were used for the calculations.

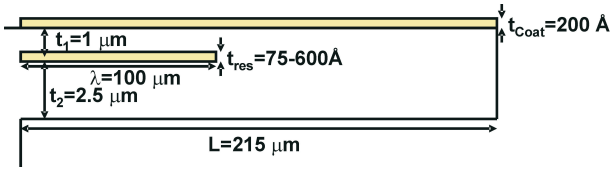

Figure 7.1: Schematic image of the sideview of a standard cantilever which has been coated with Au. The top SU-8 layer is about $t_1{=}1$ μm and the bottom layer is about $t_2{=}2.5$ μm. The thickness of the Au layer for the piezoresistor is normally $t_{res}{=}600$ Å but can be decreased down to 75 Å. The top Au coating $t_{coat}{=}$ 200 Å was used to bind molecules to the surface.

By using Eq.(6.3), the relationship between the surface stress and the output voltage becomes

$$\sigma_s = \frac{4}{(\frac{\Delta R}{R\sigma_s})} \frac{\Delta V_{out}}{V_{in}} = A \frac{\Delta V_{out}}{V_{in}} \quad (7.6)$$

where A is about 10380 N/m for a Au coated cantilever. If the cantilever is uncoated the surface stress sensitivity becomes $5.9{\cdot}10^{-4}$ $(\mathrm{N/m})^{-1}$ and $A{=}6730$ N/m. Hence, an output voltage of 1 μV corresponds to a surface stress change of about 20 mN/m for a Au coated cantilever and 13 mN/m for an uncoated cantilever.

In the following sections the results from the surface stress measurements are presented by showing both the measured output voltage change and the corresponding calculated surface stress change. Although the conversion factor, A, calculated for a standard Au coated cantilever can normally be used, some measurements have been performed using cantilever with slightly different thicknesses and thereby different conversion factors.

Parameter	Value
Young's modulus SU-8	3.5 GPa
Young's modulus Au	78 GPa
Poisson's ratio Au	0.42
Gauge factor Au	3.7
Thickness of the first SU-8 layer	1 µm
Thickness of the second SU-8 layer	2.5 µm
Thickness of the resistor	600 Å

Table 7.1: The parameters for a standard SU-8 chip. Using these parameters it is possible to calculate the surface stress sensitivity of the SU-8 cantilever.

7.2 Etching of the Au layer on a cantilever

When a Au layer is evaporated on the cantilever surface it induces a small bending of the cantilever due to the built-in stress of the layer. By etching the Au on the measurement cantilever it was possible to measure how the stress from the Au was released. A 50/600 Å Ti/Au layer was evaporated on the measurement SU-8 cantilever while the reference cantilever was left uncoated.

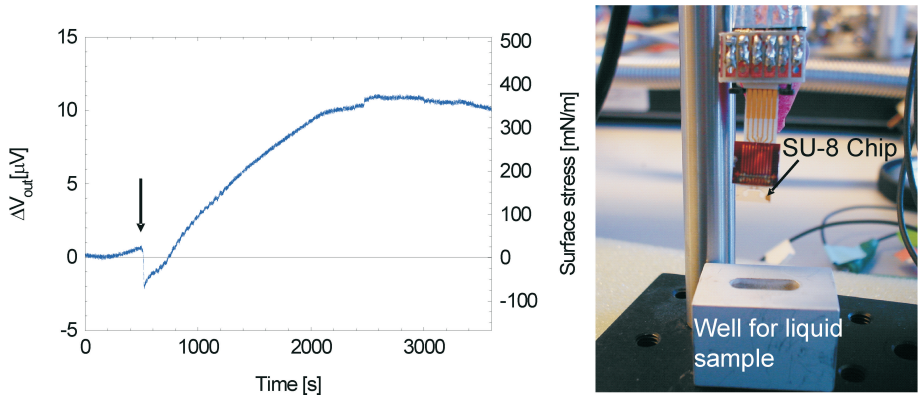

Figure 7.2: Left: Output voltage change due to etching of a 600 Å Au layer on the measurement cantilever. The arrow indicates when the Au etchant was introduced. The signal corresponded to a stress of 6 MPa in the Au layer. Right: The cantilevers were immersed in a well with liquid and the Au etchant was introduced using a syringe.

Since the measurements were done before the microfluidic system was developed, the chips were dipped in a 300 µL well containing KCl dissolved in MilliQ water, see Figure 7.2 (right). The KCl solution was used to ensure a stable salt concentration during the measurement. Once the signal was stable, 30 µl of 0.1 M KI was introduced into the well using a syringe. The KI was used to etch the Au off the cantilever. The detected change in output

voltage was about 10 μV which corresponded to a surface stress change of about 350 mN/m, see Figure 7.2 (left). Hence, the stress in the Au film was about 6 MPa. The same measurement has previously been demonstrated using a Si based cantilever where the stress in the Au layer was found to be about 30 MPa [50].

7.3 Cleaning of Au surfaces

To detect thiol immobilization by surface stress measurements, it is highly important to have a clean Au surface. Although, the Au was normally deposited maximum a few days before the experiments and stored in a closed single wafer tray, hydrocarbon and other contaminants quickly bound to the surface. Since freshly deposited Au surfaces are hydrophilic, but become hydrophobic after exposure to air for only a few minutes, the degree of contamination can be observed by measuring the contact angle [109].

Since the cantilever device is intended to be a single-use device, cleaning of the Au surface after a measurement is in principle not an issue. However, to reduce the number of chips that had to be fabricated it was an advantage to reuse the chips. Moreover, by reusing the same chip several times problems with chip to chip variations could be eliminated. Hence, it was also important that thiols could be removed from the Au surface after each experiment. Contact angle measurements were used to investigate if thiols could be removed from the Au by using an UV/ozone treatment.

7.3.1 UV/ozone treatment

To remove contaminants, Au can be cleaned in oxygen plasma, HNO_3, HCl, piranha (1:3 H_2SO_4:H_2O_2), by UV/ozone treatment or by etching the top layer of the Au surface [18][45][97]. Although thiols are known to bind almost covalently to Au they should also be removed by the mentioned cleaning processes. It was crucial that the cleaning process was compatible with the SU-8 chip so that the chips were not damaged. Although SU-8 is known to be very chemically resistant it was occasionally observed that the cantilevers with integrated readout delaminated in strong acid solution, such as HCl, or in very hot piranha. The delamination was observed between the resistor and the thin SU-8 layers for the cantilever, making the resistor exposed to the surrounding liquid. Hence, HCl and piranha were not considered to be suitable cleaning processes. To clean the Au by etching of the top layer of the Au coating, thickness variations was expected to become a problem. Since the thickness of the Au layer had a large effect on the sensitivity of the cantilevers, this method was not investigated further. However, since UV/ozone cleaning is a straightforward and mild method to use it was found to be a

promising cleaning method to remove contaminations and thiols.

UV/ozone cleaning is an effective method to remove a variety of contaminants from surfaces [110]. It is a dry process where an oxygen containing atmosphere is exposed to UV-light to produce ozone (O_3) that dissociate into oxygen radicals (O^+). The oxygen radicals are strong oxidizers that decompose organic surface contaminants (CO, CO_2, N_2) to volatile groups that desorb from the surface. The cleaning was performed in a commercial system (PR 100, UVP Inc.) having a mercury arc lamp providing UV radiation at 185 nm (to produce ozone) and 254 nm (to produce oxygen radicals).

To investigate the UV/ozone cleaning process, Au samples were prepared by evaporation of 20/200 Å Ti/Au on a Si wafer and afterwards dicing the wafer in 1.5 by 1.5 cm pieces. The contact angle was measured both on samples with immobilized thiols and on samples with contaminations from the air.

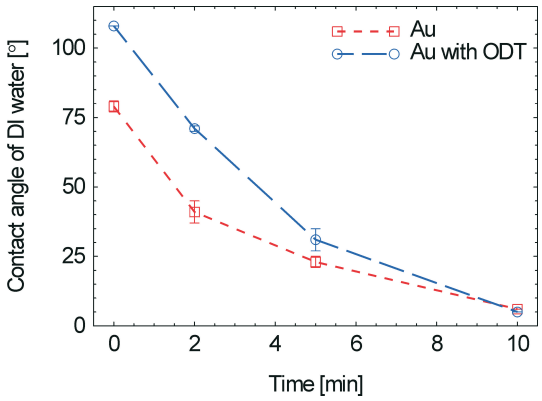

Figure 7.3: Change in contact angle of water on Au surfaces as a function of the cleaning time in UV/ozone. Au surfaces contaminated by air were compared to Au surfaces with chemisorbed ODT. After 10 min of UV/ozone cleaning both surfaces were hydrophilic and both the hydrocarbon contaminants and the ODT molecules were assumed to be fully removed.

Octadecanethiols (ODT) ($CH_3(CH_2)_{17}SH$) were chemisorbed on the Au samples that had been cleaned in UV/ozone for 20 min. The Au samples were immersed in a solution of 0.1 mM ODT in ethanol for 2 h and afterwards rinsed in ethanol and dried with a gentle stream of nitrogen. The result was a hydrophobic surface with a contact angle of 110°. This is in good agreement with reported contact angle values of 108° for ODT on Au [111]. As a reference, the contact angle was also measured on samples that had been immersed in ethanol without ODT molecules. These measurements did not indicate any increase in the contact angle. After treating the ODT

covered surfaces with UV/ozone for 10 min, it was found that the surfaces became hydrophilic (5°) which indicated that the ODT molecules were removed from the surface, see Figure 7.3. By using XPS, it has previously been observed that a UV/ozone treatment followed by a water rinse could remove self-assembled cysteamine on Au within 5 min [112].

Au samples that had been stored in a closed container for a day after evaporation had a contact angle of about 80°. This indicated that hydrocarbons had immobilized on the surface of the Au. By contact angle measurements it was observed that the hydrocarbon contaminants could be removed after 10 min UV/ozone treatment, see Figure 7.3.

These results indicated that the UV/ozone treatment was a suitable method to use for cleaning the Au surface before and after measurements. Normally, the chips were UV/ozone treated for 20 min to 30 min immediately before they were assembled in the microfluidic system.

7.3.2 Thiol binding on contaminated surfaces

To investigate if thiol molecules could bind on contaminated surfaces, Au samples were immersed in solutions of ODT in ethanol for 2 h. Three types of Au samples were used including PDMS contaminated Au, hydrocarbon contaminated Au and UV/ozone cleaned Au. The samples that had been contaminated by PDMS were prepared as described in Chapter 5 and were stored with the PDMS for one week which resulted in a contact angle of about 90°. The Au surfaces were observed to have a considerably larger contact angle compared to Si samples that had also been stored on the PDMS. The reason was probably due to a larger contamination rate due to the larger surface free energy of the Au (1.2 N/m) compared to Si (0.07 N/m)[96][113]. The hydrocarbon contaminated surfaces had also been stored for one week after evaporation in a closed single wafer tray and had a contact angle of about 80°.

After immersion in ODT, the samples were rinsed and dried and the contact angles were measured. A contact angle of about 110° was measured on all three samples. The result indicated that thiols could bind to the surface even though the surface was contaminated. However, the change in contact angle and thereby the change in the surface energy, was considerably larger on the UV/ozone cleaned surface compared to the PDMS contaminated surfaces. Since the surface stress can be related to the surface free energy it could be expected that the surface stress was considerably reduced due to contamination. Hence, PDMS and hydrocarbon contaminations can have a large influence on the measured surface stress changes.

7.4 Immobilization of thiols in vapor phase

To characterize the chips in terms of the surface stress sensitivity, the binding of 6-mercapto-1-hexanol (MCH)(SH-C_6H_{12}-OH) (Sigma-Aldrich) on Au coated SU-8 cantilevers was monitored. MCH has a six-carbon chain and is terminated in one end by a thiol group (-SH) and in the other end by a hydroxyl group (-OH). MCH is often used as a spacer molecule for DNA hybridization.

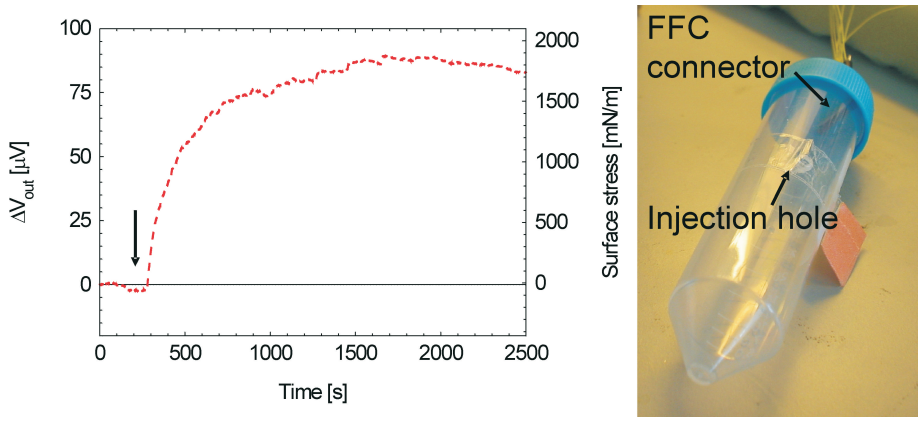

Figure 7.4: Left: The cantilever was deflecting due to immobilization of mercaptohexanol in vapor phase. Right: The chip was mounted in a tube and a droplet of mercaptohexanol was introduced through a hole in the side of the tube.

The PCB with the SU-8 chip was connected to the FFC connector which was placed inside a propylene tube, see Figure 7.4 (right). A hole was made in the lid of the tube for the electrical wires from the FFC connector. A drop of 60 µL MCH was placed inside the tube through a hole in the side (which was closed again afterwards) and was allowed to evaporate at room temperature. A signal output change of about 90 µV was detected corresponding to a surface stress change of 1750 mN/m, see Figure 7.4 (left). From the output voltage signal it was observed that the thiols induced a tensile stress in the resistor which corresponds to a compressive stress in the cantilever. For comparison, alkanethiols in vapor phase with chain lengths from 4 to 12 carbon atoms have been demonstrated by Berger et al. to result in surface stress changes of 100-200 mN/m [114]. Godin et al. have detected surface stress changes of 300-600 mN/m for dodecanethiols in vapor phase [115]. The discrepancies in the obtained signals can be explained by the different measurement setups, the amount of molecules used and the properties of the Au surface.

To reduce the size of the measurement setup, to eventually enable a portable device, an INA 125 amplifier (Burr Brown) was used instead of the lock-in

amplifier. The INA-amplifier was mounted together with an FFC connector on a printed circuit board by Jan Vasland Eriksen at DANCHIP, see Figure 7.5 (right). The signal amplification was 500 and an input voltage of 1.25 V was used. The amplifier was run on batteries and the output voltage from the Wheatstone bridge was connected to a Keithly which was connected to the laptop computer. The amplifier required that all four resistors for the Wheatstone bridge were on the chip. Hence, the external SMD resistors were not used. The signal output had a noise level which was comparable to the noise level of the lock-in amplifier setup.

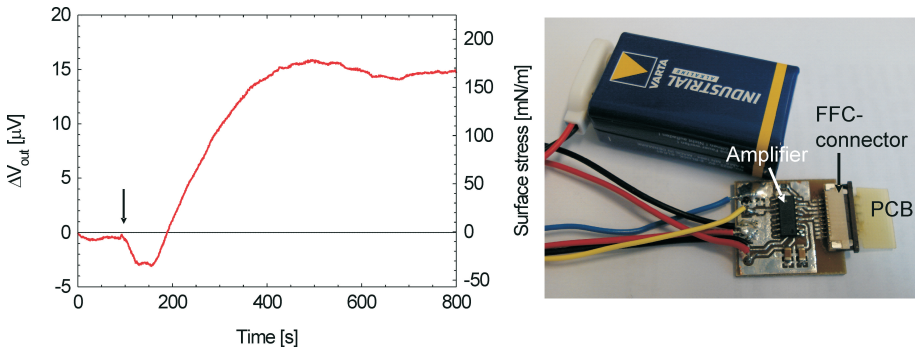

Figure 7.5: Left: Vapor phase detection of mercaptohexanol. Right: The measurement was done using a small amplifier on a print instead of the lock-in amplifier. The print is a first step towards development of a portable device.

This amplifier was used to repeat the MCH measurement described above. The only difference was that for these experiments a droplet size of 6 µl was used. Surface stress change of about 170 mN/m were obtained, see Figure 7.5 (left). The surface stress was smaller than for the previously shown result which was probably due to the reduced droplet size.

7.5 Fluidic measurement setup

The fluidic measurement setup consisted of a syringe pump (Harvard Research), a 6-port valve (Vici) and the PMMA based microfluidic system described in Chapter 5.

The pump was used to pump buffer or MilliQ water to the valve. The valve was manually switched and could be either in position B, where the solution from the pump went directly to the chip or in position A, where the solution was pumped through the sample loop, see Figure 7.6. Normally, the sample loop had a volume of about 75 µL and could be filled with the sample through a syringe connected to one of the ports of the valve. This was done while the valve was in position B. The pump rate was normally 10 µl/min.

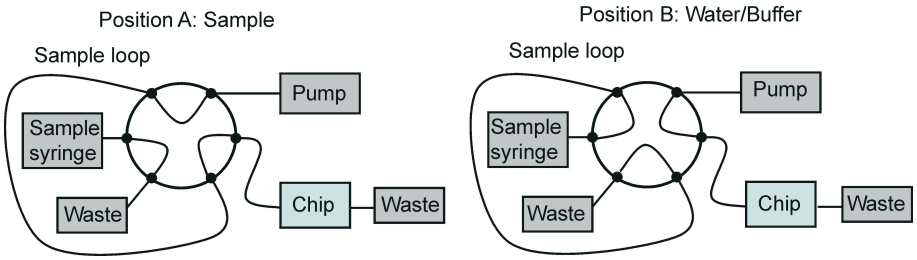

Figure 7.6: In position A (left) the sample in the loop was pumped to the chip. In position B (right) the sample loop could be filled while water or buffer was pumped to the chip from a large syringe.

Except for the silicone tubes (Reichelt Chemitechnik GmbH.) that were connected to the microfluidic system, all the other tubes were made of polytetrafluoroethylene (PTFE) (Upchurch). The silicone tube and the PTFE tube could be connected by simply inserting the PTFE tube into the silicone tube. Between every measurement, the tubes were rinsed using MilliQ water.

7.6 Immobilization of thiols in liquid phase

The surface stress sensitivity of the cantilevers was also characterized by immobilization of MCH on Au coated cantilevers in liquid. The MCH molecules were diluted in MilliQ water. MilliQ was pumped through the microsystem until a stable baseline was obtained. The valve was then switched and MCH was pumped to the chip. Concentrations of 0.2, 0.5 and 1 mM were used. Surface stress measurements using MCH are shown in Figure 7.7.

When MilliQ was again pumped through the system, the signal was observed to decrease. The reason was most likely that the MCH molecules had formed more than one monolayer on the Au surface and when the system was rinsed with MilliQ, the MCH molecules that were not chemisorbed on the Au surface were washed away, see Figure 7.8. The resulting surface stress was seen to increase for increasing concentrations from about 50 mN/m to 300 mN/m. Just as for the measurements of thiols in vapor phase, the cantilevers were bending downwards. The measured surface stress change due to binding of MCH molecules was slightly lower in liquid than in vapor phase. This was not surprising since the surface stress is generally expected to be lower in liquid than in air [96].

To investigate if there were any unspecific interactions between the MCH and the SU-8 cantilevers, hexanol (C_6H_{13}-OH) was also injected in the microfluidic system. Since hexanol does not have a thiol group it was not expected

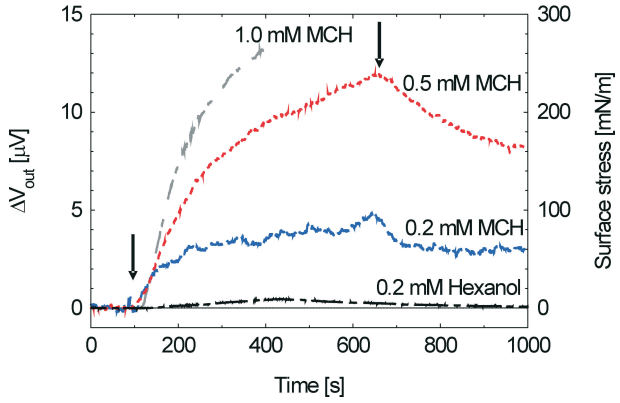

Figure 7.7: Surface stress measurements of chemisorption of mercaptohexanol on Au-coated SU-8 cantilevers. The detected surface stress change was observed to increase for increasing concentrations. When introducing hexanol there was only a small transient signal which indicated that the molecules did not bind to the surface.

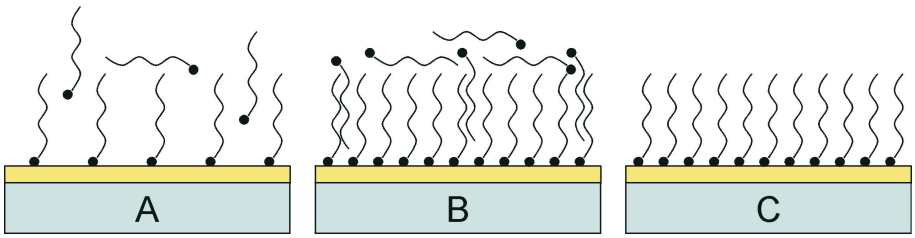

Figure 7.8: The thiol molecules were adsorbing on the Au surface (A) until a dense layer had formed (B). When the system was flushed with water the molecules that were not bound to the Au surface were washed off (C) and the surface stress decreased.

to interact with the Au surface. Although a small output signal from the hexanol measurements were often observed, the signal always returned to the baseline when switching back to MilliQ. This indicated that the hexanol molecules were not chemisorbed on the surface and could be removed by flushing with MilliQ. A typical hexanol measurement is shown in Figure 7.7. These MCH measurements have also been published elsewhere [116].

7.6.1 Thiol adsorption on SU-8 surfaces

For the presented measurements, the top surface of the measuring cantilever was covered with Au, while the top surface of the reference cantilever was left uncoated. Hence, any interactions between the thiols and the SU-8 surface would take place on the backside of both the cantilevers as well as on the top side of the reference cantilever. Although SU-8 has been used quite extensively for microfluidic components for the last few years it has not been properly investigated how molecules interact with the surface.

The SU-8 surface has both epoxy and OH-groups on the surface and this ratio can be altered by surface treatments. It is possible that electrostatic interactions occur between the OH-groups on the SU-8 cantilever surface and the OH-groups and SH-groups of the mercaptohexanol molecules, see Figure 7.9. However, due to the larger electronegativity of the O atom compared to the S atom, it is likely that the OH-groups interact more strongly with the surface than the SH-group [117].

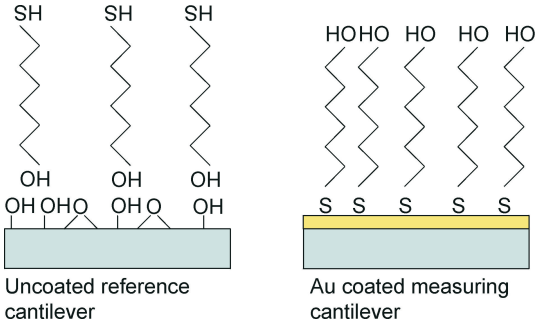

Figure 7.9: Thiol molecules, such as mercaptohexanol are expected to bind to the Au coated measuring cantilever (right). However, it might be possible that the molecules also interact with the OH- and epoxy groups on the SU-8 surface (left).

Using contact angle measurements, it was possible to investigate if the surface properties of the SU-8 were influenced by immersion in MCH. SU-8 samples were immersed in a 0.5 mM solution of MCH overnight and afterwards rinsed in MilliQ. Since the chips were UV/ozone treated before measuring, to clean the Au, the SU-8 surface was also exposed to UV/ozone. The treatment was expected to open the epoxy groups and increase the number of OH-groups on the surface. Both UV/ozone treated and untreated SU-8 samples were investigated for MCH binding.

The measured contact angle of the SU-8 surface was not observed to change significantly after immersion in MCH compared to reference samples immersed in only MilliQ, see Figure 7.10. Although the UV/ozone treatment was found to reduce the contact angle, it did not seem to have any influence on the MCH binding. However, even though the contact angle measurements indicated that the molecules did not adsorbed on the surface it is still possible that molecular interactions with the surface would take place during a measurement.

To further investigate if the uncoated cantilever was a good reference, the MCH surface stress measurements were repeated using a reference cantilever which was coated with 150 Å Ti instead of an uncoated reference cantilever. It was assumed that the MCH molecules did not bind to the Ti coating. In

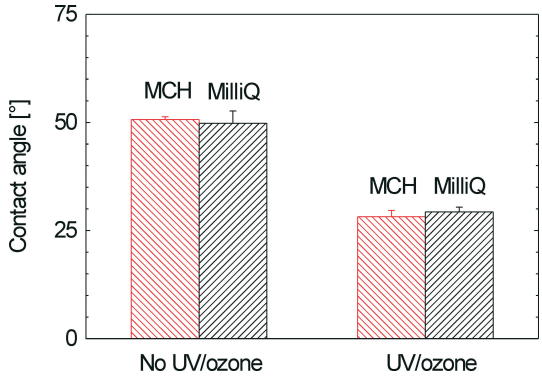

Figure 7.10: The contact angle of SU-8 samples was measured after immersion in either mercaptohexanol solution or MilliQ. The contact angle was found to be approximately the same which indicated that the molecules did not bind to the surface. The same result was observed for UV/ozone treated SU-8 surfaces.

Figure 7.11, MCH measurements using a Ti coated reference cantilever are compared to measurements using an uncoated cantilever. It is seen that the output signals were similar which indicates that an uncoated SU-8 cantilever can be used as a reference cantilever.

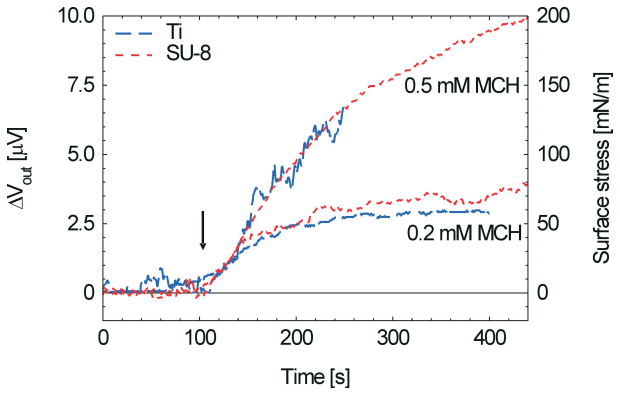

Figure 7.11: MCH immobilization on Au coated cantilevers when using either an uncoated SU-8 cantilever or a Ti coated cantilever as the reference cantilever. No significant difference was observed.

7.7 Sensitivity to pH and salt changes

To better understand the surface properties of the SU-8 cantilevers and its response to chemical stimuli, the influence of pH on Au coated SU-8 cantilevers was also investigated. Since the pH might vary during a measurement of a biochemical sample, it is important that the response of the cantilever

is small so that these variations will not interfere with the molecular recognition signal. Hence, it is desirable to use a cantilever with low sensitivity to pH, unless the cantilever was going to be used as a pH sensor.

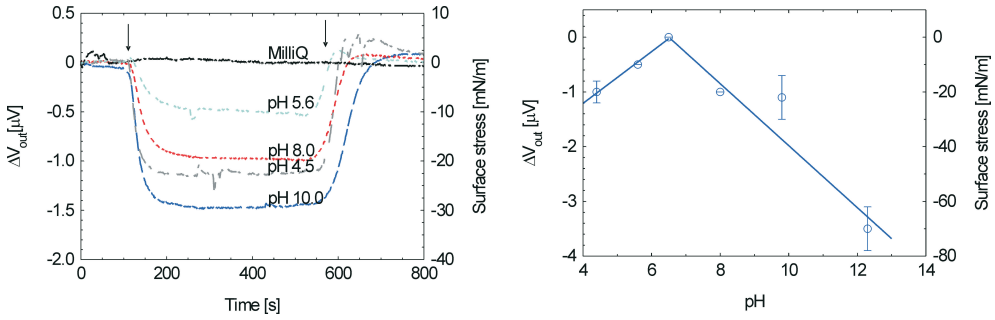

Figure 7.12: Left: The bending response of Au coated SU-8 cantilevers as a function of pH changes. The arrows indicate when then solution was introduced and when the system was flushed with water. The cantilevers were observed to bend towards the Au surface for both increasing and decreasing pH values. Right: The graph shows the output voltage as a function of pH using three different chips.

Freshly made solutions of varying concentrations of HCl and NaOH in MilliQ were used for the measurements. The pH of the solution was measured immediately before it was introduced in the microfluidic system. An output voltage change was observed when introducing the pH solution and the signal returned to baseline after switching back to MilliQ, see Figure 7.12 (left). For both increasing and decreasing pH values, the cantilevers were bending upwards, towards the Au coating. The stress change was about 10 mN/m per pH, see Figure 7.12 (right). Similar behavior has been observed for Au coated SiO_2 cantilevers [118]. The deflection of the cantilever could be due to both Cl ions interacting with the Au layer and OH-groups interacting with the SU-8 surface. pH characterizations of SU-8 cantilevers for optical readout have previously demonstrated that SU-8 cantilevers are less sensitive to pH changes than Si based cantilevers [39]. Using Au coated Si_3N_4 cantilevers, surface stress changes of about 15-20 mN/m when increasing the pH value from pH 4 to pH 10 have been reported by Butt [16]. Ji et al. have reported values that were about 10 times larger using the same type of cantilevers [118]. Cantilever based pH sensors have been demonstrated by immobilizing pH sensitive molecules with end groups such as -NH_2 or -COOH on the cantilever surface [38][118][119].

The response of the cantilevers due to salt was also measured. By introducing a salt concentration of 1 mM of either NaCl, KCl or $NaNO_3$, a voltage change of about 1.5 μV was measured, see Figure 7.13. This corresponds to a surface stress change of about 30 mN/m. As for the pH measurements, the cantilevers were observed to deflect toward the Au surface. Since the sur-

face properties of the SU-8, such as the charge, are not well-characterized more measurements are required to interpret the obtained results [120]. In comparison, when introducing 1 M NaCl, surface stress changes of either 60 mN/m or 430 mN/m have been reported for Si based cantilevers [16][121].

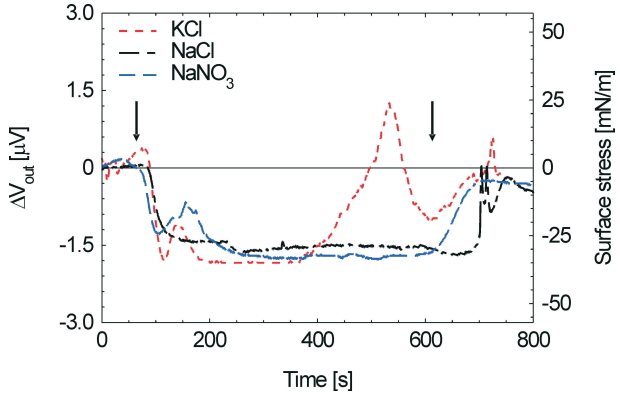

Figure 7.13: The bending response due to injection of different 1 mM salt solutions was observed to be similar.

The reproducibility of the presented measurements varied. While the thiol measurements generally had a low reproducibility, the pH measurements resulted in a relatively high reproducibility. The reason could be that thiol immobilization required a very clean Au surface while the pH measurements were less dependant on the surface properties of the Au. The cause of the possible contaminations was discussed in Chapter 5 and could be assumed to be a result of the packaging process and materials. Hence, for the device to function as a high-sensitivity biosensor with a good reproducibility, the surface properties of the sensor surface have to be well-characterized.

7.8 Minimum detectable surface stress

Are the SU-8 cantilevers with piezoresistive readout sensitive enough to be used as cantilever based biosensors for detection of DNA hybridization and antibody-antigen recognition? To answer this question we need to know the minimum detectable surface stress of the sensor and the expected surface stress due to biomolecular recognition.

The minimum detectable output voltage can be assumed to be equal to the voltage noise level,

$$\sigma_{det} = A\frac{\Delta V_{out,det}}{V_{in}} = A\frac{\Delta V_{noise}}{V_{in}} \tag{7.7}$$

where ΔV_{noise}=0.2 μV. This noise level was an average value that was obtained by observing the noise level during the surface stress measurements and was assumed to be valid when using the setup presented in Chapter 6. Hence, the minimum detectable surface stress can be calculated, see Table 7.2. The minimum detectable surface stress is about 4.2 mN/m for a Au coated cantilever and 2.7 mN/m for an uncoated cantilever.

Cantilever	t_1 [μm]	t_{res} [Å]	t_2 [μm]	V_{in} [V]	σ_{det}+Au [mN/m]	σ_{det} [mN/m]
Standard	1	600	2.5	0.5	4.2	2.7

Table 7.2: The table shows the minimum detectable surface stress for the so called standard cantilevers used in this project. A noise level of 0.2 μV has been assumed. Results for Au coated and uncoated cantilevers are compared.

To estimate the expected surface stress change from a biochemical reaction such as DNA hybridization or antigen-antibody interactions some results from the literature are presented in Table 7.3. In all cases, Au coated cantilevers were used.

Biomolecule	Conc.	σ_s [mN/m]	Method	Ref. cant.	Ref.
DNA	0.4 μM	5	optical	yes	[17]
DNA	0.5 μM	2.7	optical	yes	[122]
DNA	1 μM	15.6	piezo	yes	[18]
DNA	3-6 μM	3.75	optical	no	[23]
PSA	0.001/1 μg/ml	5/26	optical	no	[123]
Myoglobin	20/100 μg/ml	1/6	optical	yes	[19]
LDL	70 μg/ml	70	optical	no	[124]
IgG+BSA	100 μg/ml	5	optical	yes	[17]
IgG+BSA	195 μg/ml	220	optical	no	[125]

Table 7.3: Reported surface stress changes due to binding of different biomolecules.

The discrepancies in the signal outputs reported by different groups are not surprising since there are many parameters that could influence the obtained surface stress results. First, the calculation of the surface stress from the change in the optical or the electrical signal can involve some errors. Second, the cleaning of the Au surface, the time after evaporation and the evaporation rate have been suggested to have major influence on the stress [126]. For example, Godin et. al have observed that the grain size of the Au had a large influence on the surface stress change. For large grain sizes (600 nm) the surface stress change was found to be about 30 times larger than

for small grain size Au (90 nm) [127]. Third, lack of or insufficient blocking of the backside of the cantilever can reduce the signal. Fourth, the use of a reference cantilever is likely to have a large influence on the obtained signal since absolute measurement can be significantly larger than differential signals. Last, the type of buffer used might also influence the measurement. Wu et al. have observed that hybridization of DNA can cause both compressive and tensile stress depending on the ionic strength of the buffer [23].

It is seen from Table 7.3 that surface stress changes down to a few mN/m should be detectable for the cantilever chip to be promising as a biosensor. The present SU-8 cantilevers in combination with the measurement setup, might not have a sufficient resolution to detect small concentrations of DNA hybridization and antigen-antibody recognition. However, as demonstrated in Chapter 8, large concentrations can be detected. By further optimization of the cantilever and the setup, improved resolution should be obtained and the detection limit should decrease. This is discussed below.

Although the sensitivity of the cantilever is a crucial parameter for biosensor applications it is equally important to have a high reproducibility and a good selectivity. However, it has not been within the scope of this PhD project to develop a commercially competitive biosensor but rather to investigate the possibilities of using polymeric cantilevers as an alternative to Si based cantilevers.

7.8.1 Cantilever optimization

The sensitivity of the cantilevers will differ slightly depending on the thickness of the cantilever layers. In Figure 7.14, the surface stress sensitivity is plotted as a function of the thickness of the second SU-8 layer for different types of cantilevers. The surface stress sensitivity has been calculated using Eq.(7.5).

The surface stress sensitivity for a standard cantilever without Au coating, shown in Figure 7.1, is plotted in the graph (blue circles). It is seen that to achieve a maximum surface stress sensitivity for this type of cantilever, the thickness of the second SU-8 layer should be about 2 μm. For most of the fabricated cantilevers the second SU-8 layer had a thickness of 2.5 μm.

If the thickness of the first SU-8 layer is decreased to 0.5 μm (gray squares) the sensitivity can be increased. However, there are limitations to how thin the SU-8 cantilever can be before it becomes too fragile. During this project it was not possible to fabricate cantilevers where the first SU-8 layer was thinner than 0.9 μm. However, after some optimization it is not unreasonable to assume that the thickness could be reduced to 0.5 μm. In that case,

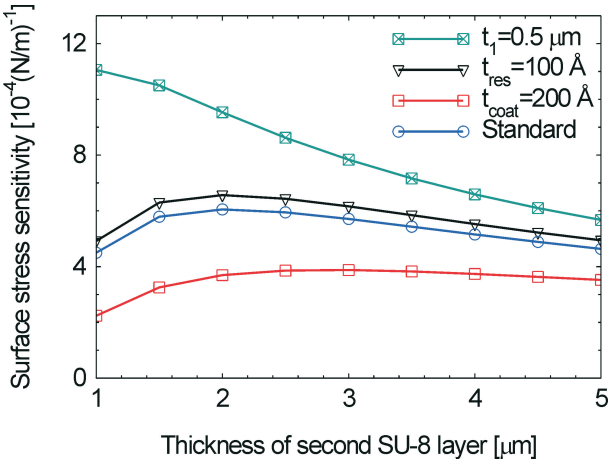

Figure 7.14: The surface stress sensitivity is plotted as a function of the thickness of the second SU-8 layer of the cantilever. The result for a standard cantilever, where the first cantilever layer was t_1=1 μm and the resistor layer was t_{res}=600 Å is shown. By reducing the thickness of the resistor or the first SU-8 layer the sensitivity can be increased. If the cantilever is coated with a Au layer having a thickness t_{coat}=200 Å the sensitivity is reduced.

the second SU-8 layer should probably be at least 2.0 μm to make the cantilever robust. The sensitivity of such a thin cantilever would increase by factor of about 1.6.

The surface stress sensitivity for a standard cantilever with a 200 Å Au coating is also plotted (red squares). It is seen that the sensitivity decreases significantly (about a factor of 0.6) due to the Au coating. Hence, it would be desirable to immobilize the biomolecules directly on the SU-8 surface instead of using a Au coating. By decreasing the thickness of the Au resistor from 600 Å to 100 Å when using a standard cantilever, the cantilever becomes slightly less stiff and the sensitivity increases with about a factor of 1.1 (black triangles). However, since the resistor layer only cover a small area of the cantilever (about 20 %) the contribution to the stiffness was assumed to be smaller than for the top coating.

It is thereby possible to estimate the minimum detectable surface stress of an optimized cantilever. The so called optimal cantilever can be assumed to have a first cantilever layer with a thickness of t_1=0.5 μm, a resistor thickness of t_{res}=75 Å and a second cantilever layer thickness of t_2=2 μm. Due to the reduced resistor thickness a larger voltage can also be applied without increasing the power dissipation. In Table 7.4, a standard cantilever is compared to an optimal cantilever and it is seen that the minimum detectable surface stress is 0.5 mN/m for a Au coated cantilever and 0.3 mN/m for an uncoated cantilever. Hence, the resolution of the optimal cantilever

design should be good enough to detect both DNA and proteins in very small concentrations.

Cantilever	t_1 [μm]	t_{res} [Å]	t_2 [μm]	V_{in} [V]	$\sigma_{det.}$+Au [mN/m]	$\sigma_{det.}$ [mN/m]
Standard	1	600	2.5	0.5	4.2	2.7
Optimal	0.5	75	2	2.5	0.5	0.3

Table 7.4: The minimum detectable surface stress for a standard and an optimal cantilever are compared. A noise level of 0.2 μV has been assumed.

In conclusion, the presented measurements demonstrate that the SU-8 chips can be used to detect surface stress changes due to binding of thiols in both vapor and liquid phase. A UV/ozone treatment was performed to clean the Au surface before and after measuring. It did not seem to make a difference whether the reference cantilever was coated with Ti or left uncoated and the thiol molecules were not observed to bind to the SU-8 surface. Furthermore, the pH measurements indicated that relatively small signals could be detected with good reproducibility. Although this chapter has demonstrated that SU-8 chips can be regarded as a promising alternative to Si based sensors, no measurements have been demonstrated using molecules for a relevant biochemical application. However, this is further discussed in the following chapter where results from antigen-antibody binding are demonstrated.

Chapter 8

Immobilization of antibodies on SU-8 surfaces

In this chapter, the possibility of using the cantilever chip as a biosensor for detection of antigens in solution is investigated. As previously mentioned, the cantilever sensor surface is normally functionalized by coating the cantilever with a Au layer on which thiol-modified biomolecules such as DNA and antibodies can bind. However, by immobilizing the biomolecules directly on the SU-8 surface, the sensitivity of the cantilever would improve. The reason is that by removing the Au layer, the cantilever becomes more soft. Moreover, by removing the Au coating, the bimorph effect will be reduced and the sensitivity to pH changes might decrease. For cantilevers with optical readout, removing the Au coating will reduce the amount of laser beam light that is reflected from the surface which lowers the sensitivity. However, for cantilevers with piezoresistive readout this is not an issue.

Investigation of protein adsorption on solid surfaces is interesting because of its importance in a wide range of biomedical applications such as medical devices and drug-delivery systems. Within the biosensor area, it is important to have a sensor surface with well-characterized properties and to understand how the surface interacts with molecules. However, although SU-8 is a well-known material within microfluidics, there are very few publications that address adsorption of molecules on SU-8 surfaces. To control the functional groups on the SU-8 surface, one approach that has been presented by Wang et al. involves using UV-mediated grafting of polymers onto the surface of the SU-8 [128].

During this PhD project, immobilization of both DNA and antibody on SU-8 surfaces were investigated. Here, only the results from the immobilization of antibody are presented while the results from the DNA immobilization experiments are described elsewhere [129]. Before any surface stress mea-

surements were done using the SU-8 cantilevers, the binding of molecules to SU-8 samples surfaces was investigated using fluorescently labelled antibodies. The results were obtained in collaboration with Gabriela Blagoi under the supervision of Martin Dufva at MIC. The results from antibody immobilization on SU-8 and the cantilever measurement have been presented elsewhere [130].

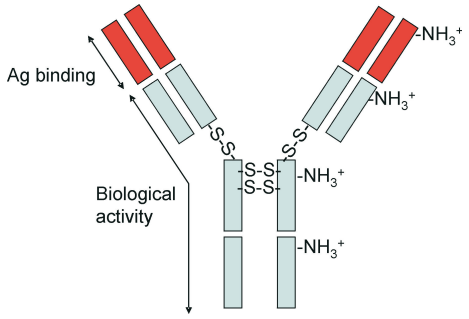

Figure 8.1: Schematic image of an antibody. The antibodies are expected to bind to the SU-8 surface through amine bonds that are present along the molecule. The fluorescent labels can bind either to the -SH or the -NH_3 groups of the antibody. The antigens bind to the variable domain of the antibody.

8.1 Antigen-antibody binding

Antibodies are antigen binding proteins that reside in the serum of the blood and are used by the immune system to identify and neutralize foreign objects such as bacteria and virions. Antibodies, or immunoglobulins as they are often called, consist of four peptide chains - two identical light chains and two identical heavy chains, see Figure 8.1. The peptides are bound together by disulfide bonds and noncovalent interactions such as hydrophobic bonds. The antibodies have a variable region that varies greatly among different antibodies and it is here that the antigens are recognized and bound. Antibodies bind to antigens through noncovalent interactions such as hydrogen bonds, ionic bonds, hydrophobic interactions and van der Waals interactions.

8.1.1 Immobilization of antibodies

Protein arrays such as Enzyme-Linked Immuno Sorbent Array (ELISA) are becoming increasingly important for protein interaction studies and diagnostics. It is of great importance that the antibody binds with the antigen binding sites exposed so that they remain active in order to recognize the antigens. Therefore, the surface material must preserve the active state of the antibody. However, in contrast to DNA, the surface charge of proteins is

variable, which can make them more complicated to immobilize [131]. Furthermore, proteins often display a hydrophilic exterior and a hydrophobic interior. Hence, immobilization on a hydrophobic surface might destabilize the structure and render the protein inactive.

Electrostatic and hydrophobic interactions between proteins and surfaces have been studied [132][133]. It was found that IgG antibodies adsorb spontaneously and with high affinity on polystyrene surfaces (having a contact angle of about 50°) even though the surface charge repels the proteins. Proteins were only fond to adsorb on hydrophilic surfaces when the electrostatic interactions were favorable. In the case of SU-8, the antibodies were expected to bind through amine groups reacting with the epoxy groups on the surface.

8.2 C-reactive protein

C-reactive protein (CRP) was used as a model system to investigate if antibodies could be immobilized directly on SU-8 surfaces. CRP is an acute-phase reactant which is present in blood. Due to an infection, trauma, surgery and other inflammatory disorders the CRP concentrations in blood may increase rapidly by as much as a factor of 1000. In addition to the increasing levels of CRP due to an infection, studies have also shown that CRP levels can predict the risk of future coronary heart disease. The concentration of CRP in blood has been divided into low risk (<1 μg/ml), average risk (1-3 μg/ml) and high risk (>3 μg/ml) [134]. Hence, since CRP detection is highly interesting for biomedical applications it could be a possible future application for the cantilever sensor.

There are already existing methods for CRP detection in the concentration range from 0.175 to 1100 μg/ml [134][135]. The detection principle is based on agglutination of antibody coated polystyrene particles that are detected by measuring the intensity of the scattered light in a nephelometer. To develop a biosensor which could compete with the existing detection methods was not within the scope of this PhD project. Instead, CRP was only used as a model molecule with relevance for clinical applications. One of the advantages of using CRP was that it is a relatively well-characterized protein that can be bought commercially.

8.3 Immobilization of antibodies on SU-8

8.3.1 Substrate preparation

SU-8 samples were prepared by crosslinking thin layers of SU-8 on pyrex wafers. Since SU-8 was found to be autofluorescent, the thickness of the SU-

8 layer should be as thin as possible to minimize the background signal. By using diluted SU-8 2002, a thickness of 0.6 µm was obtained. The wafer was cut into squares of about 1.5 mm by 1.5 mm and glued on glass slides that fitted into the fluorescent scanner.

8.3.2 Fluorescent labelling

The CRP antigens were detected by using a sandwich assay, see Figure 8.2 (right). Capture antibodies were immobilized on the SU-8 surface and the CRP antigens were detected using fluorescently labelled detection antibodies. Fluorescent molecules adsorb light at one wavelenght and emit light at another. The detections antibodies were labelled with Cy5 maleimide according to the manufacturers instructions (GE Healthcare, U.K.). To remove nonreacted Cy5 fluorophores, Micro Bio-spin P30 Tris columns (BioRad, Hercules, U.S.) were used. The CRP antibody had about 2.5 dye molecules per protein as measured by spectroscopy [136]. The fluorescent signal was detected using a CCD scanner (Array-WorX, Applied Precision, Issaquah, WA, USA). Mean values from the fluorescent density of each spot was obtained using the analysis software Data Inspector (Arrayworx). For the presented data, the background signal has been subtracted from the spot signal.

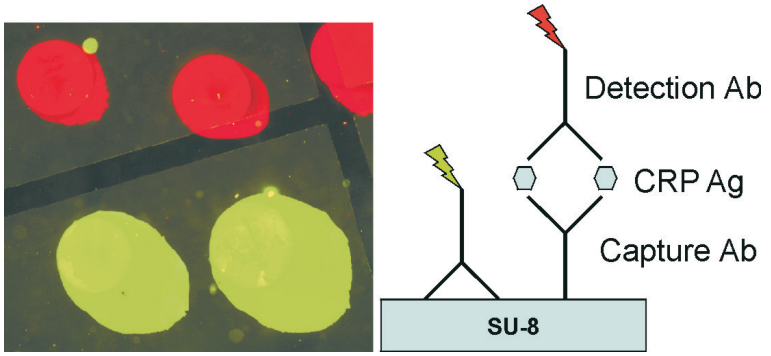

Figure 8.2: Left: The scanning image shows fluorescent spots from the CRP assay (red) and from anti-mouse antibodies immobilized directly on the SU-8 surface (green). Right: A sandwich assay, including capture and detection antibodies, was used to detect CRP molecules.

8.3.3 Fluorescent measurements

All solutions were based on phosphorous buffered saline (PBS)(pH 7.4)(Sigma, Germany). Monoclonal anti-CRP capture antibodies (Fitzgerald Industries International, U.S.) having a concentration of 5 µg/ml were immobilized on the SU-8 by manually spotting 0.5 µl spots on the surface. The antibodies

were incubated for 1 h at room temperature in a humid atmosphere. Following incubation, the samples were washed in PBS and the active sites of the SU-8 surface was blocked using bovine serum albumin (BSA) (1 µg/ml)(Sigma, Germany) for 15 min. The CRP antigen-antibody binding was obtained by covering the surface with CRP (Scripps laboratories, U.S.) with concentrations from 0.01 to 10 µg/ml. After incubation, the samples were washed and Cy5 labelled detection CRP antibodies with a concentration of 1-100 µg/ml were immobilized. The samples were washed before scanning. For surface stress measurements using the SU-8 cantilever, the fluorescently labelled detection antibodies were not necessary. Figure 8.2 (left) shows an example of a slide with red fluorescent spots due to CRP antigen-antibody binding. The green spots are due to fluorescently labelled anti-mouse antibodies that were immobilized directly on the SU-8 surface.

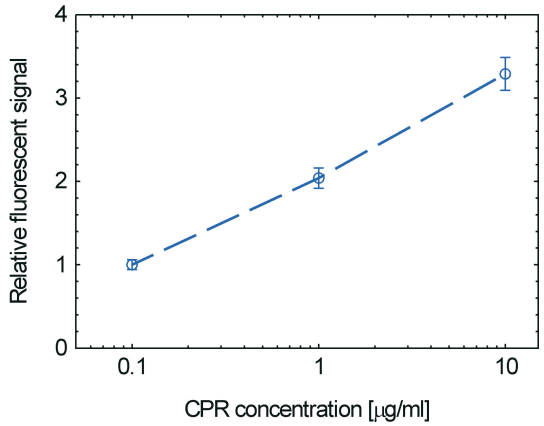

Figure 8.3: Fluorescent signal measured for varying concentrations of CRP antigen. The concentration of the capture and the detector antibody was 5 µg/ml and 100 µg/ml respectively.

The optimal concentration of the detection antibody was found to be 100 µg/ml while the detection limit for the CRP antigens was about 100 ng/ml, see Figure 8.3. This is well below the 1-3 µg/ml of CRP that is present in the serum during an infection.

8.4 SU-8 surface functionalization

The surface of the SU-8 cantilever chips was exposed to a number of chemical treatments during processing. These process steps could influence the properties of the surface by changing the functional groups that were present on the surface of the SU-8. Hence, the properties of the surface of the SU-8 samples used for the fluorescent measurements might not be the same as

the properties of the cantilever surface. This could have a large influence on the antibody immobilization. Hence, it was investigated how surface treatments such as the Cr etchants and the UV/ozone were influencing the SU-8 surface.

8.4.1 UV/ozone treatment

A UV/ozone treatment can be performed to clean the surface of the chip and to make the SU-8 surface more hydrophilic. For microfluidic systems, a hydrophilic surface is often preferable. As already mentioned, the SU-8 surface was assumed to have both epoxy and OH-groups on the surface and the number of OH-groups were expected to increase after a UV/ozone treatment. To investigate how stable the surface properties of the SU-8 was after the treatment, the contact angle of UV/ozone treated samples was measured as a function of time.

SU-8 samples were prepared by crosslinking thin layers of SU-8 on Si wafers and afterwards dicing the wafers. The contact angle of SU-8 was about 84±6° after processing and about 16±10° after a UV/ozone treatment for 20 min. The SU-8 samples were stored in a single wafer tray made from polypropylene (Entegris). The contact angle was measured by quickly opening the tray and removing one sample at a time. After the contact angle had been measured, the samples were discarded. The UV/ozone treated surface was observed to remain hydrophilic for several weeks, see Figure 8.4. In comparison, it has been observed that after treating the SU-8 surface with O_2 plasma the surface slowly becomes more hydrophobic over time [137].

As previously mentioned, antibodies preferably bind to hydrophobic surfaces. As expected, the fluorescent signal obtained from antibody immobilization on UV/ozone treated SU-8 surfaces was lower than for untreated surfaces.

8.4.2 Influence of the Cr etchant

During the release, the chips were immersed in the Cr etchant from 30 min up to several hours depending on how long it took for the chips to be fully released. Although SU-8 is known to be highly chemically stable, the surface was influenced by the Cr etchant. The reason is that the Cr etchant contains acetic acid and acids are known to be oxidizing agents that catalyzes epoxy group opening which results in more OH-groups on the surface. The contact angle was about 50° for SU-8 samples that had been immersed in Cr etchant 8002A for 1.5 h. However, the surface was not stable and the contact angle was observed to increase slowly over time, see Figure 8.4 [138].

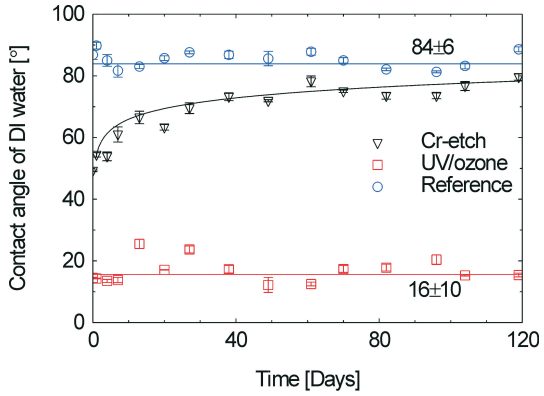

Figure 8.4: The image shows the contact angle as a function of time after different surface treatments. The contact angle of SU-8 samples that had been exposed to UV/ozone for 20 min or immersed in 8002 A for 1.5 h were compared to reference SU-8 samples that had not been surface treated.

To investigate if antibodies could be immobilized on SU-8 surfaces that had been immersed in different Cr etchants for 1 h, 5 µg/ml CRP capture antibodies were incubated on the surface. Binding of the antibodies was detected using Cy3 labelled anti-mouse antibodies and the results are shown in Figure 8.5 (left).

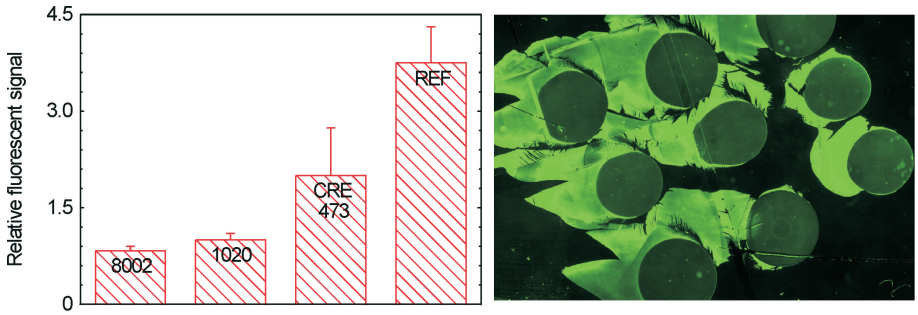

Figure 8.5: Left: The amount of immobilized CRP antibody on SU-8 was reduced by using Cr etchant treatments. Right: The spots had a strange shape which was probably caused by insufficient blocking of the SU-8 surface.

The fluorescent signal obtained from the Cr etchant treated surfaces was about 2-4 times lower than for the untreated surface. Unfortunately, 8002A which was the preferred etchant for the chip fabrication, resulted in the lowest antibody binding. As seen in Figure 8.5 (right) the spots had a strange pattern. The reason was probably that although the BSA blocked the untreated SU-8 surface well, it did not block the Cr etchant treated SU-8 surface. By adding 1% skimmed milk in the BSA solution a good blocking of the surface was obtained [136].

8.4.3 Silanization of the SU-8 surface

To increase the amount of antibodies adsorbed on the surface, the SU-8 surface was silanized using 1% 3-aminopropyl triethoxy (APS) in toluene. However, the surface coverage was inhomogeneous and the fluorescent signal was about 20 % lower than for the untreated SU-8 surfaces. The results could be improved by using a O_2 plasma treatment before incubation of the silanes [136].

8.5 Spotting

It is important to remember that if the receptor biomolecules bind to the SU-8 cantilever surface, they will also bind to all other SU-8 surfaces in the microfluidic system. If the molecules bind to both the top and the backside of the cantilever, the differential induced surface stress is zero and the cantilever will not bend. Hence, the biomolecules should not be immobilized by injecting the solution in the microfluidic system. Instead, it was necessary to either block the SU-8 surface of the backside of the cantilever, or to immobilize receptor molecules only on the top surface of the cantilever using a spotter.

Since a microspotter was not available at MIC at the start of this project, the antibody immobilization on the cantilever surface was initially done manually using a micropipette and a droplet volume of 0.5 µl. However, to manually immobilize antibodies on a specific area which was 200 µm by 200 µm was not straightforward. Since the SU-8 surface was slightly hydrophobic it was possible to place the droplet so that only an area of about 1 mm by 1 mm was covered. Hence, the top surfaces of two neighbouring cantilevers were covered by the droplet. It was assumed that there was no antibodies on the backside of the cantilevers.

To instead spot the antibody solution on the surface of only a single cantilever, a collaboration was initiated with Allan Hede Alstrup and Adama Sesay at the Centre for Microtechnology and Surface Analysis at Teknologisk Institut. Using a spotter with a droplet size down to a few picoliter it was possible to deposit antibodies on the cantilever surfaces, see Figure 8.6 (left) and (right).

8.6 Surface stress measurements

The surface stress change measurements due to CRP binding to antibodies immobilized on the SU-8 cantilever were performed. 3-8 droplets of 18 pl was spotted on two of the cantilevers on each chip. The chips were then

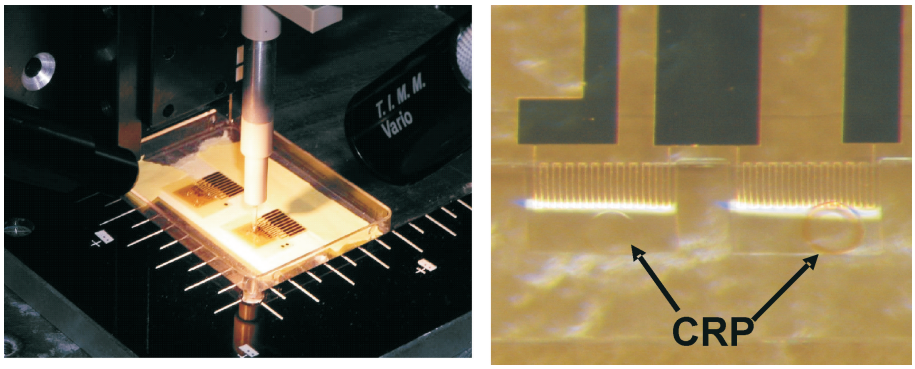

Figure 8.6: Left: A picoliter spotter was used to immobilize the antibodies on the cantilever surface. Right: Several droplets of CRP antibody solution with a volume of 18 pl were spotted to cover the cantilever surface.

transported in a closed single wafer tray providing a humid environment. Afterwards, a 20 µl drop of BSA was placed on each chip to block the SU-8 surfaces. The chips were incubated with the BSA overnight. Before measuring, the chips were rinsed in 10 mM PBS. The chips were stored in the fridge and all chips were used within four days of antibody immobilization. Figure 8.7 shows the output voltage change when injecting a CRP concentration of 10 µg/ml in the microfluidic system. However, this measurement was not reproduced and measurements using a reference antigen or antibody were not performed.

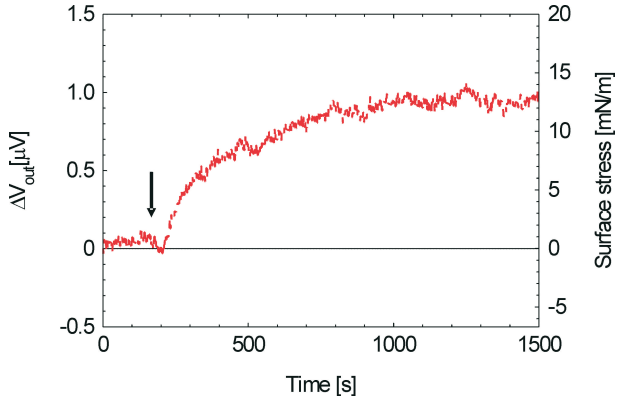

Figure 8.7: When 10 µg/ml of CRP antigen solution was introduced in the fluidic system, the cantilever with the immobilized antibodies was observed to deflect. The measured surface stress was about 13 mN/m.

CRP detection using concentrations of 100 ng/ml has previously been reported using piezoresistive Si cantilevers [139]. The CRP antibodies were immobilized on Au coated cantilevers using self-assembled monolayers of

Calixcrown. Cantion A/S has also demonstrated detection of CRP in concentrations of 5 ng/ml and 100 ng/ml, where the CRP antibodies were immobilized directly on the Si surface [82]. In neither of these articles were the resulting surface stress change calculated and although a buffer sample without CRP did not result in a deflection, the specificity of the measurements were not investigated by using a reference antigen.

In this chapter, it has been demonstrated that antibodies can bind to SU-8 surfaces and that subsequent binding of antigen/antibody is possible. These results are very interesting for future applications of SU-8 based microfluidic systems and sensors. However, it has been observed that the surface properties of the SU-8 can be influenced by different surface treatments that in turn can influence the antibody immobilization. It was also observed that the surface properties could change over time. In this chapter, it was demonstrated that the SU-8 cantilever can be used as a biosensor for detection of rather large concentration of antigens. However, cantilever measurements should be performed using reference antigens to verify that the signal change was due to specific CRP binding.

Chapter 9

The Cantion system

Since 2001, Cantion A/S has developed and sold cantilever based biochemical sensing systems based on piezoresistive Si based cantilevers. The company was started by Jakob Thaysen who developed the chip during his PhD studies in the Nanoprobe group [98]. The Cantion system, Canti^{TM} Lab4, is an instrument which consists of both an electrical readout system and a fluidic system [18][82], see Figure 9.1. An external pump and a valve are required to pump the liquid into the system. The Cantion chip, Canti^{TM} Chip4, has four piezoresistive cantilevers in a microfluidic channel and the chips are flip chip bonded on rigid-flex prints. The Cantion chip is briefly presented in Chapter 4 and is here referred to as *the Si Cantion chip*. The cantilevers can be individually functionalized using the Canti^{TM} Spot system which has a xyz-microposition stage and a camera so that 100 pl of solution can be delivered to the surface of a each cantilever.

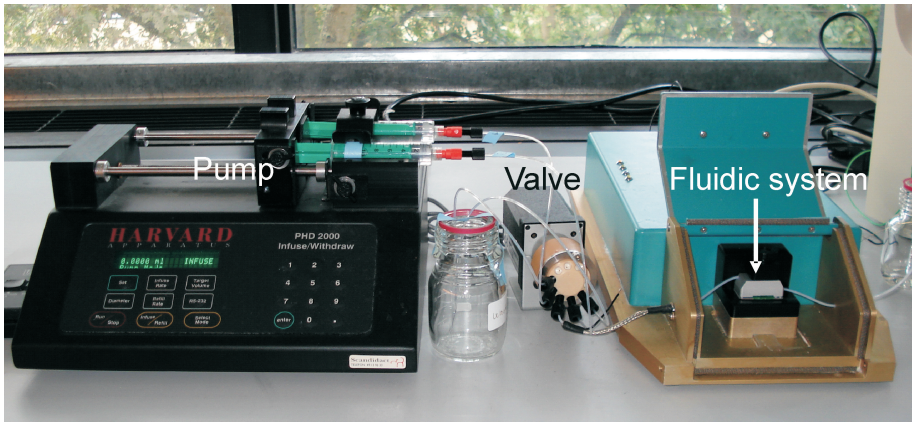

Figure 9.1: The Cantion system including the pump and the valve. The print with the flip chip bonded chip was mounted under the fluidic system.

In January 2006, MIC acquired a Cantion system. The system will primar-

ily be used to perform surface stress measurements using the Si Cantion chips but also to characterize cantilever chips that have been developed at MIC. By using the Cantion system for all measurements it will be possible to directly compare the performance of different cantilever chips. Moreover, developing of individual packaging systems and setups will not be required.

The Cantion system imposes some restrictions on the chips that can be used in the system. First, the chips must be interconnected to the rigid-flex prints which means that the contact pads on the chips have to fit with the contact pads on the print. Second, to obtain an output signal, it requires that the resistors in the cantilevers have a resistance between 3.8 and 4.2 kΩ. Third, it is only allowed to apply a voltages of either 1.25 or 2.5 V over the Wheatstone bridge. Forth, the fluidic system provides an inlet and outlet system applied on the top side of the chip but requires that the channel in the chip has a lid attached to the opposite side.

9.1 Design and fabrication of the SU-8 Cantion chip

A third generation of SU-8 chips, the so called *SU-8 Cantion chip*, which was designed to fit into the Cantion measuring system was fabricated. The SU-8 Cantion chips were smaller than the first and second generation chips and had a rectangular channel instead of a rounded channel. Although the cantilevers and the resistors had the same design as the second generation SU-8 chip, the way the resistors were connected differed, see Figure 9.2.

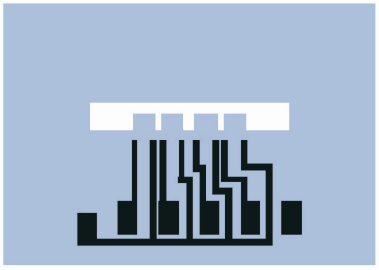

Figure 9.2: The first two mask used to fabricate the SU-8 Cantion chip. The chips were 5 by 3 mm and had four cantilevers in a microfluidic channel. The input voltage was applied to the right leg of each piezoresistor. The resistors in the cantilevers are too small to be visible.

The second generation SU-8 chip had ten contact pads while the SU-8 Cantion chip design only had six contact pads. One reason was that the SU-8 Cantion chip did not have any on-chip resistors. The other reason was that the right conductor going from each resistor was connected to the same con-

tact pad where the input voltage was applied. This design was required for the chip to function in the Cantion system and was the same as for the Si Cantion Chip. One wafer had 120 chips compared to 148 chips for the SU-8 chips.

To achieve the required resistance, which was larger than for the SU-8 chips, it was necessary to increase the length, reduce the width or reduce the thickness of the resistors. The length could not be significantly increased without increasing the dimensions of the cantilever. Since the width of the resistors was only 4 μm, line-width would become a critical issue if the width was further reduced. Hence, the most straightforward solution was to reduce the Au thickness. Alternatively, the Au could be replaced with another conductive material with a lower resistivity.

To obtain a resistance of 3.8-4.2 kΩ, a Au thickness of 100-125 Å was evaporated. The evaporation rate was normally about 2 Å/s. However, when using the Alcatel the reproducibility from batch to batch was rather low and it was occasionally required to control the thickness of the Au layer within 2 Å to obtain the desired resistance, see Figure 9.3. This was not straightforward and resulted in a low yield.

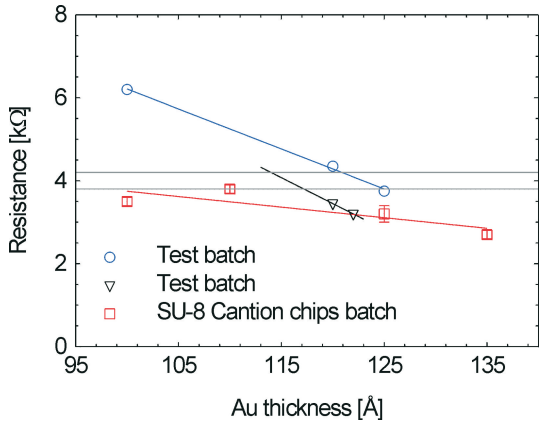

Figure 9.3: The thickness of the Au layer for the resistors had to be carefully optimized to achieve a resistance of about 4 kΩ. Two test batches and one batch of SU-8 Cantion chips were fabricated. Unfortunately, the reproducibility was rather low from batch to batch. Only one of the wafers with the SU-8 chips had a resistance within the allowed range.

Since the resistance over the SU-8 Cantion chips was larger than for the SU-8 chips, it was possible to apply a larger voltage without heating the cantilever. For a 4 kΩ resistor the dissipated power was about 0.1 mW for V_{in}=1.25 V and 0.4 mW for V_{in}=2.5 V. This is comparable to the dissipated power of 0.1 mW for a 500 Ω with an applied voltage of 0.5 V.

The resistors of the SU-8 Cantion chips had a lower yield compared to the second generation SU-8 chips. The reason was most likely that the resistors were more fragile due to the very thin Au layer. The maximum resistor yield was about 60 % compared to 90 % for the SU-8 chips.

9.2 Packaging of SU-8 Cantion chips

The chips were electrically interconnected to rigid-flex prints (Reichelt Chemitechnik GmbH.) that fitted into the Cantion system, see Figure 9.4. Although the ACF flip chip bonding process, discussed in Chapter 4, was successful when using FR-4 prints, the yield was considerably lower (about 10 %) when the rigid-flex prints were used. The reason was probably that the rigid-flex print was softer than the FR-4 print. Instead of flip chip bonding, silver paste was used to electrically interconnect the chips.

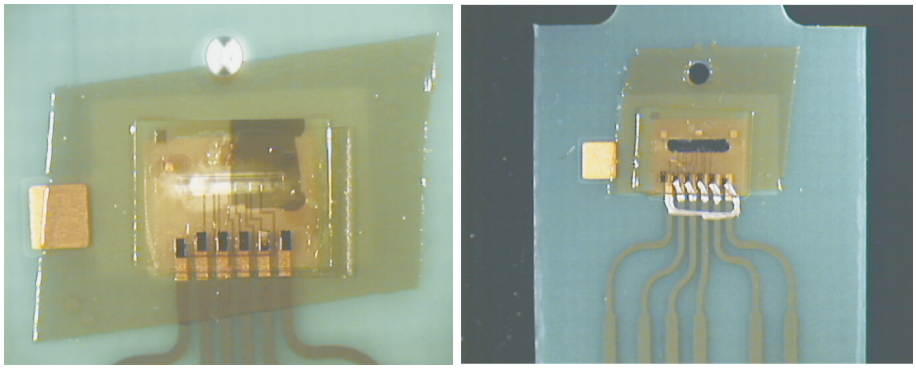

Figure 9.4: Left: An SU-8 Cantion chip has been flip chip bonded to the rigid-flex print using ACF. Unfortunately, the electrical interconnection yield was very low. Right: Electrical interconnection from the SU-8 Cantion chip to the rigid-flex was achieved by using silver paste.

The SU-8 channel lids could be adhered onto the SU-8 Cantion chips as described in Chapter 3. Another possibility was to fabricate a fluidic part that could function as a reversible attached lid of the channel. It was decided that the fluidic part should not be based on PDMS due to the possible issues with contamination. Hence, the microfluidic part was based on PMMA and a Viton O-ring. A recess for the O-ring was micromilled in a plate of PMMA. The thickness of the plate was only 0.5 mm so that it would fit into the system. The Cantion microfluidic system could be easily aligned to the print and the PMMA plate by a small pin that fitted into a hole in the print and the microfluidic part, see Figure 9.5.

Water or buffer was pumped through the system several times to test for

leakage. Normally, leakage was not observed which demonstrated that the O-ring was sealing the gap between the chip and the new fluidic part properly.

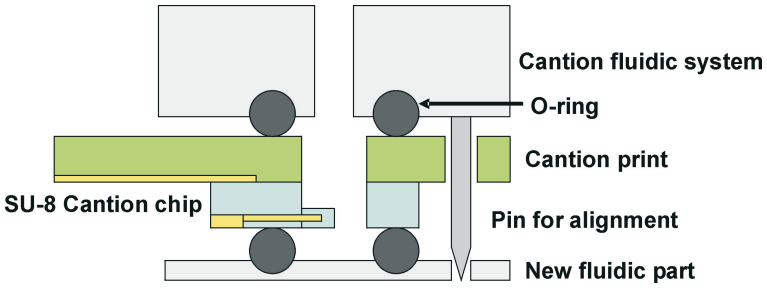

Figure 9.5: Schematic drawing of the packaging system for the SU-8 Cantion chip. The chip was interconnected using silver paste and a new fluidic part was fabricated and placed underneath the chip. The packaging did not contain PDMS and only Viton O-rings were used.

9.3 Characterization of the SU-8 Cantion chips

The greatest advantage by using the Cantion system compared to the lock-in amplifier setup was that both absolute and differential signals of the output voltage change were obtained simultaneously for all four cantilevers. For the lock-in amplifier setup only the differential response between two cantilevers could be observed. Although it is the differential value that is interesting for the measurements, the absolute value can provide information about how each cantilever reacts to changes in the fluidic flow, the temperature or due to molecular binding. The absolute signal gives a better understanding of how the measuring cantilever responds in comparison to the reference. Moreover, it can be used to quickly identify cantilevers that behave abnormal.

To compare the performance of the SU-8 Cantion chips with the Si Cantion chips, the chips were characterized in terms of the drift and the noise level in air. Measurements were done over several hours to observe signal changes due to temperature fluctuations. However, no significant difference in drift was observed between the Si and the SU-8 Cantion chips. However, the SU-8 Cantion chips turned out to have more resistors that behaved abnormal, meaning that the drift was much larger than expected. The reason was probably due to defects in the Au resistor. By performing drift measurements in air using absolute mode, these cantilevers could easily be identified and removed.

By using an input voltage of 2.5 V, the noise level in air was observed to be

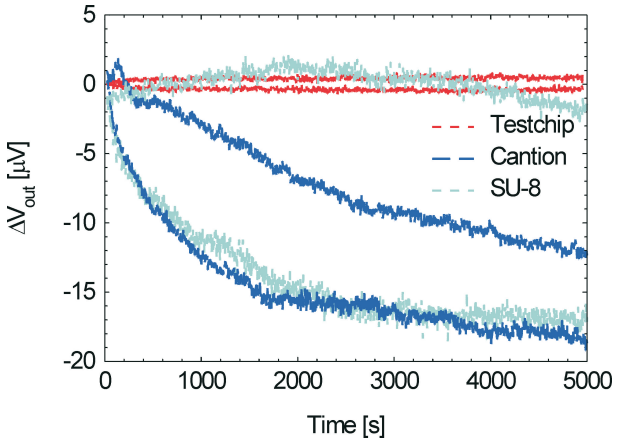

Figure 9.6: The drift and noise levels for the Cantion chips, the SU-8 Cantion chips and testchips based on thin film resistors were characterized. The graph shows typical measurements in air. The SU-8 Cantion chips were observed to have a very similar behavior to the Si Cantion chips.

approximately 1 μV which was comparable to the noise level for the Cantion chips, see Figure 9.6. This is surprising since the noise level was expected to be lower for the Au resistor than for a Si resistor. A test chip with four SMD resistors was also used to measure the noise and drift level of the Cantion system. The noise level was found to be slightly lower than for the Si and the SU-8 Cantion chips which indicated that it was not the noise level of the Cantion system that set the limit on the minimum detectable signal.

Assuming that the minimum detectable signal is 1 μV, the minimum detectable surface stress can be calculated for the SU-8 Cantion chips using Eq.(7.5)-(7.7). Table 9.1 compare the sensitivity of the SU-8 Cantion chip to the sensitivity of the SU-8 chips presented in Chapter 7. It is seen that the minimum detectable surface stress of the SU-8 Cantion chip, when using an input voltage of 2.5 V, is comparable to the standard SU-8 chip using the lock-in amplifier setup. The results can be compared to the minimum detectable surface stress of the Si Cantion chip. According to Cantion A/S the A-factor is 3125 N/m which results in a minimum detectable surface stress of 1.25 mN/m when using an input voltage of 2.5 V and a noise level of 1 μV.

In conclusion, the performance of the SU-8 chips in terms of noise level and drift in air using the Cantion system has been found to be comparable to the Si Cantion chips. Hence, in the future it should be possible to use the Cantion system to perform biomolecular measurements using both Si and SU-8 based cantilevers with integrated readout. It would thereby be possible to compare the performance in terms of sensitivity to pH, salt and unspecific

Cantilever	t_1 [μm]	t_{res} [Å]	t_2 [μm]	V_{in} [V]	σ_{det}+Au [mN/m]	σ_{det} [mN/m]
Standard	1	600	2.5	0.5	4.2	2.7
Optimal	0.5	75	2	2.5	0.5	0.3
SU-8 Cantion	1	125	2.5	1.25	7.8	5
SU-8 Cantion	1	125	2.5	2.5	3.9	2.5

Table 9.1: The minimum detectable surface stress for the SU-8 Cantion chip has been calculated for an input voltage of 1.25 V or 2.5 V. The values are compared to the results obtained from the SU-8 chip using the lock-in amplifier setup which had a lower noise level.

binding on the backside of the cantilever. However, due to the relatively high noise level observed when using the Cantion system, it is not suitable for detection of small surface stress changes. Moreover, the system is not flexible since it requires that the resistors have a specific resistance and that the input voltage is either 1.25 V or 2.5 V. Hence, unless these issues are solved in future generations of the Cantion system, it is not recommended that the system is used to characterize new designs of piezoresistive cantilever chips.

Chapter 10

Conclusion and Outlook

This thesis describes the fabrication, packaging and characterization of a polymeric cantilever chip. The aim was to develop a micromechanical biosensor for surface stress detection due to binding of biomolecules. The microchip was fabricated in the photosensitive polymer SU-8 and the cantilevers had integrated Au resistors for readout. To the author's knowledge, this is the first time that surface stress measurements are presented using a polymeric cantilever based biosensor with integrated readout.

The motivation for fabricating the chip in SU-8 instead of Si, was to reduce the fabrication time and the material and equipment expenses. Since SU-8 is a relatively novel material for microfabrication, the processing is normally less reproducible than Si processing. However it was demonstrated that the SU-8 chips could be fabricated with a yield of up to 90%.

The theory describing surface stress sensing using piezoresistive readout was presented in this thesis. It was theoretically demonstrated that for piezoresistive readout, a short and wide cantilever has a similar or improved surface stress sensitivity compared to long and narrow cantilevers which are normally used for optical readout. To increase the surface stress sensitivity, the thickness of the cantilever and the piezoresistor should be reduced.

Electrical interconnection methods such as flip chip bonding were investigated and it was found that although it was feasible to obtain a robust electrical interconnection using the SU-8 chips, it was significantly more difficult than for the Si based chips. To enable surface stress measurements in liquid, a PMMA/PDMS microfluidic system was fabricated.

The chips were characterized in terms of the gauge factor of the piezoresistors, the resonant frequency of the cantilevers, the temperature sensitivity and the noise level. The gauge factor was found to be about 3.7 which is in

very good agreement with theoretical estimations. Although the piezoresistors were sensitive to temperature changes most of this effect could be balanced out by using a symmetrical Wheatstone bridge configuration. Heating of the cantilevers was observed due to the applied voltage but could be reduced to an acceptable level by lowering the voltage or by increasing the resistance of the piezoresistors.

The surface stress sensitivity of the cantilevers was characterized by measuring the surface stress change due to etching of a Au layer on the cantilever surface, immobilization of mercaptohexanol in vapor and liquid phase and by changing the pH and the salt concentration. The stress in the Au layer was found to be 6 MPa, while the immobilization of mercaptohexanol resulted in a surface stress change of about 170-1750 mN/m in vapor phase and 50-300 N/m in liquid phase depending on the concentration. pH changes in the range from pH 4.5 to pH 12 were found to result in surface stress changes of about 10 mN/m per pH. Finally, the device was characterized as a biosensor by immobilizing CRP antibodies on the cantilever surface and subsequently detecting CRP antigens in buffer. The surface stress change was 13 mN/m for an antigen concentration of 10 μg/ml. The CRP antibodies were immobilized directly on the SU-8 surface instead of using thiol/Au chemistry. The minimum detectable surface stress of the SU-8 cantilever was found to be about 2.7 mN/m for uncoated cantilevers and 4.2 mN/m for Au coated cantilevers using the measurement setup presented in this thesis. However, by reducing the thickness of the cantilever and the piezoresistor the sensitivity could be further improved.

It was also demonstrated that the SU-8 chip could be integrated in the commercial measurement system developed by Cantion A/S, which was designed for piezoresistive Si based chips. Although the yield of the polymer chips was slightly lower than the commercial chips, the performance was found to be similar in terms of drift and noise level.

Further work should include the fabrication of a cantilever with an optimized sensitivity. Moreover, it would be desirable to exchange the Au resistors with a material with a higher gauge factor and lower temperature sensitivity without increasing the noise level. In terms of the characterization of the chips, it would be interesting to further compare the performance of the SU-8 chips with the Si chips. This requires that the same setup can be used.

A more detailed study of the SU-8 surface and how molecules interact with the surface would be desirable. This issue is interesting, not only for cantilever based biosensors but for all bio/medical applications where SU-8 is used as the device material. The study should also include the long term

stability of the mechanical properties of the cantilever as well as the stability of the surface properties. For cantilever based biosensors, more research is required to understand how surface stress changes are generated and how they can be enhanced. It could for example be interesting to perform simultaneous optical and piezoresistive readout. For biosensors, it is important to focus not only on the sensitivity but also on the selectivity and the reproducibility. Finally, for microsystems for biochemical applications, it is important to learn more about the materials involved in terms of biocompatibility and contamination.

In short, the main achievement of this PhD work was that it was demonstrated that polymeric cantilever biosensors offer a promising alternative to Si based devices due to the lower cost without reducing the sensitivity.

Bibliography

[1] Image by Daniel Haefliger, MIC, DTU

[2] G. Binning, C. F. Quate and Ch. Gerber, *Physical Review Letters*, **56** 930-933 (1986)

[3] J. Thaysen, A. Boisen, O. Hansen and S. Bouwstra, *Sensors and Actuators*, **83** 47-53 (2003)

[4] P. -F. Indermühle, G. Schürman, G. -A. Racine and N. F. de Rooij, *Journal of Micromechanics and Microengineering*, **7** 218-220 (1997)

[5] D. R. Baselt, B. Fruhberger, E. Klaassen, S. Cemalovic, C. L. Britton Jr., S. V. Patel, T. E. Mlsna, D. McCorkle and B. Warwick, *Sensors and Actuators B*, **88** 120-131 (2003)

[6] G. Shekhawat, S. -H. Tark and V. P. Dravid, *Science*, **311** 1592-1595 (2006)

[7] http://en.wikipedia.org/wiki/Atomic_force_microscopy

[8] L. M. Lechuga, J. Tamayo, M. Álvarez, L. G. Carrascosa, A. Yufera, R. Doldán, E. Peralías, A. Rueda, J. A. Plaza, K. Zinoviev, D. Domínguez, A. Zaballos, M. Moreno, C. Martínez-A, D. Wenn, N. Harris, C. Bringer, V. Bardinal, T. Camps, C. Vergnenegre, C. Fontaine, V. Díaz and A. Bernad, *Sensors and Actuators B*, **118** 2-10 (2006)

[9] M. Tortonese, H. Yamada, R. C. Barrett and C. F. Quate, *Solid-State Sensors ans Actuators, TRANSDUCERS '91*, 448-451 (1991)

[10] B. Ilic, Y. Yang, H. G. Craighead, *Applied Physics Letters*, **85** 2604-2606 (2004)

[11] R. Berger, Ch. Gerber, J. K. Cimzewski, E. Meyer and H. J. Güntherodt, *Applied Physics Letters*, **69** 40-42 (1996)

[12] F. J. Norton, U. S. Patent No. 2,307,800 (1943)

[13] P. J. Shaver, *The Review of Scientific Instruments*, **40** 901-905 (1969)

[14] R. Raiteri and H. -J. Butt, *Journal of Physical Chemistry*, **99** 15728-15732 (1995)

[15] G. Y. Chen, T. Thundat, E. A. Wachter and R. J. Warmack, *Journal of Applied Physics*, **77** 3618-3622 (1995)

[16] H. -J. Butt, *Journal of Colloid and Interface science*, **180** 251-260 (1996)

[17] J. Fritz, M. K. Baller, H. P. Lang, H. Rothuizen, P. Vettiger, E. Meyer, H. -J. Güntherodt, Ch. Gerber and J. K. Gimzewski, *Science*, **288** 316-318 (2000)

[18] R. Mukhopadhyay, M. Lorentzen, J. Kjems and F. Besenbacher, *Langmuir*, **21** 8400-8408 (2005)

[19] Y. Arntz, J. D. Seeling, H. P. Lang, J. Zhang, P. Hunziker, J. P. Ramseyer, E. Meyer, M. Hegner and Ch. Gerber, *Nanotechnology*, **14** 86-90 (2003)

[20] M. Álvarez, A. Calle, J. Tamayo, L. M. Lechuga, A. Abad and A. Montoya, *Biosensors and Bioelectronics*, **18** 649-653 (2003)

[21] L. A. Pinnaduwage, T. Thundat, A. Gehl, S. D. Wilson, D. L. Hedden and R. T. Lareau, *Ultramicroscopy*, **100** 211-216 (2004)

[22] H. Jensenius, J. Thaysen, A. A. Rasmussen, L. H. Veje, O. Hansen and A. Boisen, *Applied Physics Letters*, **76** 2615-2617 (2000)

[23] G. Wu, H. Ji, K. Hansen, T. Thundat, R. Datar, R. Cote, M. F. Hagan, A. K. Chakraborty and A. Majumdar, *Proceedings of the National Academy of Science*, **98** 1560-1564 (2001)

[24] R. Bogue, *Sensor Review*, **25/3** 180-184 (2005)

[25] M. A. Cooper, *Drug Discovery World*, 68-82 (2006)

[26] N. Backmann, C. Zahnd, F. Huber, A. Bietsch, A. Plückthun, H. -P. Lang, H. -J. Güntherodt, M. Hegner and C. Gerber, *Proceedings of the National Academy of Science*, **102** 14587-14592 (2005)

[27] N. V. Lavrik and P. G. Datskos, *Applied Physics Letters*, **82** 2697-2699 (2003)

[28] S. Kurosawa, M. Nakamura, J, -W. Park, H. Aizawa, K. Yamada and M. Hirata, *Biosensors and Bioelectronics*, **20** 1134-1139 (2004)

[29] L. Huang, G. Reekmans, D. Saerens, J. -M. Friedt, F. Frederix, L. Francis, S. Muyldermans, A. Campitelli and C. van Hoof, *Biosensors and Bioelectronics*, **21** 483-490 (2005)

[30] G. Genolet, J. Brugger, M. Despont, U. Drechsler, P. Vettiger, N. F. de Rooij and D. Anselmetti, *Review of Scientific Instruments*, **70** 2398-2401 (1999)

[31] A. W. McFarland and J. S. Colton, *Journal of Microelectromechanical Systmes*, **14** 1375-1385 (2005)

[32] A. W. McFarland, M. A. Poggi, L. A. Bottomley and J. S. Colton, *Review of Scientific Instruments*, **75** 2756-2758 (2004)

[33] X. R. Zhang and X. Xu, *Applied Physics Letters*, **85** 2423-2425 (2004)

[34] Z. Bayindir, Y. Sun, M. J. Naughton, C. N. LaFratta, T. Baldacchini, J. T. Fourkas, J. Stewart, B. E. A. Saleh and M. C. Teich, *Applied Physics Letters*, **86** 064105 (2005)

[35] M. Calleja, J. Tamayo, A. Johansson, P. A. Rasmussen, L. Lechuga and A. Boisen, *Sensor Letters*, **1** 1-5 (2003)

[36] J. Zou, X. Wang, D. Bullen, K. Ryu, C. Liu and C. A. Mirkin, *Journal of Micromechanics and Microengineering*, **14** 204-211 (2004)

[37] R. Katragadda and Y. Xu, *International Workshop on Nanomechanical Sensors*, Copenhagen, Denmark (2006)

[38] J. H. T. Ransley, M. Watari, D. Sukumaran, R. A. McKendry and A. A. Seshia, *Microelectronic Engineering*, **83** 1621-1625 (2006)

[39] M. Calleja, J. Tamayo, M. Nordström and A. Boisen, *Applied Physics Letters*, **88** 113901 (2006)

[40] Anja Boisen, PhD thesis, MIC, DTU (1997)

[41] D. Haefliger, O. Hansen and A. Boisen, *Advanced Materials*, **18** 238-241 (2006)

[42] J. Thaysen, A. D. Yalcinkaya, P. Vettiger and A. Menon, *Journal of Physics D: Applied Physics*, **35** 2698-2703 (2002)

[43] M. Calleja, P. Rasmussen, J. Johansson, A. Boisen, *Smart Sensors, Actuators, and MEMS, Proceedings of the SPIE*, Gran Canaria, Spain (2003)

[44] Rodolphe Marie, PhD thesis, MIC, DTU (2003)

[45] A. G. Hansen, M. W. Mortensen, J. E. T. Andersen, J. Ulstrup, A. Kühle, J. Garnæs and A. Boisen, *Probe Microscopy*, **2** 139-149 (2001)

[46] S. D. Senturia, Microsystems Design, Kluwer Academic Publishers (2001)

[47] Image by Maria Nordström

[48] G. C. Kuczynski, *Physical review*, **94** 61-64 (1954)

[49] C. Reale, *Czechoslovak Journal of Physics B*, **21** 663-673 (1971)

[50] Peter A. Rasmussen, PhD thesis, MIC, DTU (2003)

[51] R. L. Parker and A. Krinsky, *Journal of Applied Physics*, **34** 2700-2708 (1963)

[52] S. U. Jen, C. C. Yu, C. H. Liu and G. Y. Lee, *Thin Solid Films*, **434** 316-322 (2003)

[53] C. Li, J. Hesketh and G. J. Maclay, *Journal of Vacuum Science and Technology A*, **12(3)** 813-819 (1994)

[54] M. Hopcroft, T. Kramer, G. Kim, K. Takashima, Y. Higo, D. Moore and J. Brugger, *Fatigue and Fracture of Engineering Materials and Structures*, **28** 735-742 (2005)

[55] L. Dellmann, S. Roth, C. Beuret, G. -A. Racine, H. Lorenz, M. Despont, P. Renaud, P. Vettiger and N. F. de Rooij, *Sensors and Actuators A*, **70** 42-47 (1998)

[56] X. Yu, J. Thaysen, O. Hansen and A. Boisen, *Journal of Applied Physics*, **92** 6296-6301 (2002)

[57] G. Villanueva, J. Montserrat, F. Pérez-Murano, G. Ruis and J. Bausells, *Microelectronic Engineering*, **73-74** 480-486 (2004)

[58] N. C. LaBianca and J. D. Gelorme, *Proceedings of SPIE- The international society for optical engineering*, **2438** 846-852 (1995)

[59] P. Alpuim, V. Chu and J. P. Conde, *IEEE sensors journal*, **2** 336-341 (2002)

[60] J. D. Gelorme, R. J. Cox and S. A. R. Guterrez, U. S. Patent No. 4882245 (1989)

[61] J. El-Ali, I. R. Perch-Nielsen, C. R. Poulsen, D. D. Bang, P. Telleman and A. Wolff, *Sensors and Actuators A*, **110** 3-10 (2004)

[62] S. Balslev, A. Mironov, D. Nilsson and A. Kristensen, *Optics Express*, **14** 2170-2177 (2006)

[63] Z. Wang, J. El-Ali, M. Engelund, T. Gotsæd, I. R. Perch-Nielsen, K. B. Mogensen, D. Snakenborg, J. P. Kutter and A. Wolff, *Lab on a chip*, **4** 372-377 (2004)

[64] G. Voskerian, M. S. Shive, R. S. Shawgo, H. von Recum, J. M. Anderson, M. J. Cima and R. Langer, *Biomaterials*, **24** 1959-1967 (2003)

[65] Private conversation with Jan Hales at MIC, DTU

[66] www.microchem.com

[67] A. Johansson, M. Calleja, P. A. Rasmussen and A. Boisen, *Sensors and Actuators A*, **123-124** 111-115 (2005)

[68] Alicia Johansson, Master thesis, MIC, DTU (2003)

[69] D. Haefliger and A. Boisen, *Journal of Micromechanics and Microengeering*, **16** 951-957 (2006)

[70] M. Nordström, A. Johansson, E. Sánchez-Noguéron, B. Clausen, M. Calleja and A. Boisen, *Journal of Micromechanics and Microengineering*, **78-79** 152-157 (2005)

[71] W. Dai, K. Lian and W. Wang, *Microsystem Technology*, **11** 526-534 (2005)

[72] L. Gammelgaard, P. A. Rasmussen, M. Calleja, P. Vettiger and A. Boisen, *Applied Physics Letters*, **88** 113508 (2006)

[73] Jan Tue Ravnkilde, PhD Thesis, MIC, DTU (2001)

[74] D. Haefliger, M. Nordström, P. A. Rasmussen and A. Boisen, *Microelectronic Engineering* **78-79** 88-92 (2005)

[75] P. Abgrall, C. Lattes, V. Conédéra, X. Dollat, S. Colin and A. M. Gué, *Journal of Micromechanics and Microengineering*, **16** 113-121 (2006)

[76] Y. Song, C. S. S. R. Kumar and J. Hormes, *Journal of Micromechanics and Microengineering*, **14** 932-942 (2004)

[77] Malene Erup Larsen, Master thesis, MIC, DTU (2005)

[78] G. Genolet, PhD thesis, EPFL, Lausanne (2001)

[79] C. Chung and M. Allen, *Journal of Micromechanics and Microengineering*, **15** N1-N5 (2005)

[80] F. J. Blanco, M. Agirregabiria, J. Garcia, J. Berganzo, M. Tijero, M. Arroyo, J. M. Ruano, I. Aramburu and K. Mayora, *Journal of Micromechanics and Microengineering*, **14** 1047-1056 (2004)

[81] T. Velten, H. H. Ruf, D. Barrow, N. Aspragathos, P. Lazarou, E. Jung, C. K. Malek, M. Richter, J. Kruckow and M. Wackerle, *IEEE Transactions on Advanced Packaging*, **28** 533-546 (2005)

[82] J. Thaysen, M. Havsteen Jacobsen and L. Kildemark Nielsen, *NSTI-Nanotechnology*, **2** 262-265 (2005)

[83] A. Johansson, J. Janting, P. Schultz, K. Hoppe, I. N. Hansen and A. Boisen, *Journal Micromechanics and Microengineering*, **16** 314-319 (2006)

[84] R. R. Tammala, Fundamentals of Microsystems Packaging (McGraw Hill Companies inc.) (2001)

[85] N. Kuan, D. Liepmann and A. P. Pisano, *Micro-Electro-Mechanical-Systems (MEMS)*, **2** 591-594 (2000)

[86] Z. Zhong, *Microelectronics International*, **18/3** 15-19 (2001)

[87] A. Seppälä and E. Ristolainen, *Microelectronics Reliability*, **44** 639-648 (2004)

[88] www.telephus.com

[89] D. Snakenborg, G. Perozziello, H. Klank, O. Geschke, J. P. Kutter, *Journal of Micromechanics and Microengineering*, **16** 375-381 (2006)

[90] J. Li, C. R. Friedrich and R. S. Keynton, *Journal of Micromechanics and Microengineering*, **12** 219-228 (2002)

[91] A. Johansson, G. Perozziello, M. J. Jensen, O. Geschke and A. Boisen, *Proceedings of the 1st International Conference on Multi-Material Micro Manufacture (4M)*, Karlsruhe (2005)

[92] L. H. U. Andersson, P. Johander and T. Hjertberg, *Journal of Applied Polymer Science*, **90** 3780-3789 (2003)

[93] N. L. Jeon, D. T. Chiu, C. J. Wargo, H. Wu, I. S. Choi, J. R. Anderson and G. M. Whitesides, *Biomedical Microdevices*, **4:2** 117-121 (2002)

[94] L. H. U. Andersson and T. Hjertberg, *Journal of Applied Polymer Science*, **88** 2073-2081 (2003)

[95] Y.-S. Lo, N. D. Heufner, W. S. Chan, P. Dryden, B. Hagenhoff and T. P. Beebe Jr., *Langmuir*, **15** 6522-6526 (1999)

[96] N. V. Lavrik, C. A. Tipple, M. J. Sepaniak and P. G. Datskos, *Biomedical Devices*, **3:1** 35-44 (2001)

[97] M. Calleja, M. Nordström, M. Álvarez, J. Tamayo, L. Lechuga and A. Boisen, *Ultramicroscopy*, **105** 215-222 (2005)

[98] Jakob Thaysen, PhD thesis, MIC, DTU (2001)

[99] F. N. Hooge, T. G. M. Kleinpennig and L. K. J. Vandamme, *Reports of Progress in Physics*, **44** 479-532 (1981)

[100] Stanford lock-in amplifier: http://www.thinksrs.com/products/SR810830.htm

[101] A. Johansson, O. Hansen, J. Hales and A. Boisen, *accepted by Journal of Micromechanics and Microengineering*

[102] N. Chronis and L. P. Lee, *Journal of Microelectromechanical systems*, **14** 857-863 (2005)

[103] Y. H. Cho, D. Collard, L. Buchaillot, F. Conseil and B. J. Kim, *Microsystem Technologies*, **12** 30-37 (2005)

[104] P. G. Datskos, N. V. Larvik and S. Rajic, *Review of Scientific Instruments*, **75** 1134-1148 (2004)

[105] S. O. Kasap, Principles of electronic materials and devices, second edition, (McGraw Hill, 2002)

[106] Y. -S. Lo, J. Simons and T. P. Beebe Jr., *Journal of Physical Chemistry B*, **106** 9847-9852 (2002)

[107] P. A. Rasmussen, J. Thaysen, O. Hansen, S. C. Eriksen and A. Boisen, *Ultramicroscopy*, **97** 371-376 (2003)

[108] G. Gerald Stoney, *Proceedings of the Royal Society of London. Series A, Containing Papers of a Mathematical and Physical Character*, **82 (553)** 172-175 (1909)

[109] T. Smith, *Journal of Colloid and Interface Science*, **75** 51-55 (1980)

[110] J. R. Vig, *Journal of Vacuum Science and Technology A*, **3 (3)** 1027-1034 (1985)

[111] Y. -K. Kim, J. P. Koo and J. S. Ha, *Applied Surface Science*, **249** 7-11 (2005)

[112] C. G. Worley and R. W. Linton, *Journal of Vacuum Science and Technology A*, **13 (4)** 2281-2284 (1995)

[113] Results obtained by Stephan Keller at MIC, DTU

[114] R. Berger, E. Delamarche, H. P. Lang, Ch. Gerber, J. K. Gimzewski and H. -J. Güntherodt, *Science*, **276** 2021-2024 (1997)

[115] M. Godin, O. Laroche, V. Tabard-Cossa, L. Y. Beaulieu and P. Grütter, *Review of scientific instruments*, **74** 4902-4907 (2003)

[116] A. Johansson, G. Blagoi and A. Boisen, *accepted by Applied Physics Letters*

[117] H. Soscún, O. Castellano and J. Hernández, *Journal of Physical Chemistry B*, **108** 5620-5626 (2004)

[118] H. -F. Ji, K. M. Hansen, Z. Hu and T. Thundat, *Sensors and Actuators B*, **72** 233-238 (2001)

[119] J. Fritz, M. K. Baller, H. P. Lang, T. Strunz, E. Meyer, H. -J. Güntherodt, E. Delamarche, Ch. Gerber and J. K. Gimzewski, *Langmuir*, **16** 9694-9696 (2000)

[120] T. Sikanen, S. Tuomikoski, R. A. Ketola, R. Kostiainen, S. Franssila and T. Kotiaho, *Lab on a chip*, **5** 888-896 (2005)

[121] S. Cherian and T. Thundat, *Applied Physics Letters*, **80** 2219-2221 (2002)

[122] R. McKendry, J. Zhang, Y. Arntz, T. Strunz, M. Hegner, H. P. Lang, M. K. Baller, U. Certa, E. Meyer, H. -J. Güntherrodt and C. Gerber, *Proceedings of the National Academy of Science*, **99** 9783-9788 (2002)

[123] G. Wu, R. H. Datar, K. M. Hansen, T. Thundat, R. J. Cote and A. Majumdar, *Nature biotechnology*, **19** 856-860 (2001)

[124] A. M. Moulin, S. J. O'Shea and M. E. Welland, *Ultramicroscopy*, **82** 23-31 (2000)

[125] A. M. Moulin, S. J. O'Shea, R. A. Badley, P. Doyle and M. E. Welland, *Langmuir*, **15** 8776-8779 (1999)

[126] J. Mertens, M. Calleja and J. Tamayo, *Proceedings of the International Workshop on Nanomechanical sensors*, Copenhagen, Denmark (2006)

[127] M. Godin, P. J. Williams, V. Tabard-Cossa, O. Laroche, L. Y. Beaulieu, R. B. Lennox and P. Grütter, *Langmuir*, **20** 7090-7096 (2004)

[128] Y. Wang, M. Bachman, C. E. Sims, G. P. Li and N. L. Allbritton, *Langmuir*, **22** 2719-2725 (2006)

[129] R. Marie, S. Schmid, A. Johansson, L. Ejsing, M. Norström, D. Haefliger, C. B. V. Christensen, A. Boisen and M. Dufva, *Bioelectronics and Bioengineering*, **21** 1327-1332 (2006)

[130] G. Blagoi, A. Johansson, S. Keller and A. Boisen, *International Workshop on Nanomechanical Sensors*, Copenhagen, Denmark (2006)

[131] P. Angenendt, J. Glökler, J. Sobek, H. Lehrach and D. J. Cahill, *Journal of Chromatography*, **1009** 97-104 (2003)

[132] J. Buijs, J. W. Th. Lichtenbelt, W. Norde and J. Lyklema, *Coloids and Surface B: Biointerfaces*, **5** 11-23 (1995)

[133] W. Norde, *Journal of Dispersion Science and Technology*, **13(4)** 363-377 (1992)

[134] P. H. Lolekha, A. Chittamma, W. L. Roberts, P. Sritara, S. Cheepudomwit and P. Suriyawongpaisal, *Clinical Biochemistry*, **38** 31-35 (2005)

[135] Nycocard: http://www.axis-shield-poc.com/esite/esite.nsf/pub/JTHD5WRHZ2?Open

[136] G. Blagoi, S. Keller, A. Johansson and A. Boisen, *in preparation*

[137] M. Norström, R. Marie, M. Calleja and A. Boisen, *Journal of Micromechanics and Microengineering*, **14** 1614-1617 (2004)

[138] Z. Wang, M. Stangegaard, M. Dufva, J. P. Kutter and A. Wolff, microTAS, Boston, USA (2005)

[139] K. W. Wee, G. Y. Kang, J. Park, J. Y. Kang, D. S. Yoon, J. H. Park and T. S. Kim, *Biosensors and Bioelectronics*, **20** 1932-1938 (2005)

Appendix A

SU-8 processing

- **Spin coating**: The SU-8 was spin coated on four inch Si wafers using a Karl-Süss Spinner (KS) (MA/BA6) or a Speedline Technologies Spinner (SS) (P6204) using a spin rate of 1000 rpm to 6000 rpm depending on the desired thickness of the SU-8 layer, see Table A.1. The acceleration was 200-600 rpm for the KS spinner while for the SS spinner the acceleration was unknown. To achieve an SU-8 layer thickness of below 1.2 μm, the Speedline Spinner was preferably used. For thin layers the SU-8 was dispensed by pouring directly from the bottle, while for thick layers (2075) a syringe attached to a pressure pump was used.

SU-8	Spinner	Spin rate/acc. [rpm]/[rpm/s]	Time [s]	Thickness [μm]	SU-8 layer
2002	SS	6000	60	1.0	First
2002	KS	4000/400	30	2.5	Second
2075	KS	5000/600	60	25-35	Lid
2075	KS	1000/200	30	150	Channel

Table A.1: Typical spin parameters for the SU-8 processing using two different spinners.

- **Soft bake**: After spin coating, the SU-8 was soft baked on a hotplate to evaporate some of the solvent from the SU-8. In general, the soft baking temperatures and times recommended by MicroChem Corp. were used [66]. A programmable hotplate was used to perform a two-step bake process where the temperature was slowly ramped to 60°C and then to 90°C. The ramp time was about 3 min in both cases. The baking times at 60°C and 90°C for the different layer thicknesses is seen in Table A.2. The wafers were left on the hotplate until they had cooled down to at least below the glass temperature, T_g, of SU-8 which is about 55°C, but preferably to room temperature. The ramp process

and the slow cooling were done to minimize stress in the SU-8.

SU-8 thickness [μm]	Soft bake [min]	
	60°C	90°C
1-3	2	2
25-35	5	30
150	5	45

Table A.2: Typical soft baking times for various SU-8 layer thicknesses. A two-step baking process was used.

- **UV-Exposure**: The SU-8 layer was patterned by UV-lithography using a KS Aligner, see Table A.3. The light intensity of the KS Aligner is normally 9 mW/cm^2. The masks were supplied by Delta masks (Netherlands). Since SU-8 is a negative resist, the exposed area becomes crosslinked while the non-exposed parts can be removed by a developer. Since both the cantilevers and the distance between them are rather large, line-width was generally not an issue. Hence, the SU-8 was normally overexposed to obtain a good adhesion to the substrate and to avoid cracks in the material.

SU-8 thickness [μm]	Exposure dose	
	[s]	[mJ/cm^2]
1-3	50	450
25-35	100	900
150	150	1350

Table A.3: The UV-exposure times and the exposure dose for different layer thicknesses of SU-8.

- **Post-exposure bake**: The crosslinking process takes place during the post-exposure bake. Although, the SU-8 will also crosslink at room temperature the process is accelerated by increasing the temperature. The SU-8 was post-exposure baked using the same two-step baking process as for the soft bake but the baking times differed, see Table A.4.
- **Development**: The non-exposed SU-8 was developed in propylene glycol methyl ether acetate (PGMEA). The wafers were developed in two beakers, one (FIRST) to remove most of the resist and the other (FINAL) to rinse off any last residues, see Table A.5. After development the wafers were rinsed in isopropanol (IPA) and dried gently with nitrogen. To ensure that the SU-8 was sufficiently developed, twice the recommended developing times were normally used.

SU-8 thickness [μm]	Post-exposure bake [min]	
	60°C	90°C
1-3	2	2
25-35	5	15
150	5	15

Table A.4: Typical post-exposure baking times for various SU-8 layer thicknesses.

SU-8 thickness [μm]	FIRST [min]	FINAL [min]
1-3	2	2
25-35	10	10
150	20	20

Table A.5: The developing times in PGMEA for different SU-8 layer thicknesses.

Although SU-8 has been widely used for the last few years the process parameters are not standardized and might vary significantly from process to process and from lab to lab. The reason is that there are a wide range of process parameters to vary, including baking temperatures and exposure dose, and they are all influenced by each other. Moreover, the process parameters have to be optimized for each SU-8 layer thickness which is further complicated when several SU-8 layers are processes on top of each other. In addition to the parameters that have been presented here, the process might also be influenced by the wait time between process steps, the substrate under the SU-8 layer, the humidity in the cleanroom, the equipment and how fresh the SU-8 is.

Appendix B

Process sequence

RELEASE LAYER:
1. Leybold: Cr/Au/Cr 50/500/500 Å

FIRST CANTILEVER LAYER:
2. Spin SU-8 2002: Speedline technologies spinner, 6000 rpm, 60 s
4. Hotplate: (ramp 3 min) 2 min at 60°C and (ramp 3 min) 2 min at 90°C
5. UV-Exposure: Cantilever mask, Soft Contact, 50 s, 9.0 mW/cm^2
6. Hotplate: (ramp 3 min) 2 min at 60°C and (ramp 3 min) 2 min at 90°C
7. Development: 2 min in PGMEA (FIRST) and 2 min in PGMEA (FINAL), rinse IPA
8. Dektak: measure thickness

RESIST FOR LIFT-OFF:
8. Spin resist: KS Spinner, AZ5214E, PR1_5
9. UV-Exposure: Resistor mask, Hard Contact, ∼8 s, 9.0 mW/cm^2
10. Reverse Bake: 100 s at 120°C
11. UV-Exposure: Flood-exposure, 40 s, 9.0 mW/cm^2
12. Development: 70 s in NaOH:$H_2$0 (1:5), rinse in DI water

METAL:
13. Plasma: 240/40 O_2/N_2, 400 W, 4 min
14. Alcatel: 20/75-600 Å Ti/Au, rate 10 Å/s
15. Acetone lift-off: ∼30 min (do not use ultra sound!), rinse in DI water
16. Plasma: 240/40 O_2/N_2, 400 W, 4 min

CONTACT PADS:
17. Spin resist: KS Spinner, AZ 5214E, PR2_2
18. UV-Expose: Electroplating mask, Hard contact, ∼10 s, 9 mW/cm^2
19. Development: 90 s in NaOH:$H_2$0 (1:5), rinse in DI water
20. Etch Cr at the edge of the wafers, rinse in DI water

21. Plasma: 240/40 O_2/N_2, 400 W, 4 min
22. Electroplate: Bath Ni1, 4 A/dm^2, 40 °C
23. Acetone lift-off: ∼30 min (do not use ultra sound!), rinse in DI water
24. Dektak: measure thickness of contact pad
25. Probe station: measure resistance over contact pads
26. Plasma: 240/40 O_2/N_2, 400 W, 4 min

ENCAPSULATION:
23. Spin SU-8 2002: KS Spinner, 4000 rpm/400 rpm/s, 30 s
24. Hotplate: (ramp 3 min) 2 min at 60°C and (ramp 3 min) 2 min at 90°C
25. UV-Exposure: Encapsulation mask, Soft Contact, 50 s, 9 mW/cm^2
26. Hotplate: (ramp 3 min) 2 min at 60°C and (ramp 3 min) 2 min at 90°C
27. Development: 2 min in PGMEA (FIRST) and 2 min in PGMEA (FINAL), rinse IPA
28. Dektak: measure thickness of cantilever

SUPPORT LAYER:
29. Spin SU-8 2075: KS Spinner, 1000 rpm/200 rpm/s, 30 s
30. Hotplate: (ramp 3 min) 5 min at 60°C and (ramp 3 min) 45 min at 90°C
31. UV-Exposure: Proximity mode (chuck for thick resist), Channel mask, Multiple exposure: 30/30·5, 9.0 mW/cm^2
32. Hotplate: (ramp 3 min) 5 min at 60°C and (ramp 3 min) 15 min at 90°C
33. Development: 15 min in PGMEA (FIRST) and 15 min in PGMEA (FINAL), rinse IPA

RELEASE:
34. Release: Underetch the chips in Cr etchant 8002A for 30 min to 4 h
35. Rinse in DI water

Appendix C

Calculations

The following equations were obtained from Ole Hansen at MIC.

C.1 Resistance change due to the bimorph effect

Here, we assume that the contribution from the piezoresistor on the bimorph effect is negligible and only consider the top coating. The bimorph effect will bend the cantilever to a circular arc with the radius r_0 to the neutral plane of the cantilever. The arc length at the neutral plane is that same as the initial length of the cantilever. Hence, we have assumed that there is no elongation due to the bimorph effect. The length of the cantilever at the neutral plane can be expressed as

$$L = \theta r_0 \tag{C.1}$$

where θ is the arc angle of the cantilever. At the distance s from the neutral axis the arc length is $L_s{=}L{+}\Delta L{=}\theta(r_0{+}s){=}\theta r_0\ (1{+}s/r_0){=}\theta r_0(1{+}\epsilon_x)$. Hence, the axial strain due to bending is

$$\epsilon_x = \frac{s}{r_0} \tag{C.2}$$

The deflection $|z|$ at the end of the cantilever is obtained by using Phytagoras and that $z \ll r_0$

$$|z| = r_0(1 - cos\theta) \simeq \frac{1}{2} r_0 \theta^2 = \frac{1}{2}\frac{L^2}{r_0} \tag{C.3}$$

The piezoresistor is placed at a distance d from the neutral plane. The relative resistance change is proportional to the strain in the piezoresistor

$$\frac{\Delta R}{R} = K\epsilon_x = K\frac{d}{r_0} = 2K\frac{d|z|}{L^2} \tag{C.4}$$

C.2 Experimental thermal resistance

The resistors in the measuring and the reference cantilever can be assumed to be temperature dependant,

$$R_m = R_{m0}(1 + \alpha_{TCR}\Delta T_m) \tag{C.5}$$

$$R_r = R_{r0}(1 + \alpha_{TCR}\Delta T_r) \tag{C.6}$$

where α_{TCR} is the coefficient of thermal expansion, ΔT is the change in temperature, R_m and R_r is the resistance of the measuring and the reference cantilever respectively. The resistances of the two other resistors in the bridge are assumed to be constant and independent of temperature. The temperature increase in the resistors is due to the dissipated power and any change in the ambient temperature is assumed to be negligible.

$$\Delta T_m = R_{THm}P_m = R_{THm}\frac{R_m V_{in}^2}{(R_m + R_r)^2} \tag{C.7}$$

$$\Delta T_r = R_{THr}P_r = R_{THr}\frac{R_r V_{in}^2}{(R_m + R_r)^2} \tag{C.8}$$

The initial resistances are assumed to be the same for the measuring and the reference cantilever, R_{m0}=R_{r0}=R_0, but the thermal resistances are slightly different, R_{THm}≠R_{THr}, hence

$$\Delta T_m \cong R_{THm}\frac{V_{in}^2}{4R_0} \tag{C.9}$$

$$\Delta T_r \cong R_{THr}\frac{V_{in}^2}{4R_0} \tag{C.10}$$

and

$$\Delta T_m - \Delta T_r = (R_{THm} - R_{THr})\frac{V_{in}^2}{4R_0} = \Delta R_{TH}\frac{V_{in}^2}{4R_0} \tag{C.11}$$

The change in the output voltage from the Wheatstone bridge can be written as

$$\Delta V_{out} = \frac{1}{4}\frac{\Delta R}{R_0}V_{in} \cong \frac{V_{in}}{4}\alpha_{TCR}(\Delta T_m - \Delta T_r) \tag{C.12}$$

which can be rewritten as

$$\Delta V_{out} = \frac{\alpha_{TCR}\Delta R_{TH}}{16R_0}V_{in}^3 \tag{C.13}$$

and it is seen that ΔV_{out} is proportional to V_{in}^3 and the expression for the thermal resistance is found

$$\Delta R_{TH} = (\frac{\Delta V_{out}}{V_{in}^3})\frac{16R_0}{\alpha_{TCR}} \tag{C.14}$$

Appendix D

Dansk resumé

En cantilever baseret biosensor kan bruges til at måle overflade stress på grund af en biologisk reaktion med et specifikt molekyle. Formålet med dette PhD projekt har været at udvikle en mikromekanisk sensor, som muliggør så kaldet label-free detektion af biomolekyler såsom antistoffer. Da sensoren desuden er meget lille, er det muligt at lave målinger med stor følsomhed selv ved brug af små mængder af væske. Denne PhD afhandling beskriver udviklingen af en SU-8 cantilever chip med integreret piezoresistiv udlæsning i form af en Au modstand. SU-8 er en epoxy baseret negativ fotoresist, som er blevet meget udbredt indenfor mikrovæske systemer i løbet af de seneste år. Si bliver normalt brugt til at fremstille cantileverer, men da SU-8 er både et blødere og billigere materiale, er det fordelagtigt at bruge SU-8 i stedet for Si. SU-8 chippen er blevet elektrisk interkonnekteret med en print plade ved hjælp af flip chip bondning, og for at kunne lave målinger i væske er et mikrovæske system blevet fremstillet ved hjælp af mikrofræsning. Karakteriseringen af chippen er sket blandt andet ved at måle piezoresistorens gauge faktor, cantileverens resonans frekvens og chippens følsomhed over for temperatur forandringer. For at bestemme cantileverens følsomheden over for overflade stress fremlægges teoretiske beregninger, og det mindste målbare overflade stress bliver estimeret. Thiol molekyler har fået lov til at binde til Au belagte cantileverer i både luft og væske og det opståede overflade stress er blevet beregnet ud fra det elektriske signal. Resultaterne er sammenlignelige med resultater fra lignende målinger, hvor Si baserede cantileverer er blevet brugt. Au belagte cantileverer er også blevet brugt til at teste følsomheden over for pH variationer. Med hjælp af fluorescerende antistoffer er det blevet vist, at det er muligt at binde antistoffer direkte til SU-8 overfladen. Disse resultater viser, at cantilever-chippen kan bruges som en biosensor til at påvise forekomsten af antigener i væske.

Appendix E

List of publications

E.1 Published articles

A. Johansson, G. Blagoi and A. Boisen, "Polymeric cantilever-based biosensors with integrated readout", accepted by *Applied Physics Letters*

A. Johansson, O. Hansen, J. Hales and A. Boisen, "Temperature effects in Au piezoresistors integrated in SU-8 cantilever chips", accepted by *Journal of Micromechanics Microengineering*

A. Johansson, J. Janting, P. Schulz, K. Hoppe, I. N. Hansen and A. Boisen, "SU-8 cantilever chip interconnection", *Journal of Micromechanics and Microengineering*, 16 (2006) 314-319

R. Marie, S. Schmid, **A. Johansson**, L. Ejsing, M. Nordström, C. B. V. Christensen, A. Boisen and M. Dufva, "Immobilisation of DNA to polymerised SU-8 photoresist", *Biosensors and Bioelectronics*, 21 (2006) 1327-1332

M. Nordström, **A. Johansson**, E. Sánchez Noguerón, B. Clausen, M. Calleja and A. Boisen, "Investigation of the bond strength between the photosensitive polymer SU-8 and gold", *Microelectronics Engineering*, 78-79 (2005) 152-157

A. Johansson, M. Calleja, P. A. Rasmussen and A. Boisen, "SU-8 cantilever sensor with integrated readout", *Sensors and Actuators A*, 123-124 (2005) 111-115

A. Johansson, M. Calleja, M. Dimaki, P. Rasmussen, P. Bøggild and A. Boisen, "Polymer cantilever platform for dielectrophoretic assembly of carbon nanotubes", *Sensor Letters* 2 (2004) 117-120